Inventorying trees in an urban landscape using small-footprint discrete return imaging lidar

Rupesh Shrestha

Dissertation submitted to the faculty of Virginia Polytechnic Institute and State University in partial fulfillment of the requirements for the degree of

Doctor of Philosophy
in
Forestry

Randolph H. Wynne, Chair
James B. Campbell
A. Lynn Abbott
Ross F. Nelson

March 28, 2011
Blacksburg, Virginia

Keywords: remote sensing, carbon, biomass, urban forestry, tree identification

Inventorying trees in an urban landscape using small-footprint discrete return imaging lidar

Rupesh Shrestha

(ABSTRACT)

Automation of urban tree inventory using remote sensing is needed not only to reduce inventory costs but also to support carbon accounting for urban planners and policy-makers. However, urban areas are heterogeneous and complex, and a more sophisticated approach is needed for using remote-sensing technology like lidar for tree inventory in urban areas than is required for forested environments. Based on remote sensing and field data from a suburban residential area in the central United States, this dissertation presents a methodology for utilizing airborne small-footprint lidar data to inventory urban trees. This dissertation proposes approaches that have the potential to automate three main activities of urban tree inventory – identifying the locations of trees, classifying the trees into taxonomic categories, and estimating biophysical parameters of individual trees – using airborne lidar data.

Mathematical morphological operations followed by a marker-controlled watershed segmentation were found to perform well (r = 0.82 to 0.92) to delineate individual tree crowns in urban areas, especially when the trees occur in relatively isolated conditions. Using various distribution metrics of lidar returns, random forests were used to classify individual trees into different taxonomic classes (broadleaves/conifers, genera, and species). A classification accuracy of 80.5% was obtained when separating trees only into broadleaf and conifer classes, 50.0% for genera, and 51.3% for species. Using spectral metrics from high-resolution satellite imagery in addition to lidar-derived predictors improved the classification accuracies by 10.4% (to 90.9%) for broadleaf and conifer, 8.4% (to 58.4%) for genera and 8.8% (to 60.1%) for species compared to using lidar metrics alone. Prediction models to estimate several biophysical parameters such as height, crown area, diameter at breast height, and biomass were developed using lidar point cloud distributional metrics from individual trees. A high level of accuracy was attained for estimating tree height (R^2=0.89, *RMSE*=1.3m), diameter at breast height (R^2=0.82, *RMSE*=9.1cm), crown diameter (R^2=0.90, *RMSE*=0.7m) and biomass (R^2=0.67, *RMSE*=1.2t).

Our results indicate that, while using lidar data alone can achieve the automation of major urban forest inventory tasks to an acceptable level of accuracy, a synergistic use of lidar data with other spectral data such as hyperspectral or orthoimagery, which are usually available at least in the United States for most urban areas, can considerably improve the performance of the lidar-based method.

ACKNOWLEDGEMENTS

First and foremost, I would like to thank my supervisor Dr. Randy Wynne. When I first arrived at Virginia Tech, some of his previous students were telling me that I was lucky to have him as my supervisor. It did not take me long to realize it. He is the greatest mentor and the kindest human being I could have had. I will forever be indebted to him for everything he has done for me both personally and professionally.

I also appreciate my committee members Dr. Jim Campbell, Dr. Ross Nelson, and Dr. Lynn Abbott for their guidance and constructive comments to improve my dissertation. Thanks also to Dr. Eric Wiseman for helping me understand urban forestry perspective. I would like to also thank Jennifer McKee for data collection; Jessica Dorr for providing lidar data; and NASA and USDA for funding my doctoral study.

I am thankful to my colleagues, staffs and professors at CEARS and the department for their support and help. Thanks to my apartment-mates Richard, Zuoli and Jhalendra, and all friends from Blacksburg for being part of my life and making my stay a pleasant memory.

I would like to thank my parents who made so many sacrifices so that I can continue my graduate study abroad. They both went through life-threatening illnesses during my Ph.D., but never stopped blessing me.

Thanks to my wife, Surya, for her unconditional love, and for her companionship and constant encouragement which kept me going whenever I started to falter.

I am especially grateful to Dr. Nancy Glenn, my post-doctoral mentor, who has been both family and friend to me, and whose guidance was crucial in finishing this dissertation.

My Ph.D. has been quite a journey. But, I must indeed be incredibly lucky and blessed to have so many nice people around me whose love and support have helped me come this far. Thank you all!

TABLE OF CONTENTS

LIST OF FIGURES

LIST OF TABLES

1: INTRODUCTION AND OBJECTIVES

1.1 Inventory of Urban Trees

Urbanization is increasing at an unprecedented rate both globally and locally. By 2050, the world's population is expected to increase by 3 billion and the growth will occur primarily in urban areas (United Nations, 2007). In the US, there was a 34% increase in urban areas between 1982 and 1997 (Alig et al., 2004) and it is projected to increase a further 8.1% by 2050 (Nowak and Walton, 2005).

Urbanization often degrades the environment due to concentrated human activity in a smaller area. However, trees in urban areas can improve environmental quality and provide several social benefits (Tyrväinen et al., 2005; Nowak and Dwyer, 2007). They provide amenities and provide a multitude of ecosystem services including carbon sequestration (McPherson et al., 1997). Urban trees in the USA store 700 million tons of carbon (tC), valued at $14,300 million with a gross carbon sequestration rate of 22.8 million tC/year ($460 million/year) (Nowak and Crane, 2002). Trees contribute to ozone formation by emitting volatile organic compounds (VOC) in the presence of nitrogen oxide from vehicle exhaust (Cardelino and Chameides, 1990).

Urban trees can be defined as the woody vegetation in and around dense human settlements, from small communities to large metropolitan cities (Gann, 2003). Only 10% of the total trees in urban areas in the US are publicly-owned and the remaining 90% are on private property (Miller, 1996). As such, the management and cultural practices on the trees vary immensely. At the same time, urban trees are subjected to different stresses – they often grow on compacted soil, are subjected to intense pruning, roots are given very little space to grow, trees are improperly staked, etc. (Duryea and Malavasi, 1995). All these factors affect the rate of growth as well as the shape and form of the trees.

Although urban trees improve environmental quality, and provide ecological and economical benefits, they can also be a source of public hazards and incur management costs for municipalities. To assess these benefits and costs, an inventory of urban trees is necessary. Information about urban trees – their species, condition, and biophysical parameters – is now an integral part of urban planning. Urban tree inventory involves locating, evaluating,

characterizing, and documenting individual trees or groups of trees in an urban area (Escobedo and Andreu, 2008). Urban tree inventories can provide estimates of total percent canopy cover, which is used for urban planning, and for assessing carbon sequestration and other ecological services. Inventory of urban trees assists city planners with scheduling tree maintenance, creating a budget plan for maintenance trees, and setting priorities for tree care and management (Escobedo and Andreu, 2008).

An urban forest inventory can be a partial, complete, or sample inventory. A partial inventory is used when information is required for only a portion of urban areas, such as a particular neighborhood, a park, or specific street segments with trees of particular interest. A complete inventory includes all the trees of urban areas including those in streets, parks, public lands, and other public right-of ways and even potential planting sites. Finally an urban forest sample inventory consists of collecting data from randomly selected areas throughout the urban area and requires less effort and cost than that required for a complete inventory. Depending on the variability of an urban forest, a sample street tree inventory can consist of collecting information on about 5% to 10% of all the trees in the area (Escobedo and Andreu, 2008).

Most urban inventories of individual tree include information about what the tree is, where it is, and what it needs (Grey, 1996). This includes information such as location, tree species, size (diameter at breast height and crown size), condition, health, hazard potential, and necessary maintenance needs. This information can be collected in one of several ways. One of the basic options is to conduct a “windshield survey” in which tree data are collected from a slow-moving car to gather data for conducting a partial or complete inventory (Escobedo and Andreu, 2008). Or, an inventory can be a statistical sample of the entire urban forest with up to several hundred study plots located randomly across a large metropolitan community.

Computerized inventory systems are usually involved in management of information from urban tree inventories. Olig and Miller (1997) and Andreu et al. (2009) have done a synthesis of currently available urban tree management software. Of the fifteen software packages available in 2009 surveyed by Olig and Miller (1997), twelve have some form of GIS capabilities. It is apparent that spatial information has become important to urban foresters. The type of inventory system that is best for particular urban area depends on the ultimate use of the information and budgetary constraints. Apart from the type of inventory used, the cost of

inventory also depends upon whether a professional or amateur conducts the inventory and the extent of the area.

Urban trees have different characteristics compared to trees in traditional forests. There are different factors in play that affect the rate of growth as well as the shape and form of the trees. One of the important factors is stresses due to urban environment (Duryea and Malavasi, 1995). As the impervious surfaces and soil compaction prevent recharge of soil water, urban trees experience frequent water stress. They also experience a heavy heat load, due to re-radiation of the heat absorbed by surrounding pavement, buildings, and automobiles parked under trees (Rhoades and Stipes, 1999). Urban trees generally face reduced competition for light and other resources with surrounding trees than in forests, and there is no 'after-thinning effect', which is a period of increased cambial activity and radial growth toward the base experienced by trees in forests right after thinning (McHale et al., 2009). Because urban trees often receive additional nutrients and water, they have higher rates of trunk growth than of those in traditional forests (Rhoades and Stipes, 1999). All these factors changes from one urban area to another. This makes the ability to predict inventory parameters such as tree height, biomass, and crown dimensions even more difficult in urban landscapes than in forests, where trees are more or less homogeneous in their growth and form for a particular locality and species.

In contrast to traditional forest inventory for estimating woody volume or biomass, urban tree inventory often requires estimation of a wider range of parameters. Urban tree inventory is also labor intensive because it often places emphasis on measuring individual trees (Wood, 1999). This makes the field inventory of urban trees expensive and there are often calls to look for alternative cost-effective approaches.

1.2 Measuring Urban Trees Using Remote Sensing

Application of remote sensing in change detection is an efficient way of reducing the labor cost and time. Traditionally, remote sensing of urban forests was done using visual interpretation of aerial photographs combined with field inventory (Nowak et al., 1996). Approaches involving use of remote sensing methods have proven to be an effective way to identify and measure urban trees (Zhang, 2001; Imai et al., 2004; Meinel and Hecht, 2004; Secord and Zakhor, 2007; Sugumaran and Voss, 2007). Use of moderate resolution sensors

(such as Landsat, sensors on the Indian Remote Sensing (IRS), and Satellite Pour l'Observation de la Terre (SPOT) satellites) was limiting because of the difficulty in separating urban trees of diverse types. This often results in spectral mixing, and hence makes the data less suitable for statistical methods. Development of high-resolution remote sensing instruments, such as Quickbird and IKONOS, along with novel classification algorithms, such as neural networks (Tatem et al., 2001) and object-oriented approaches (Yu et al., 2006), has increased the ability to discriminate not only the trees that occur in clumps but also the isolated trees.

There are several challenges in using remote sensing for urban forest inventory. Urban areas are so complex due to the mixture of all kinds of man-made and natural features. There is difficulty in separating the trees and man-made objects in urban areas because of the similarity of the texture (Zhang, 2001). This can be overcome, in most cases, by fusing the lidar-based digital surface model with optical remote sensing data, but in areas where trees and buildings are close to each other, it is still difficult to separate them (Zhang, 2001). Because of this complexity, a synergistic approach with use of different data sources (such as lidar data and optical data) is often employed, because a single sensor may not be able to present a complete characterization (Gamba et al., 2005).

The availability of airborne lidar data, which are able to characterize vertical profiles more accurately, has added another dimension to urban forest inventory using remote sensing. In recent years, the ability of lidar systems to collect high density data, as well as the availability of different software and algorithms for processing lidar data, has made them more useful for various forest inventory applications.

Lidar (light detection and ranging) is an active sensor that measures distances using precisely defined and carefully timed pulses of laser (Campbell, 2002) and positional measuring devices. There are two major classes of lidar systems – large-footprint, full-wave form systems and small-footprint, discrete-return systems. The differences between waveform and discrete-return lidar involve the area actively sensed by the laser pulse and the spatially explicit information returned to the sensor (Jensen et al., 2006). Systems with a footprint size of 1 m diameter or smaller are categorized as a small-footprint, and those with a footprint size between 10 and 30 meters are categorized as a large-footprint lidar. Large footprint systems enable penetration of laser energy deep into the canopy that reaches the ground surface, even in very

dense forests (Ogunjemiyo et al., 2006), but large-footprint systems have limitations due to their low spatial resolution and high per unit area acquisition costs (Lee, 2006).

A typical lidar device consists of (1) an orientation unit, consisting of a geographic positioning system (GPS) and an inertial navigation system (INS) to provide the spatial and attitude positioning of a laser vector, (2) a ranging unit to provide the magnitude (range) of the laser vector and – optionally – auxiliary information about the footprint, (3) a scanning unit that deflects the laser beam into different directions to obtain specific footprint patterns, and (4) a control unit to control the sub-systems and their interaction, record the data, and perform real-time processing (Schenk, unpublished). The device may be operated from aircraft or helicopters. Most systems also record the intensity of the reflected return, which is to some extent a measure of the surface reflectance (Forlani et al., 2006). A typical lidar data acquisition is shown in Figure 1.1.

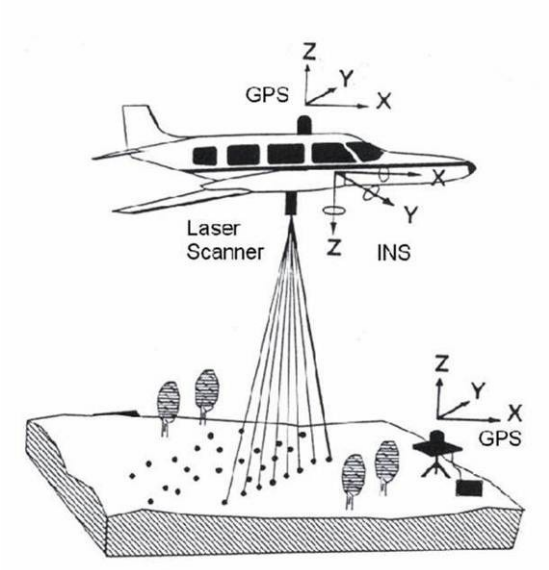

Figure 1.1. Airborne lidar data acquisition (Source: Kao et al., 2006, used with permission of the authors)

Lidar systems of the present day are capable of achieving vertical accuracies of 15 cm root mean square error (RMSE) and horizontal accuracies about two times the footprint size (usually at sub-meter) (Renslow et al., 2000). Lidar scans produce a very large and dense cloud of point returns. Often the first step of the lidar data processing is to reduce the number of points clouds by filtering operations, such as those used to separate returns from ground and non-ground objects. For computing digital terrain model (DTM), the returns from non-ground objects

like buildings and trees have to be eliminated, but for detection of buildings and trees, those returns are needed.

With availability of sensors with denser sampling rates and higher precisions, lidar technology has broadened its range of applications. As much as lidar remote sensing is used in surface reconstruction (Lohr, 1998; Petzold et al., 1999; Schenk, unpublished), its use in automatic extraction of non-ground objects, especially trees and buildings, has been primary in applied research in recent years (Brenner, 2003; Wang et al., 2006).

Lidar data have been widely used for extraction, 3D reconstruction, and visualization of urban features like buildings, with applications in urban planning, mobile communication, disaster management, virtual reality, and navigation among others (Haala and Brenner, 1999; Verma et al., 2006; Miriam Rehor, 2008; Qihong, 2008; Alexander et al., 2009).

One of the approaches to extract urban features is to fuse lidar data with another optical data set. This approach is especially suited for urban areas because, due to the mixture of different man-made and natural features, they are so complex that a single sensor may not be able to present a complete characterization (Gamba et al., 2005). Csatho et al. (2003) used a region growing approach from seed pixels with fused LIDAR and AVIRIS (Airborne Visible/Infrared Imaging Spectrometer) imagery to classify and segment urban areas automatically. Rottensteiner et al. (2005) used the Dempster–Shafer method (Le Hegarat-Mascle et al., 1997) to fuse LIDAR data and multi-spectral images to detect buildings. They used height differences between the first and last returns, the digital surface model (DSM) derived from the last return, surface roughness properties, and the normalized differential vegetation index (NDVI) (Lu and Trinder, 2003) to classify urban areas into buildings, trees, grasslands and bare soil. Alonso and Malpica (2008) used a support vector machine (SVM) on lidar data combined with SPOT imagery to classify vegetation and buildings in urban areas. Chen et al. (2009) used a hierarchical object-oriented method to classify urban areas using Quickbird imagery and lidar data.

Other approaches to extract urban features of interest are based on using only the lidar data set, achieved either using the interpolated surface from lidar returns or using the raw lidar returns without the interpolation. The latter methods avoid the loss of information and accuracy due to interpolation (Cho et al., 2004). The most common method to extract buildings is using a

region growing approach. Some studies (e.g., Oda et al., 2004; Overby et al., 2004; Tarsha-Kurdi et al., 2007) have used the 3-D Hough transform to extract the buildings from the lidar data. Others (e.g., Bretar and Roux, 2005; Forlani et al., 2006; Tarsha-Kurdi et al., 2007; Miriam Rehor, 2008) have used the Random Sample Consensus (RANSAC) algorithm for detecting building roof planes. RANSAC (Fischler and Bolles, 1981) is a robust estimator, most frequently used in computer vision to detect geometric primitives. Weidner and Förstner (1995) and Weidner (1997) used parametric models in a normalized DSM (equivalent to the Canopy Height Model (CHM) in forests) to detect buildings. Cho et al. (2004) used the concept of a 'pseudo-grid' to extract 3-D vectors of buildings. Pseudo-grids are virtual 3-D grids containing lidar data points, the size of the grid being dependent on the density of the points and the maximum and minimum height difference of the returns. Their method involves pseudo-grid creation, noise removal, segmentation using maxima filters, grouping within the pseudo-grid for building detection, and linearization and simplification of the resulting building boundary.

Lidar has been used widely in recent years to detect individual trees in forest (Persson et al., 2002; Popescu and Wynne, 2004; Yu et al., 2004), to identify species of individual trees (Holmgren and Persson, 2004; Holmgren et al., 2008) and to estimate several forest biophysical parameters like tree height, aboveground biomass, leaf area index, crown diameter, etc. (Nelson et al., 1988; Hyyppä and Hyyppä, 2001; Brandtberg et al., 2003; Riaño et al., 2003; Todd et al., 2003; Popescu and Wynne, 2004; Bortolot and Wynne, 2005; Boudreau et al., 2008; Dean et al., 2008). Use of lidar remote sensing in forestry and ecological applications has been reviewed by Dubayah and Drake (2000), Lefsky et al. (2002), Lim et al. (2003), and Hyyppä et al. (2008). However, methods and algorithms developed for forested environments may not be very useful for detecting and inventorying trees in urban environments, because the complex backgrounds and different tree shapes in the latter are more complicated (Liu et al., 2006).

1.3 Objectives

The overall goal of this dissertation is to develop a methodology using of small-footprint lidar coupled with optical imagery and field inventory data, to inventory trees in urban landscapes. Specific objectives of the research are to:

1. Develop an algorithm for detecting trees in an urban environment using small-footprint lidar data
2. Classify the taxonomic group of individual trees using both a lidar point cloud and canopy height models
3. Investigate various approaches to estimate biophysical parameters of the trees in an urban environment using small-footprint lidar data

The objectives are discussed in Chapter 2 to 4 of the dissertation as three independent research manuscripts. Chapter 2 discusses an image morphology based approach for detection and delineation of individual trees. Chapter 3 evaluates a method using lidar and high-resolution Quickbird metrics with Random Forests for taxonomic classification of individual trees. Chapter 4 uses distributional metrics from lidar point clouds of individual trees to estimate several biophysical parameters.

1.4 Literature Cited

Alexander, C., Smith-Voysey, S., Jarvis, C. and Tansey, K., 2009. Integrating building footprints and LiDAR elevation data to classify roof structures and visualise buildings. Computers, Environment and Urban Systems, 3(4): 285-292.

Alig, R.J., Kline, J.D. and Lichtenstein, M., 2004. Urbanization on the US landscape: looking ahead in the 21st century. Landscape and Urban Planning, 69(2-3): 219-234.

Alonso, M. and Malpica, J., 2008. Classification of multispectral high-resolution satellite imagery using LIDAR elevation data, Advances in Visual Computing, pp. 85-94.

Andreu, M.G., Brown, E.M., Friedman, M.H., Northrop, R.J. and Thornhill, M.E., 2009. Comparison of urban forest tree inventory and management software systems, School of Forest Resources and Conservation, Florida Cooperative Extension Services, Institute of Food and Agricultural Sciences, University of Florida, Gainesville, FL.

Bortolot, Z.J. and Wynne, R.H., 2005. Estimating forest biomass using small footprint LiDAR data: An individual tree-based approach that incorporates training data. ISPRS Journal of Photogrammetry & Remote Sensing, 59(6): 342-360.

Boudreau, J., Nelson, R.F., Margolis, H.A., Beaudoin, A., Guindon, L. and Kimes, D.S., 2008. Regional aboveground forest biomass using airborne and spaceborne LiDAR in Québec. Remote Sensing of Environment, 112(10): 3876-3890.

Brandtberg, T., Warner, T.A., Landenberger, R.E. and McGraw, J.B., 2003. Detection and analysis of individual leaf-off tree crowns in small footprint, high sampling density lidar data from the eastern deciduous forest in North America. Remote Sensing of Environment, 85(3): 290-303.

Brenner, C., 2003. Building reconstruction from laser scanning and images, Proceedings of ITC Workshop on Data Quality in Earth Observation Techniques, Enschede, The Netherlands.

Bretar, F. and Roux, M., 2005. Hybrid image segmentation using lidar 3D planar primitives, ISPRS Proceedings on Laser scanning, Enschede, the Netherlands.

Campbell, J.B., 2002. Introduction to Remote Sensing. The Guilford Press, 621 pp.

Cardelino, C.A. and Chameides, W.L., 1990. Natural hydrocarbons, urbanization, and urban ozone. Journal of Geophysical Research, 95(D9): 13971-13979.

Chen, Y., Su, W., Li, J. and Sun, Z., 2009. Hierarchical object oriented classification using very high resolution imagery and LIDAR data over urban areas. Advances in Space Research, 43(7): 1101-1110.

Cho, W., Jwa, Y., Chang, H. and Lee, S., 2004. Pseudo-grid based building extraction using airborne LIDAR data. International Archives of Photogrammetry and Remote Sensing, 35(B3): 378-381.

Csatho, B., Schenk, T. and Suyoung, S., 2003. Spectral interpretation based on multisensor fusion for urban mapping, 2nd GRSS/ISPRS Joint Workshop on Remote Sensing and Data Fusion over Urban Areas, 2003., pp. 8-12.

Dean, T.J., Cao, Q.V., Roberts, S.D. and Evans, D.L., 2008. Measuring heights to crown base and crown median with LiDAR in a mature, even-aged loblolly pine stand. Forest Ecology and Management, 257(1): 126-133.

Dubayah, R.O. and Drake, J.B., 2000. Lidar remote sensing for forestry. Journal of Forestry, 98(6): 44-46.

Duryea, M.L. and Malavasi, M.M., 1995. Tree growth in the urban forest. Forestry Report R8-FR, USDA Forest Service, Southern Region, Atlanta, Georgia.

Escobedo, F. and Andreu, M., 2008. A community guide to urban forest inventories, School of Forest Resources and Conservation, Florida Cooperative Extension Services, Institute of Food and Agricultural Sciences, University of Florida, Gainesville, FL.

Fischler, M.A. and Bolles, R.C., 1981. Random sample consensus: a paradigm for model fitting with applications to image analysis and automated cartography. Graphics and Image Processing, 24(6): 381-395.

Forlani, G., Nardinocchi, C., Scaioni, M. and Zingaretti, P., 2006. Complete classification of raw LIDAR data and 3D reconstruction of buildings. Pattern Analysis & Applications, 8(4): 357-374.

Gamba, P., Dell'Acqua, F. and Dasarathy, B.V., 2005. Urban remote sensing using multiple data sets: Past, present, and future. Information Fusion, 6(4): 319-326.

Gann, S.B., 2003. A methodology for inventorying stored carbon in an urban forest. M.S. Thesis, Virginia Polytechnic Institute and State University, Blacksburg, Virginia. http://scholar.lib.vt.edu/theses/available/etd-08052003-135647/.

Grey, G.W., 1996. The Urban Forest: Comprehensive Management. John Wiley & Sons Inc., New York, 156pp.

Haala, N. and Brenner, C., 1999. Extraction of buildings and trees in urban environments. ISPRS Journal of Photogrammetry and Remote Sensing, 54(2-3): 130-137.

Hecht, R., Meinel, G. and Buchroithner, M.F., 2008. Estimation of urban green volume based on single-pulse LiDAR data. IEEE Transactions on Geoscience and Remote Sensing, 46(11): 3832-3840.

Holmgren, J. and Persson, Å., 2004. Identifying species of individual trees using airborne laser scanner. Remote Sensing of Environment, 90(4): 415-423.

Holmgren, J., Persson, Å. and Soderman, U., 2008. Species identification of individual trees by combining high resolution lidar data with multi-spectral images. International Journal of Remote Sensing, 29(5): 1537-1552.

Hyyppä, H.J. and Hyyppä, J.M., 2001. Effects of stand size on the accuracy of remote sensing-based forest inventory. Geoscience and Remote Sensing, 39(12): 2613-2621.

Hyyppä, J., Hyyppä, H., Leckie, D., Gougeon, F., Yu, X. and Maltamo, M., 2008. Review of methods of small-footprint airborne laser scanning for extracting forest inventory data in boreal forests. International Journal of Remote Sensing, 29(5): 1339-1366.

Imai, Y., M., S., Y., Y. and N, F., 2004. Tree-height measuring characteristics of urban forests, Proceedings of XXth ISPRS Congress 'Geo-Imagery Bridging Continents', Commission VII, 12-23 July 2004, Istanbul, Turkey.

Jensen, J.L.R., Humes, K.S., Conner, T., Williams, C.J. and DeGroot, J., 2006. Estimation of biophysical characteristics for highly variable mixed-conifer stands using small-footprint lidar. Canadian Journal of Forest Research, 36(5): 1129-1138

Kao, D.L., Kramer, M.G., Love, A.L., Dungan, J.L. and Pang, A.T., 2006. Visualizing Distributions from Multi-Return Lidar Data to Understand Forest Structure. The Cartographic Journal, 42(1): 35–47.

Le Hegarat-Mascle, S., Bloch, I., and Vidal-Madjar, D., 1997. Application of Dempster-Shafer evidence theory to unsupervised classification in multisource remote sensing. IEEE Transactions on Geoscience and Remote Sensing, 35(4): 1018-1031.

Lee, A., 2006. Utilizing airborne scanning laser (LiDAR) to improve the estimation of Australian forest structure and biomass. Ecological Management & Restoration, 7(s1): 77-78.

Lefsky, M.A., Cohen, W.B., Parker, G.G. and Harding, D.J., 2002. Lidar remote sensing for ecosystem studies. BioScience, 52(1): 19-30.

Lim, K., Treitz, P., Wulder, M.A., St-Onge, B.A. and Flood, M., 2003. LiDAR remote sensing of forest structure. Progress in Physical Geography, 27(1): 88-106.

Liu, J., Li, D., Qin, X. and Yang, J., 2006. Automatic extraction of tree crowns from aerial imagery in urban environment, Geoinformatics 2006: Remotely Sensed Data and Information. SPIE, pp. 64190G-5.

Lohr, U., 1998. Laserscanning for DEM generation. In: C.A. Brebbia and P. Pascolo (Editors), GIS technologies and their environmental applications Computational Mechanics Publications, Southampton, UK, pp. 243-249.

Lu, Y. H., and Trinder, J., 2003. Data fusion applied to automatic building extraction in 3D reconstruction. Proceedings of Annual ASPRS Conference, Anchorage, Alaska, May 2003, pp. 114–122.

McHale, M., Burke, I., Lefsky, M., Peper, P. and McPherson, E., 2009. Urban forest biomass estimates: is it important to use allometric relationships developed specifically for urban trees? Urban Ecosystems, 12(1): 95-113.

McPherson, E.G., Nowak, D., Heisler, G., Grimmond, S., Souch, C., Grant, R. and Rowntree, R., 1997. Quantifying urban forest structure, function, and value: the Chicago Urban Forest Climate Project. Urban Ecosystems, 1(1): 49-61.

Meinel, G. and Hecht, R., 2004. Urban vegetation volume on the basis of laser-scan data at non-leaf aerial flight times. In: M. Thies, B. Koch, H. Spiecker and H. Weinacker (Editors), ISPRS Working Group VIII/2 Laser-Scanners Forest and Landscape Assessment, Vol. XXXVI, No. 8/W2, 03-06 October 2004, Freiburg, Germany, pp. 334-339.

Miller, R.W., 1996. Urban Forestry: Planning and Managing Urban Greenspaces. Prentice Hall, New Jersey, USA, 480 pp.

Miriam Rehor, H.-P.B., Fayez Tarsha-Kurdi, Tania Landes, Pierre Grussenmeyer, 2008. Contribution of two plane detection algorithms to recognition of intact and damaged buildings in lidar data. The Photogrammetric Record, 23(124): 441-456.

Nelson, R., 1997. Modeling forest canopy heights: The effects of canopy shape. Remote Sensing of Environment, 60(3): 327-334.

Nelson, R., Krabill, W. and Tonelli, J., 1988. Estimating forest biomass and volume using airborne laser data. Remote Sensing of Environment, 24(2): 247-267.

Nowak, D. and Dwyer, J., 2007. Understanding the benefits and costs of urban forest ecosystems. In: J.E. Kuser (Editor), Urban and Community Forestry in the Northeast. Springer, pp. 25-46.

Nowak, D.J. and Crane, D.E., 2002. Carbon storage and sequestration by urban trees in the USA. Environmental Pollution, 116(3): 381–389.

Nowak, D.J., Rowntree, R.A., McPherson, E.G., Sisinni, S.M., Kerkmann, E.R. and Stevens, J.C., 1996. Measuring and analyzing urban tree cover. Landscape and Urban Planning, 36(1): 49-57.

Nowak, D.J. and Walton, J.T., 2005. Projected urban growth (2000-2050) and its estimated impact on the US forest resource. Journal of Forestry, 103(8): 383-389.

Oda, K., Takano, T., Doihara, T. and Shibasaki, R., 2004. Automatic building extraction and 3D city modeling from lidar data based on Hough transformation. International Archives of Photogrammetry and Remote Sensing, XXXV part B3.

Ogunjemiyo, S., Roberts, D., Ustin, S. and Parker, G., 2006. Comparison of small and large footprint lidar systems in predicting forest structural characteristics, Remote Sensing and Modeling of Ecosystems for Sustainability III. SPIE 6298, 629803, San Diego, CA, USA.

Olig, G. and Miller, R., 1997. A Guide to Street Tree Inventory Software, U.S. Dept. of Agriculture.

Overby, J., Bodum, L., Kjems, E. and Ilsøe, P., 2004. Automatic 3D building reconstruction from airborne laser scanning and cadastral data using Hough transform, Proceedings of ISPRS 20th Congress - Commission III, Istanbul, Turkey, pp. 296–301.

Persson, A., Holmgren, J. and Soderman, U., 2002. Detecting and measuring individual trees using an airborne laser scanner. Photogrammetric Engineering & Remote Sensing, 68(9): 925-932.

Petzold, B., Reiss, P. and Stössel, W., 1999. Laser scanning – surveying and mapping agencies are using a new technique for the derivation of digital terrain models. ISPRS Journal of Photogrammetry and Remote Sensing, 54(2-3): 95-104.

Popescu, S.C. and Wynne, R.H., 2004. Seeing the trees in the forest: using lidar and multispectral data fusion with local filtering and variable window size for estimating tree height. Photogrammetric Engineering & Remote Sensing, 70(5): 589-604.

Qihong, Z., 2008. Data filtering and feature extraction of urban typical objects from airborne lidar point cloud. International Archives of the Photogrammetry, Remote Sensing and Spatial Information Sciences, 36(B3b): 153-156.

Renslow, M., Greenfield, P. and Guay, T., 2000. Evaluation of multi-return LIDAR for forestry applications, San Dimas Technology & Development Center, San Dimas, CA.

Rhoades, R. and Stipes, R., 1999. Growth of trees on the Virginia Tech campus in response to various factors. Journal of Arboriculture, 25(4): 211-217.

Riaño, D., Meier, E., Allgöwer, B., Chuvieco, E. and Ustin, S.L., 2003. Modeling airborne laser scanning data for the spatial generation of critical forest parameters in fire behavior modeling. Remote Sensing of Environment, 86(2): 177-186.

Rottensteiner, F., Trinder, J., Clode, S. and Kubik, K., 2005. Using the Dempster-Shafer method for the fusion of LIDAR data and multi-spectral images for building detection. Information Fusion, 6(4): 283-300.

Schenk, T., unpublished. Surface Reconstruction from Airborne Laser Scanning. In: T. Schenk (Editor), Digital Photogrammetry-Volume II. TerraScience LLC, pp. 1-70.

Secord, J. and Zakhor, A., 2007. Tree detection in urban regions using aerial lidar and image data. IEEE Geoscience and Remote Sensing Letters, 4(2): 196-200.

Sugumaran, R. and Voss, M., 2007. Object-oriented classification of LIDAR-fused hyperspectral imagery for tree species identification in an urban environment. In: M. Voss (Editor), Proceedings of 2007 Urban Remote Sensing Joint Event, 11-13 April 2007, Paris, France.

Tarsha-Kurdi, F., Landes, T. and Grussenmeyer, P., 2007. Hough-transform and extended RANSAC algorithms for automatic detection of 3D building roof planes from lidar data. International Archives of Photogrammetry, Remote Sensing and Spatial Information Sciences, 36(3/W52): 407-412.

Tatem, A.J., Lewis, H.G., Atkinson, P.M. and Nixon, M.S., 2001. Super-resolution mapping of urban scenes from IKONOS imagery using a Hopfield neural network, Proceedings of IEEE International Geoscience and Remote Sensing Symposium, 9-12 July, 2001, Sydney, Australia, pp. 3203-3205.

Todd, K.W., Csillag, F. and Atkinson, P.M., 2003. Three-dimensional mapping of light transmittance and foilage distribution using lidar. Canadian Journal of Remote Sensing, 29(5): 544-555.

Tyrväinen, L., Pauleit, S., Seeland, K. and Vries, S., 2005. Benefits and uses of urban forests and trees. In: C.C. Konijnendijk, K. Nilsson, T.B. Randrup and J. Schipperijn (Editors), Urban Forests and Trees. Springer, pp. 81-114.

UnitedNations, 2007. World Urbanization Prospects: The 2007 Revision Population Database. U.N. Department of Economic and Social Affairs, New York, New York, U.S.A.

Verma, V., Kumar, R. and Hsu, S., 2006. 3D Building Detection and Modeling from Aerial LIDAR Data, Computer Vision and Pattern Recognition, 2006 IEEE Computer Society Conference on, pp. 2213-2220.

Wang, Y., Weinacker, H. and Koch, B., 2006. Automatic non-ground objects extraction based on multi-returned Lidar data. Photogrammetrie Fernerkundung Geoinformation (PFG), 6(2): 127-137.

Weidner, U., 1997. Digital surface models for building extraction. Automatic Extraction of Man-Made Objects from Aerial and Space Images (II): 193-202.

Weidner, U. and Förstner, W., 1995. Towards automatic building extraction from high-resolution digital elevation models. ISPRS Journal of Photogrammetry and Remote Sensing, 50(4): 38-49.

Wood, J.P., 1999. Tree inventories and GIS in urban forestry. M.F. Paper, Virginia Polytechnic Institute and State University, Blacksburg, Virginia, USA. http://scholar.lib.vt.edu/theses/available/etd-012499-141520.

Yu, Q., Gong, P., Clinton, N., Biging, G., Kelly, M. and Schirokauer, D., 2006. Object-based detailed vegetation classification with airborne high spatial resolution remote sensing imagery. Photogrammetric Engineering & Remote Sensing, 72(7), 799-811.

Yu, X., Hyyppä, J., Kaartinen, H. and Maltamo, M., 2004. Automatic detection of harvested trees and determination of forest growth using airborne laser scanning. Remote Sensing of Environment, 90(4): 451-462.

Zhang, Y., 2001. Texture-integrated classification of urban treed areas in high-resolution color-infrared imagery. Photogrammetric Engineering & Remote Sensing, 67(12): 1359-1365.

2: IMAGE MORPHOLOGY BASED ALGORITHM TO DELINEATE TREES IN AN URBAN LANDSCAPE USING SMALL FOOTPRINT DISCRETE-RETURN IMAGING LIDAR

2.1 Abstract

Urban areas are more heterogeneous and complex than forested environments, and, to account for this complexity, a different and more sophisticated approach is needed for tree detection in urban areas. We have demonstrated use of mathematical morphological operations followed by a marker-controlled watershed segmentation to delineate individual tree crowns in urban areas using small footprint lidar data. When tested using a leaf-on lidar dataset collected from an Optech ALTM 2050 system over a typical suburban area of the United States, the morphological approach was largely able to separate tree cover from urban structures. In four test areas, mean tree detection errors were 24.15% for Type I error and 23.9% for Type II error. Field measured crown area was highly correlated with automatically measured crown area (r = 0.82 to 0.92). The best results were achieved when the trees occur in relatively isolated conditions. Our approach can be useful for measuring individual trees as well as tree cover in urban areas using lidar data.

2.2 Introduction

In urban landscapes, detection of objects, especially man-made objects, has been a domain of photogrammetry. Obtaining the precise geometric boundary of buildings and other cultural objects for urban planning has been one of the primary tasks of a photogrammetrist. Objects in urban areas are detected traditionally using manual analytical plotters, and more recently using digital photogrammetric workstations, but both of these methods, while giving a high accuracy, are very time-consuming and expensive (Schenk and Csatho, 2002). This has necessitated the development of automated or semi-automated methods of extracting urban objects, through use of digital photogrammetry, remote sensing, and computer vision techniques (Gruen et al., 1998; Mayer, 1999; Chen et al., 2004; Guan et al., 2007).

Algorithms such as region-based methods, template-matching, probabilistic methods, and contour matching have been developed to detect individual trees in optical imagery. Wulder et al.

(2000), Bortolot and Wynne (2005) and Eriksson et al. (2006) have provided a review of these available tree detection algorithms.

Dralle and Rudemo (1997) used Gaussian smoothing followed by local maxima filtering for automatic detection of trees in aerial photos. The exact positions of trees at ground level are estimated by use of a displacement model incorporating the angle to the sun, the camera position, and estimated tree heights. Gougeon (1995) and Culvenor (2002) used a valley-following algorithm – growing local maxima constrained by local minima representing shade in the image – to delineate tree crowns. Wulder et al. (2000) used a local maximum filter to identify the location of individual trees in high resolution imagery and found that a variable size window has lower commission error than a fixed size window. Brandtberg and Walter (1998) developed a multiple-scale approach to segment individual tree crowns using local maxima and region growing in high resolution aerial images.

Approaches involving use of remote sensing methods have been proven as an effective way to identify and measure trees in urban areas (Zhang, 2001; Imai et al., 2004; Meinel and Hecht, 2004; Secord and Zakhor, 2007; Sugumaran and Voss, 2007). However use of digital imagery alone may not be effective due to difficulty in separating trees from other urban objects (Zhang, 2001) and optical images are easily influenced by topography, vegetation cover types and weather conditions (Chen et al., 2005).

Lidar, with its high spatial resolution and horizontal and vertical accuracy, has been used widely in recent years to detect individual trees in forests, and many algorithms have been proposed (Persson et al., 2002; Popescu and Wynne, 2004; Yu et al., 2004). Most of the algorithms rely on finding the local maxima on the lidar-based canopy height model (CHM) and often rely on prior knowledge of the relationship between crown diameter and height. Leckie et al. (2003) used the valley following approach of Gougeon (1995) for individual tree detection in a CHM created from high-density lidar data over a Douglas-fir forest of varying densities. Falkowski et al. (2007) used discrete wavelet transformation of lidar data to detect trees. They convolved two-dimensional Mexican hat wavelets, over a range of likely tree crown diameters, with lidar CHM and determined the location of individual trees by the identification of local maxima within the resultant wavelet transformation image. Without using any prior information,

they were able to obtain a RMSE comparable to the variable window filter method of Popescu and Wynne (2004).

The accuracy of tree delineation depends on the density of lidar data and the applied processing techniques (Hyyppä et al., 2005). Accurate location of tree tops is difficult especially in low density data because of the high probability of the lidar to miss the top of tree. Varying tree heights and crown sizes, the absence or presence of leaves, the overlap of tree crowns in dense forests, and the variety of crown shapes also contribute to the lower accuracy in tree detection (Palenichka and Zaremba, 2007). The ISPRS/EuroSDR Tree Extraction Project (Kaartinen and Hyyppä, 2008) evaluated the performance of twelve different automatic and semi-automatic tree extraction algorithms in various forest conditions and lidar point densities. One conclusion was that despite much research the accurate location of individual trees is still to be achieved (Hyyppä et al., 2007).

Imai et al. (2004) used a combination of IKONOS imagery and digital height models at two different resolutions (1m and 2m) based on helicopter-borne lidar data to measure heights of urban trees in Tokyo, Japan. They found that the tree height accuracy does not depend on the resolution of lidar data but instead on the species and density of the trees. Hecht et al. (2008) used the lidar data collected during leaf-off condition to reconstruct and estimate the leaf-on (green) volume of the trees in urban areas. Omasa et al. (2008) used lidar CHM to estimate the height of trees in an urban park. They also used portable on-ground lidar to complement airborne lidar CHM for estimation of canopy volume, trunk volume, and canopy cross-sectional area.

Weidner (1997) found that the size criterion separating vegetation and buildings in a digital surface model (DSM) is not sufficient for larger vegetation areas or vegetation areas close to buildings. While the roughness of the surface measured by differential geometric quantities, like gradients or curvatures, are more effective in separating vegetation in DSM, such image morphological approaches may not work where vegetation canopies are smooth, similar to a bare topographic surface or roof patches (Weidner, 1997).

Filin (2002) developed a clustering method based on a surface structure analysis to classify lidar data into low and high vegetation, buildings and ground. Cho et al. (2004) used the minimum building area and circularity to separate trees from buildings in the ‘pseudo-grid’ but they could not separate the trees with sizes and shapes similar to the buildings.

Palenichka and Zaremba (2007) used a multi-scale isotropic matched filtering (MIMF) to detect trees in lidar data using a nonlinear image operator optimized for object detection and recognition. The method provides a robust scale- and orientation-invariant localization of the objects of interest. The local maxima of the matched-filtering operator are located at the potential centers of the objects of interest such as the trees. They found a lower tree detection rate in an urban area compared to that in a forested area.

Few of the above algorithms can achieve crown delineation of individual trees, which is essential for the estimation of individual tree biophysical characteristics like height, volume, and biomass, and possibly the classification of species. Due to the complex background and different tree shapes in urban environments, crown delineation algorithms developed for forested environments may not be very useful for trees in urban environments (Liu et al., 2006). To account for the complexity of urban landscapes, a more sophisticated method needs to be developed.

Mathematical morphology provides the tools for extracting image components that are useful in representation and description of region shapes, such as boundaries, skeletons and convex hulls, in binary or grey images (Gonzalez and Woods, 2002). The basic morphological operation involves probing an image with a structuring element, a set whose size and shape depends on the type of the shape information to be extracted from the image. Morphological operations have been applied in filtering lidar data using a filter of fixed-size window (Kilian et al., 1996; Lohmann et al., 2000) or progressive variable window (Zhang et al., 2003). The variable window filter is effective in preserving features and their boundaries that are larger than the filtering window size (Zhang and Whitman, 2005). Rottensteiner and Briese (2002) developed a technique based on "terrain roughness" to discriminate buildings from vegetation in a high-resolution LIDAR data of urban areas. Regions with an area greater than a minimum area (40 m^2) were classified as buildings. A large (e.g., 9 x 9) integration kernel was used in the DSM to compute the first derivative of the image, and based on anisotropic variations, texture of the image was classified as homogeneous, linear or point-like. Regions containing more than 50% of pixels classified as being "point-like" were categorized as vegetation. Morphological opening with a square structural element was used to separate the trees connected to the buildings. Andersen et al. (2001) used morphological analysis of a high-resolution lidar-based CHM to

detect individual tree tops. Zhang (2008) developed a top-hat mathematical morphological transformation to extract gap features in a mangrove forest using lidar data.

Extraction of trees from lidar data is a two step process – first, returns from non-ground objects have to be separated from ground returns, and then returns from trees have to be separated from other non-ground objects. A mixture of different objects like buildings, wires, vehicles, trees, and often close to each other or sometimes overlapping, makes urban areas a complex environment in which to extract trees. This necessitates more sophisticated methods such as mathematical morphology to extract trees in urban areas. Although mathematical morphology was originally developed for two-dimensional binary images, it has now been extended to three-dimensional gray-scale images. When lidar returns from urban areas are interpolated into a normalized digital surface model (nDSM), the same principle of gray-scale mathematical morphology can be applied to extract urban trees. In nDSM, objects such as buildings and trees have higher gray scale values than the ground, so that urban objects can be separated from ground returns by the change in gray scale values.

This study builds upon previous work applying mathematical morphological operations followed by segmentation to delineate individual tree crowns in urban areas using small foot-print lidar data. Our methodology is based on the premise that the lidar returns from trees have more variation than those from building roofs and most other urban structures (Figure 2.1). The resulting variation in texture of nDSM should enable morphological operations to separate trees from buildings. The objective of this study is to evaluate use of image morphology in identifying trees (defined as vegetation 1m or greater in height) in an urban landscape.

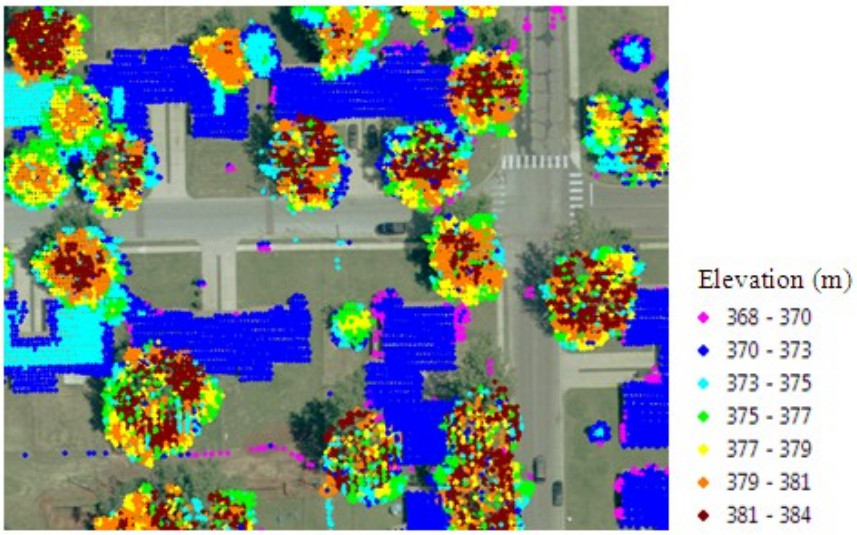

Figure 2.1. Variation in lidar elevation in buildings and trees. Color represents the elevation values of the lidar returns. Lidar data is from a residential area in Tinker, Oklahoma, and collected using an Optech ALTM 2050 in July 2004.

2.3 Morphological Operators

Morphological operators extract relevant structures of an image set by probing the image with another set of known shape called the structuring element.

2.3.1.1 Dilation

If A⊕B represents the dilation of an image A by structuring element B, dilation can be defined as the locus of points *a* such that B hits A when its origin coincides with *a* (Haralick et al., 1987; Soille, 2003):

$$A \oplus B = \{a \mid B_a \cap A \neq \varnothing\} \tag{1.1}$$

which can be also written as a union of set translations:

$$A \oplus B = \bigcup_{b \in B} (A)_b \tag{1.2}$$

where $(A)_b$ represents the translation of A by b. Dilation operation is similar to convolution and fills "holes" of a size equal to or smaller than the structuring element.

2.3.1.2 Erosion

If A⊖B represents the erosion of an image A by structuring element B, then erosion is defined as the locus of points ***a*** such that B is included in A when its origin is placed at ***a*** (Haralick et al., 1987; Soille, 2003):

$$A \ominus B = \{a | B_a \subseteq A\} \tag{1.3}$$

which can also be written as an intersection of set translations:

$$A \ominus B = \bigcap_{b \in B} (A)_{-b} \tag{1.4}$$

The erosion operation takes the minimum of a set of differences. The erosion operation removes noise and small objects.

2.3.1.3 Morphological gradient

Morphological gradients are the operators enhancing variations of pixel intensity in a neighborhood determined by a structuring element (Soille, 2003). A morphological gradient operation is performed in the image to highlight the boundaries of objects. The basic morphological gradient ρ is called Beucher gradient (Rivest et al., 1993) and is defined as the arithmetic difference between the dilation and erosion of the original image by the structuring element B:

$$\rho_B = \delta_B - \varepsilon_B$$

where δ_B and ε_B are respectively the dilation and erosion of the image with structuring element B. In continuous case, ρ is defined as:

$$\rho_B = \lim_{\lambda \to 0} \frac{\delta_{\lambda B} - \varepsilon_{\lambda B}}{2\lambda}$$

where $\delta_{\lambda B}$ and $\varepsilon_{\lambda B}$ are respectively the dilation and erosion of the image with circular structuring element B with radius λ. This is equivalent to the norm of the gradient vector of the image:

$$\rho(f) = \|\nabla f\|, \quad \nabla f = \left(\frac{\partial f}{\partial x}, \frac{\partial f}{\partial y}\right)$$

2.3.1.4 Morphological opening

Morphological opening γ is defined as the erosion operation of image *f* by a structuring element *B* followed by the dilation operation with the structure element $\check{B}$:

$$\gamma_B(f) = \delta_{\check{B}}[\varepsilon_B(f)]$$

where $\delta_{\check{B}}$ is the dilation with the reflected structural element $\check{B}$ and ε_B is the erosion with structural element *B*. The opening operation is the union of all sets containing the structuring element *B* in the original image *A*:

$$\gamma_B(A) = \bigcup_a \{B_a | B_a \subseteq A\}$$

The opening operation smoothes the contour, breaks narrow isthmuses, and eliminates small islands and sharp peaks or capes (Haralick et al., 1987). The opening operation is an idempotent operator, and thus applying it more than once produces no further effect.

2.3.1.5 Morphological closing

Morphological closing φ is defined as the dilation operation of image *f* by a structuring element *B* followed by the erosion operation with the structure element $\check{B}$:

$$\varphi_B(f) = \varepsilon_{\check{B}}[\delta_B(f)]$$

where ε_B is the erosion with the reflected structural element $\check{B}$ and $\delta_{\check{B}}$ is the dilation with the structural element *B*. The closing operation is the intersection of all complement sets containing the structuring element *B* in the original image *A*:

$$\varphi_B(A) = \bigcap_a \{B_a^C | A \subseteq B_a^C\}$$

The closing operation smoothes the contours, fuses narrow breaks and long thin gulfs, eliminates small holes, and fills gaps on the contours (Haralick et al., 1987).

2.3.1.6 Top-hat operator

The top-hat operator *TH* is usually implemented by first applying the opening operator γ to the original image *f*, then subtracting the result from the original image:

$$TH(f) = f - \gamma(f)$$

This kind of top-hat operator is also called white top-hat because the grey scale values of such top-hat operator are always greater than or equal to zero. A top-hat operator identifies the brightest peaks in the image.

2.3.1.7 Hit or miss operator

Let B_{FG} be the set of pixels matching the foreground and B_{BG} be the set of pixels matching the background of the image *A*. The hit or miss operator *HMO* of *A* by a composite structuring element B = (B_{FG} ,B_{BG}) is defined as the set of points *a,* such that when the origin of B coincides with *a*, B_{FG} fits A while B_{BG} fits A^C:

$$HMO_B(A) = \{a|(B_{FG})_a \subseteq A, (B_{BG})_a \subseteq A^C\}$$

The hit-or-miss operator is implemented as the intersection of an erosion operation with B_{FG} structuring element to the original image *f* and an erosion operation to the complement of the original image with a B_{BG} structuring element:

$$HMO_B(f) = \varepsilon_{B_{FG}}(f) \cap \varepsilon_{B_{BG}}(f^C)$$

2.3.1.8 Morphological Thinning

The thinning operator A O B is implemented by first applying a hit or miss operator to the original image A with composite structuring elements *B*, and then subtracting the result from the original image (Theo, 1982):

$$A \text{ O } B = A - HMO_B(A)$$

Sequential iteration of thinning generates a medial axis or skeleton of the input set.

2.3.1.9 Pruning

The pruning operation iteratively removes the end points of an image until only pixels with 2 or more neighbors remains, so that all the skeleton branches are removed or shortened, leaving only the closed paths. Pruning with a structure element *B* of a given size *n* consists in removing *n* pixels of each branch of the skeleton in the image *A*, starting from each end point:

$$PRUNE^{(n)}(A) = (A \circ B)^{(n)}$$

A thinning and pruning operation removes the lidar returns coming from electric wires, poles and other noises in urban areas and only the closed skeleton of the tree crowns remain.

2.3.1.10 Dual rank operator

Rank operators of rank *k* with a finite discrete window of arbitrary shape *B* sorts the pixel values falling within the window centered at the considered pixel in ascending order and selects the k^{th} value in the sorted array. Each rank operator has a corresponding dual with respect to complementation. The dual rank consists of two successive rank operators. The first rank operator is applied with given rank value and the second operator uses the complementary value. The rank value 1 results in morphological opening and the value of *n* results in morphological closing. Let *p* be a pixel, *R* be a rank operator for the given neighborhood and *r* be the rank value, then the dual rank operator *DF* is defined as:

$$DF(p,r) = R(p,r) \circ R(p,n-r)$$

The dual rank operator is described in Eckstein and Munkelt (1995) and Soille (2002).

2.3.1.11 Alternative sequential filter

When an image contains noisy structures over a wide range of scales, alternately closings and openings, a small structuring element is applied to start with and then proceeding with ever increasing structural elements until a given size is reached. This sequential application of open-close (or close-open) filters is called an alternate sequential filter (ASF). If γ_i be an opening and φ_i be the dual closing of size *I*, then following sequential combinations are all morphological filters:

$m_i = \gamma_i \varphi_i, \quad r_i = \varphi_i \gamma_i \varphi_i$

$n_i = \varphi_i \gamma_i, \quad s_i = \gamma_i \varphi_i \gamma_i,$

Then ASF of size *i* is defined as the sequential combination of one of these filters, starting the sequence with filter of size 1, and terminating it with filter of size *i:*

$M_i = m_i \ldots m_2 m_1, \quad R_i = r_i \ldots r_2 r_1$

$N_i = n_i \ldots n_2\, n_1, \quad S_i = s_i \ldots s_2\, s_1$

The alternative sequential filter is described by Soille (2003) and Zhang et al.(2003).

2.4 Tree-Finding Algorithm

Detecting individual trees involve indentifying the location of the tree-top and delineating the crown boundary. Locating trees using lidar can be done either using regularly interpolated surfaces (like canopy height models) or using lidar point clouds based on criteria like local-maxima and nearness of the points. Because it is easier to handle and process interpolated images than the point returns, a method based on the interpolated surface was used. The algorithm was developed in Interactive Data Language (IDL) version 6.4 (ITT Corporation, NY), Appendix A. The algorithm applies different morphological operators and a marker-based segmentation to separate trees from other urban non-tree structures and delineate the crown (Figure 2.2).

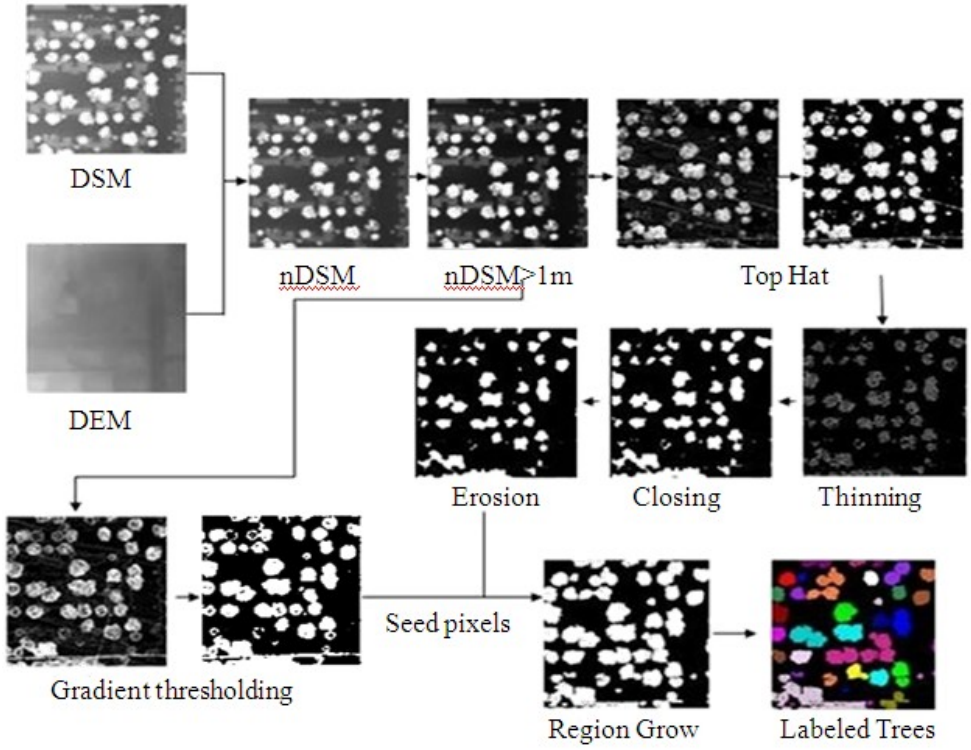

Figure 2.2. Detailed steps of the algorithm to detect individual trees. The digital surface model (DSM) was computed by interpolating all lidar returns, and the digital elevation model (DEM) was computed by interpolating all bare-earth returns of the lidar data.

A formal description of the algorithm is presented in the psuedocode below:

Algorithm: Individual tree detection using morphological operators and a marker-based segmentation

input: N, where N is an image array of dimension r rows and c columns, representing normalized surface (*nDSM*) obtained by subtracting lidar-derived digital surface model from bare-earth digital terrain model

1: **begin**

2: **if** $N_{i,j} \leq 2$ **then** $N_{i,j} := 0$ for $0 \leq i < r$ and $0 \leq j < c$

3: define S_i for $0 \leq i < 5$, where S is a circular structural element

4: $E := N \ominus S$

5: $T := N - [E \oplus \check{S}]$, where $\check{S}$ is the reflection of S

6: **if** $T_{i,j} \leq 3$ **then** $T_{i,j} := 0$ for $0 \leq i < r$ and $0 \leq j < c$

7: $H := T - \left[E \cap \left[T \ominus S^C\right]^C\right]$, where S^C is the complement of S

8: **for each** $y \in N_8(H_{i,j})$ **do**

9: **begin**

10: **if** y >2 **then** $H \leftarrow H \cup \{y\}$

11: **end**

12: define R_i for $(0 \leq i < 2)$, where R is a circular structural element

13: $C := [H \oplus R] \ominus \check{R}$, where $\check{S}$ is the reflection of S

14: $G := [N \oplus R] - [N \ominus R]$

15: **for each** $p \in C$ **do**

16: **begin**

17: $D_{i,j} := \min_k\{d(p, q_k) : (C(q_k) = 0) \wedge (1 \leq k)\}$, where $d(p,q_k)$ is distance transform function for $p = (x_1, x_2, ..x_i)$, and $q = (y_1, y_2, ..y_j)$, and k is all the pixels in the image

18: **end**

19: $W :=$ watershed (C,D), where W is morphological watershed segmented image of C with marker D

20: $R :=$ region_label (W), where R is region labelled image

21: return R

22: **End**

Algorithm: Individual tree detection using morphological operators and a marker-based segmentation

Definition of operators and variables

Variables		Operators	
N	nDSM image array	$\ominus$	Symmetric difference (here to denote erosion)
S, R	Structural element	$\oplus$	Direct sum (here to denote dilation)
$\check{S}, \check{R}$	Reflection of S, R	$\cap$	Intersection
S^C	Complement of S	$\cup$	Union
$d(p,q_k)$	Distance transform function	$\wedge$	Logical and
		$\in$	Element of

To do away with any complications arising from classifying lidar data using height-filtering algorithms in urban areas, the DEM delivered by the vendor (Tobin Aerial Surveys, Texas) was used. The DEM was evaluated by the vendor using ground control points and vertical accuracy within ± 15cm was reported. First, the elevation of each lidar point was subtracted from the digital elevation model (DEM) of the area to give the height from the ground surface. A 0.5 m x 0.5 m grid was overlaid on the lidar points and the grid cells were populated with the maximum height of the lidar point in each cell. This grid represents a normalized Digital Surface Model (nDSM). Pixel values in nDSM reflect the height of objects above ground instead of height above datum. Areas with less than 2m height are thresholded from the nDSM to remove small objects like shrubs, cars, etc. and to remove the errors due to filtering and subsequent interpolation during DEM generation.

A top-hat operator T with a structural element S of radius 5 pixels is applied to the nDSM to identify the peak heights. The top-hat operator is implemented by first applying the opening operator to the original nDSM, then subtracting the result from the original image. The top-hat image is then thresholded (>3m) to remove the building boundaries and some other non-tree objects. To remove the lidar returns coming from electric wires, poles and other noises, a thinning and pruning operation is performed after which only the closed skeleton of the tree crowns remain. The pruning operation removes pixels with single neighbors iteratively until

only pixels with 2 or more neighbors remains, so that all the skeleton branches are removed, and only the closed paths remains.

A dilation operation followed by erosion is performed on the thinned image to fill the pixels inside the skeleton. The closed image represents the approximate center of each tree crown, which is then used as a seed pixel or marker for segmentation of the crown.

2.5 Segmentation of Individual Tree Crowns

Morphological watershed segmentation is one of the efficient approaches for automatic segmentation of images, and has been used, in its different variations, for segmenting individual tree crowns (Chen et al., 2006; Kwak et al., 2007; Andersen, 2009). We used a marker-based watershed morphological segmentation to delineate the tree crowns. Morphological based segmentation groups the image around the regional minima of the image and the boundaries of the adjacent groupings are precisely located along the crest line of the gradient image (Soille, 2003). This kind of segmentation is called 'watershed segmentation'. If we invert an nDSM image, the tree-tops will represent the minima and the whole set of points of the crown surface whose steepest slope path reach the minima will make the 'catchment basin' associated with the particular minima. The 'watersheds' constitute the zone dividing the adjacent catchments or tree crowns, in our case. Watershed segmentation is described in detail by Soille (2003). If the regional minima R_{MIN} of the input image *f* are first set to minimum value h_{min}, the resulting image is denoted by *f':*

$$f'(x) = \begin{cases} h_{min}, if\ p\ \in R_{min}(f) \\ f(x), \quad \text{otherwise} \end{cases}$$

In nDSM, the direct computation of watershed segmentation produces over-segmentation due to the presence of spurious minima. The marker-based method uses a marker function to mark the relevant image objects (minima) and their background, and the corresponding markers are used as a set of minima to impose to the watershed segmentation function. We used the seed pixels from the centre of the crown extracted using morphological operations (section *1.3.2*) as the marker to perform the segmentation. A marker image f_m is defined as a two-state image containing markers of the object and the background of the segmentation function f_1 and defined as follows for pixels x (Soille, 2003):

$$f_m(x) = \begin{cases} 0, & \text{if } x \text{ belongs to a marker} \\ t_{max}, & \text{otherwise.} \end{cases}$$

Once the minima of f_1 has been imposed by an appropriate marker function f_m, the image is segmented by applying an watershed transformation.

An n-dimensional distance map, which consisted of the distance to the nearest background pixels from the markers, was computed and used to identify the tree centers with the largest distance values. This additional marker from the distance transformed image was used with markers from nDSM to segment the tree crown using marker-controlled watershed segmentation. Chen et al. (2006) used markers from a similar distance transformed image and found accuracy increased by up to 10%.

After segmentation, each tree crown was defined as a region and assigned a unique label using a region labelling procedure. For each crown region, maximum height, minimum height, crown area and the X, Y coordinates of the tree top were recorded.

2.6 Algorithm Validation

2.6.1 Lidar Data

Lidar data collected using an Optech ALTM 2050 lidar system in July 2004 over Tinker Air Force Base in central Oklahoma, USA (latitude: 35° 25' 35.43"N; longitude: 97° 24' 37.73"W) (Figure 2.3) were used for validation. The area represents a typical suburban residential area of United States with detached and row houses with trees, both broadleaves and conifers, growing along roads and in yards and parks. The base is around 20 km^2 (5000 acres) in area and has 472 buildings (TAFB, 2009), and is dominated by Eastern red cedar (*Juniperus virgiana*), Austrian pine (*Pinus nigra*), and Siberian elm (*Ulmus pumila*) (Otey, 2007).

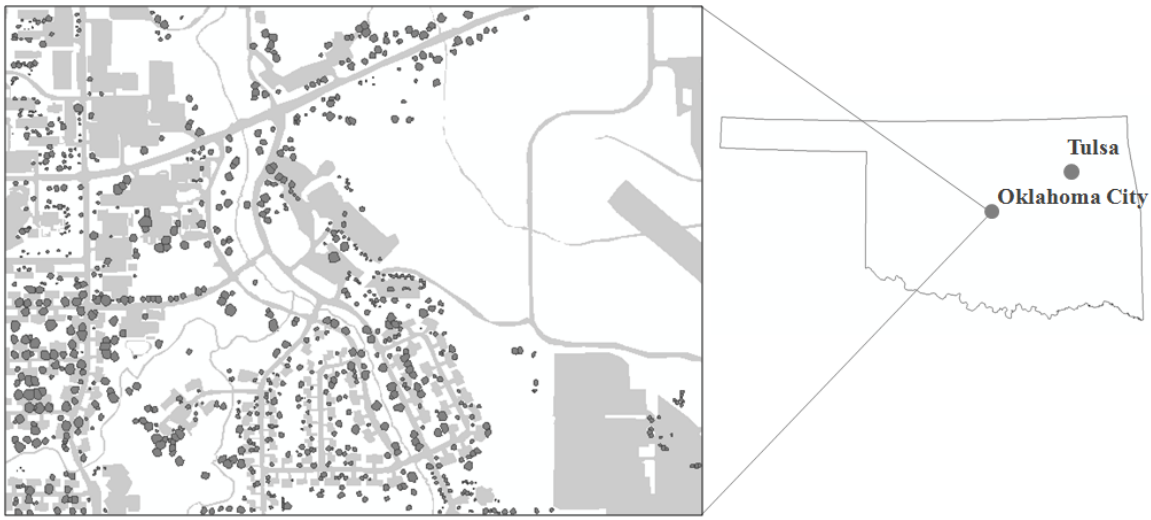

Figure 2.3. Study area at Tinker Air Force Base, Oklahoma. Trees measured in the field are shown in darker shades.

The system was flown at a 640 m flight height with a swath overlap of 40%. The pulse repetition frequency was 50 KHz and the scan frequency 45 Hz. The scan angle was less than 15 degrees. The Optech ALTM 2050 is a small-footprint multiple-return lidar system which uses a 1064 nanometer laser. There were about 8 returns per m^2.

2.6.2 Field Data

Base line data of the urban trees used for this study were collected in the summer of 2006. The coordinates of each individual tree were recorded using a GPS unit. A high resolution digital orthoimage was used in the field to verify the location of each tree. Various tree attributes were recorded including species, diameter at breast height, tree height, condition of tree, crown radius, age class, etc. (Otey, 2007). Height of the tree was measured to the nearest foot (0.3048m) using an Opti-Logic100 LH Laser Rangefinder Hypsometer. On windy days several measurements were taken and averaged. Crown radius was measured at two directions perpendicular to each other with a logger's tape to the nearest foot from the center of the trunk to the dripline of the canopy by using a nail to secure the tape to the trunk.

2.6.3 Accuracy Assessment

Four sample areas of size 200m x 200m were used to quantitatively assess the accuracy of the location and the crown size of the trees delineated by the algorithm (Figure 2.4). The sample areas were chosen such that they represented varied conditions and different mixtures of urban objects such as isolated and clumped trees of different sizes and large and small buildings. The sizes and distribution of trees within each sample area is shown in Table 2.1.

Table 2.1. Characteristics of field-measured trees within four sample areas

Sample Area	Number of trees*			Tree height (ft)			Crown radius (m)		
	I	O	B	Min	Mean	Max	Min	Mean	Max
1	34	13	4	10	28	47	1.4	5.6	9.6
2	25	15	34	11	36	72	1.2	5.1	10.7
3	11	111	6	9	44	79	0.7	6.5	15.9
4	27	21	23	4	17	34	0.7	2.6	5.3

*I = isolated, O = overlapping with other trees, B=overlapping with buildings/wires

Because of global positioning system (GPS) errors, spatial positions of the trees measured in the field using a GPS differed from the actual positions of the trees. This sometimes caused problems with matching automatically delineated trees with field measured trees. In some areas, not all the trees were measured during field inventory. To compensate for this, we also manually delineated the trees on the lidar data. All the returns with <1m surface height from the study area were eliminated, which resulted in the lidar returns from the trees and other above-ground urban objects such as buildings and wires. Tree crowns were then manually delineated in ArcGIS using the lidar returns and orthoimagery. Orthoimagery was obtained from 1:4500 scale color aerial photography acquired in February 17, 2004. Orthoimages consisted of 3 bands and the spatial resolution was 4 inches (10.2cm). A visual assessment was performed using both sets of reference trees – field measured and manually delineated - within the sample area.

Sample Area 1
(Isolated trees in open area with electric wires passing through)

Sample Area 2
(Trees adjacent to residential buildings)

Sample Area 3
(Large trees occurring in clumps and residential buildings)

Sample Area 4
(Small trees in the area of parking lot and large buildings)

Figure 2.4. Four sample areas used for accuracy assessment. Each sample is of 200mx200m size. Locations of trees measured during field survey are indicated with green dots.

In Sample Area 1, which was a fairly open space with mostly isolated trees and limited building edges, separating individual trees and buildings was achieved accurately but separating trees from electrical wire and removing bushes along the stream was a major challenge (Figure 2.5). However, the morphological thinning operation was able to remove most of the returns coming from the wire. Only when the wires were passing over the area of the tree crown, some pixels with returns from wires were mixed with those of crown thus increasing the area of crown (shown by red arrows in Figure 2.5d). Bushes along the stream were completely removed. Most

of the tall objects such as poles were removed (shown by red arrows in Figure 2.5c). But still a few non-tree objects were identified as trees (shown by red arrows in Figure 2.5d).

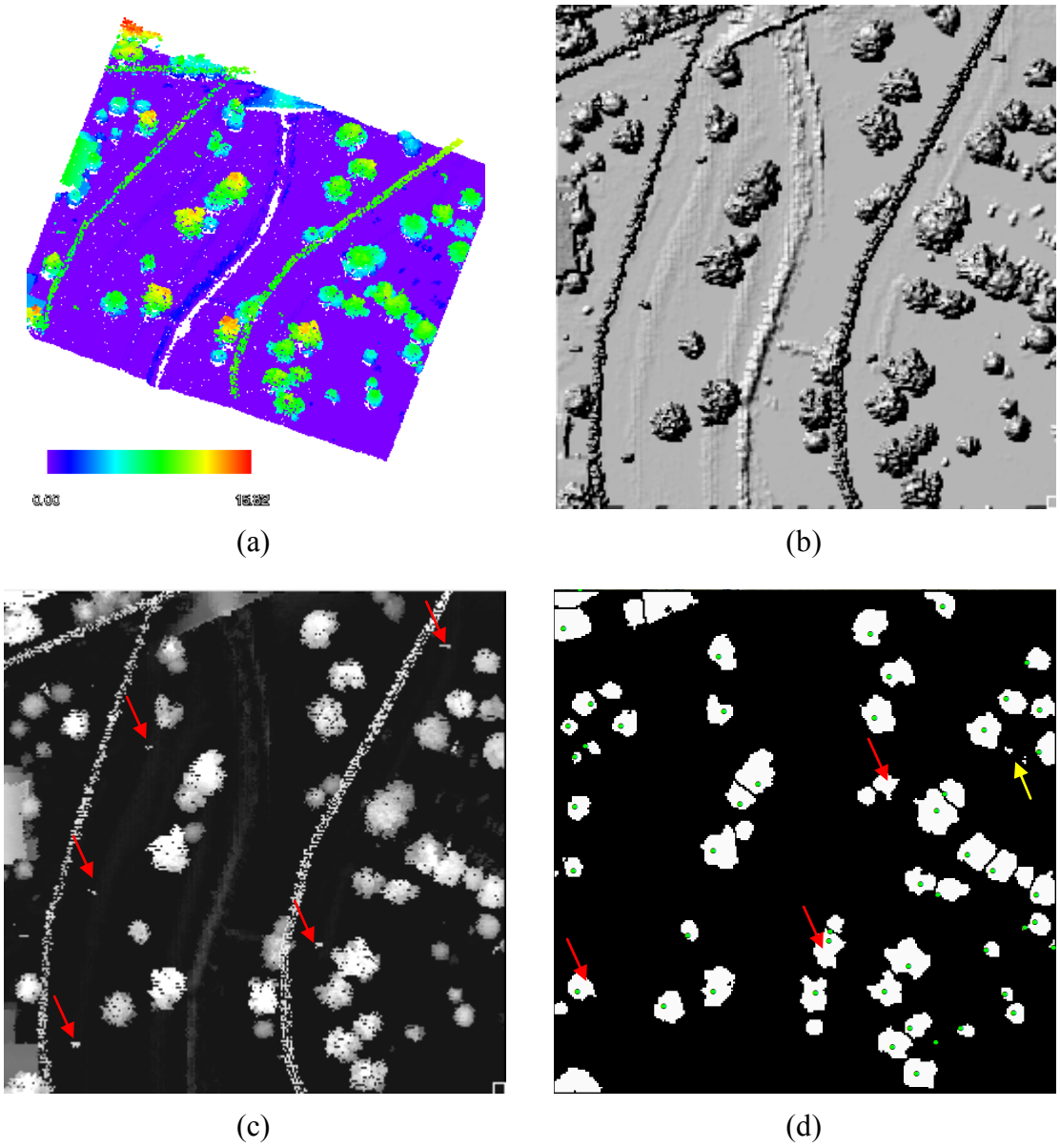

Figure 2.5. Individual tree detection in Sample Area 1. (a) Lidar point cloud. Color represents the height above ground. (b) Hillshade of nDSM. Note wire lines and a row of bushes along the stream (c) Grayscale representation of nDSM. Brighter pixels are taller in height. (d) Delineated individual trees. Locations of field-measured trees are indicated with green dots.

In Sample Area 2, which mainly consisted of isolated trees in the backyard of residential buildings and electrical wire lines passing through the area (Figure 2.6a and b), separation of buildings from the trees was achieved very well. There were a few problems when trees were

located beneath or adjacent to electric wires (shown by yellow arrows in Figure 2.6d). This was because a result of the processing carried out in the raster domain instead of in the point cloud itself. Also, there was a problem separating some of the trees occurring in clumps (shown by red arrows in Figure 2.6d). This effect is a common issue with lidar data in general when overlapping trees having no distinct tree tops.

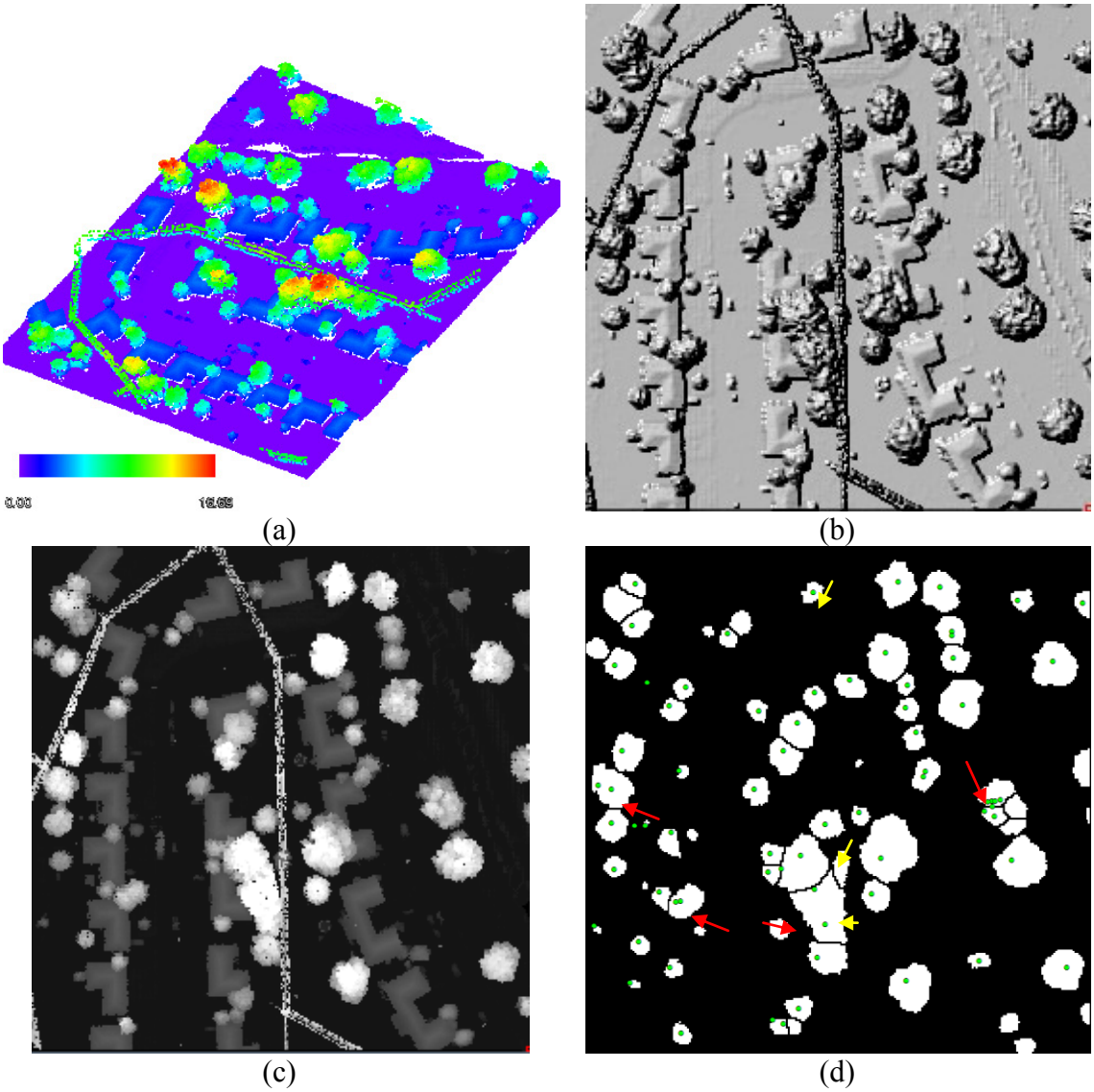

Figure 2.6. Individual tree detection in Sample Area 2. (a) Lidar point cloud. Color represents the height above ground. (b) Hillshade of nDSM. Note wire lines and a row of bushes along the stream (c) Grayscale representation of nDSM. Brighter pixels are taller in height. (d) Delineated individual trees. Locations of field-measured trees are indicated with green dots.

Sample area 3 is characterized by large trees up to 25m height and occurring in clusters with only a few isolated trees. There were few residential buildings and some distinct wall structures appearing in the nDSM (Figure 2.7a, b, c). While the morphological algorithm was able to remove the buildings and the walls, and segment most of the individual trees, there were still larger clumps where individual tree segmentation was not working as expected (shown by red arrows in Figure 2.7b).

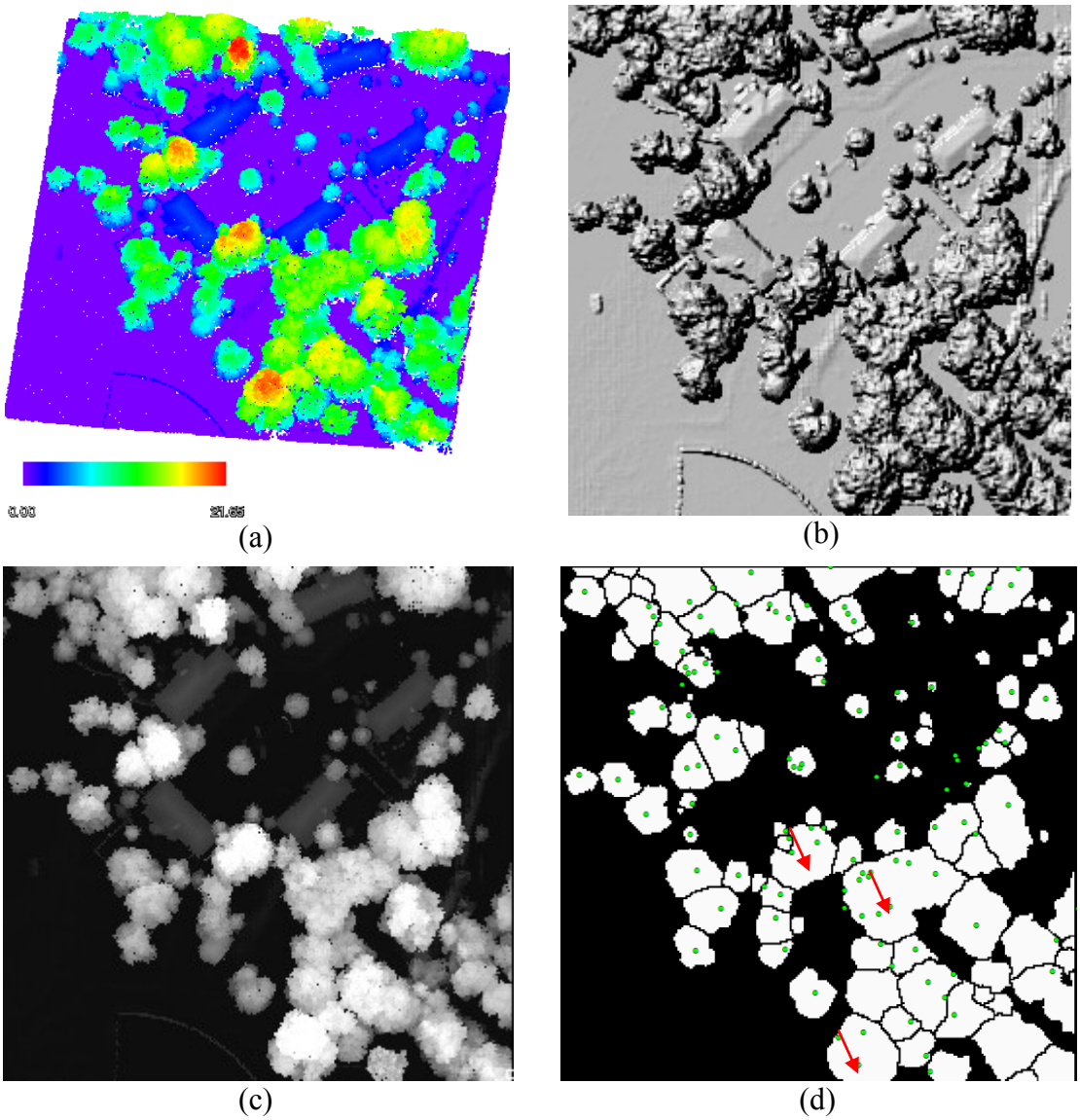

Figure 2.7. Individual tree detection in Sample Area 3. (a) Lidar point cloud. Color represents the height above ground. (b) Hillshade of nDSM. The area is mostly dominated by larger trees occurring in clumps. (c) Grayscale representation of nDSM. Brighter pixels are taller in height. (d) Delineated individual trees. Locations of field-measured trees are indicated with green dots.

In Sample area 4, (Figure 2.8a, b, c), the challenge was to remove the large buildings and cars in order to detect small trees. Small trees in the open parking lots with cars could not be detected (shown in lower left corner of Figure 2.8d). This was probably due to the time gap between the lidar data collection in 2004, when the trees were very small, and the field survey in 2006. Other problem areas were small trees very close to the buildings – these trees were not detected at all.

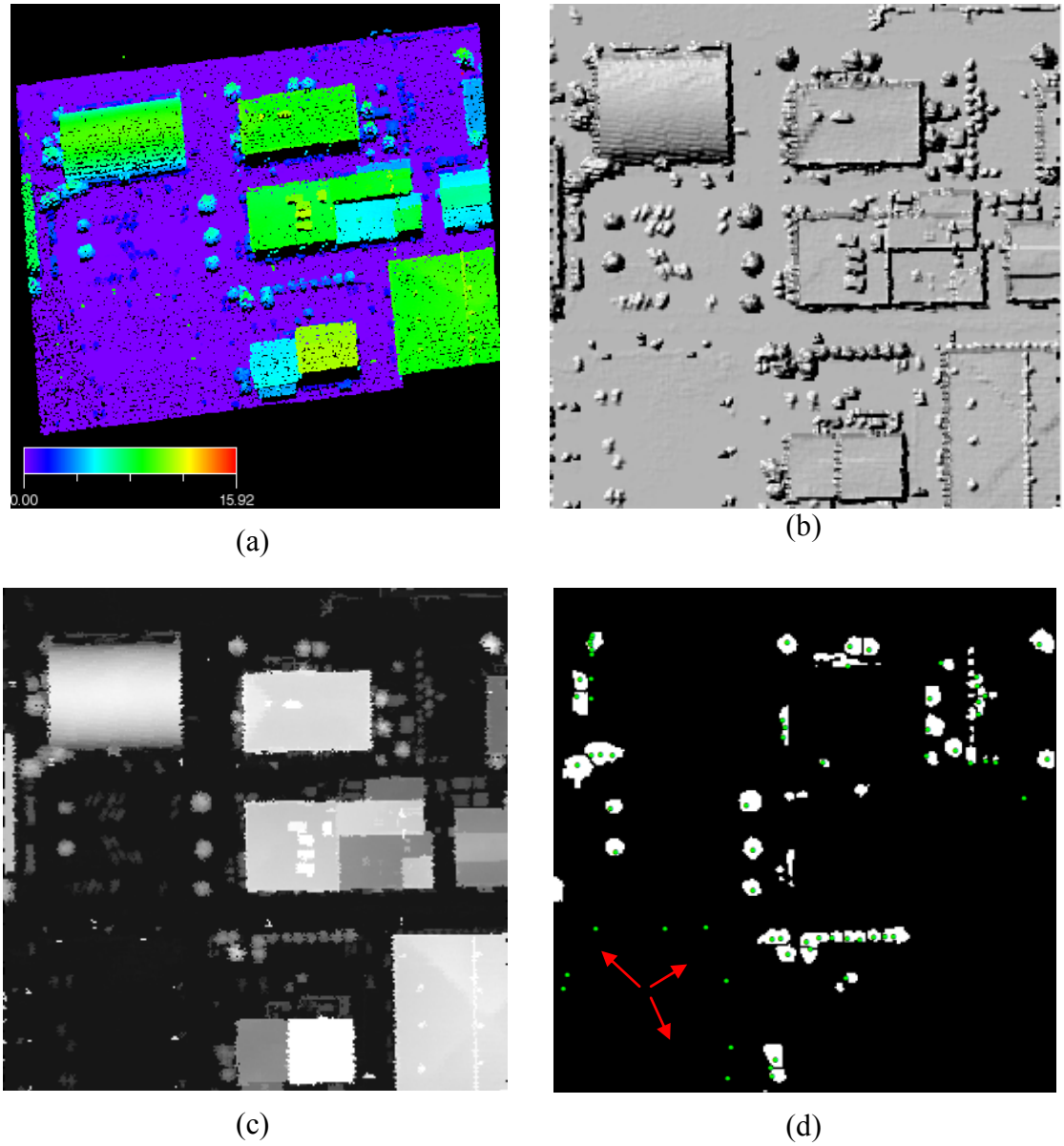

Figure 2.8. Individual tree detection in Sample Area 4. (a) Lidar point cloud. Color represents the height above ground. (b) Hillshade of nDSM. (c) Grayscale representation of nDSM. Brighter pixels are taller in height. (d) Delineated individual trees. Locations of field-measured trees are indicated with green dots.

The errors of automatic tree detection were assessed against field measured trees (Table 2.2). Both Type I and Type II errors were generally higher than expected although visual comparison of the results with the orthophoto and lidar data suggested the algorithm performed reasonably well. In some samples, the higher errors are merely due to not all the trees being measured during the field survey, and in others, as previously noted, smaller trees were too small to detect with lidar data collected two years before the field measurement. During the two year period between the lidar survey and field measurement, there were some significant changes – some of the trees were removed and some areas were reconstructed.

Table 2.2. Errors of automatically identified tree vs. field measured trees in 4 sample areas

Sample area	Total trees from field measurement	Total trees from automatic detection	Type I error (%)* (False positive)		Type II error (%)* (False negative)	
			A	*B*	*A*	*B*
1	51	66	27.27	25.76	3.03	3.92
2	74	76	19.74	17.11	15.79	2.70
3	118	107	35.51	33.64	40.19	7.63
4	71	61	14.08	27.87	36.62	16.90
Weighted Mean			**25.65**	**26.77**	**25.59**	**7.96**

**A* columns represent errors due to improper crown delineation, computed by one-to-one matching of field-measured trees with automatically detected trees. *B* columns represent errors due to improper tree detection, computed by matching field-measured with automatically detected tree area irrespective of one-to-one individual tree matching.

The total number of field measured trees in the samples is not much different from the total number of automatically detected trees (Table 2.2). Even if the Type II errors were generally higher for one-to-one matching error (Column *A*), the errors were much lower for Column *B,* which was computed irrespective of one-to-one individual tree matching. This indicates that the algorithm was able to detect most of the tree areas, even though it failed to properly delineate individual trees. If the algorithm were to be used for tree cover detection instead of individual trees, the error rate should be considerably lower.

In samples 1 and 2, which consisted of mostly individual trees in open areas, errors due to false positives were higher than error due to false negatives, meaning the algorithm was able to detect most of the trees. Relative to Sample 1, the higher false negatives in Sample 2 were mainly due to the algorithm not being able to find smaller trees that were beneath larger trees. Sample 3 had the highest Type I and Type II errors largely due to overlapping crowns of the

trees and the trees occurring in clumps. In Sample 4, the higher false negatives are mainly due to the two years between field data collection and the lidar flight.

The crown sizes of the detected trees were compared with the field-measured crown size. Because of GPS error, the locations of some field measured trees were slightly off the original trees; so only those trees whose locations were matched one-to-one with the field-measured trees and not lying across the sample boundary were considered (Figure 2.9). The crown area of field-measured trees was computed using the mean (*r)* of two field-measured crown radii as πr^2.

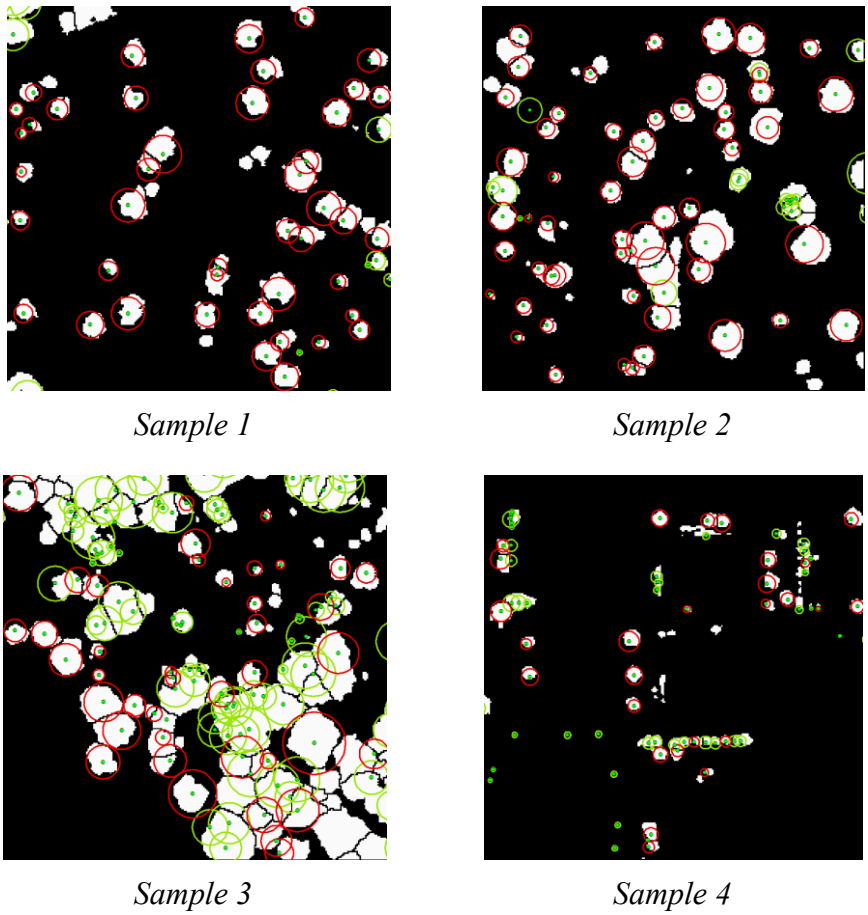

Sample 1 *Sample 2*

Sample 3 *Sample 4*

Figure 2.9. Trees considered for comparison of crown-sizes. White areas show the crowns of automatically delineated trees and circles show the crown area of field measured trees. Red circles were considered for the comparison and green circles were left out.

There was a good correlation (*R* varying between 0.82 and 0.92) between field measured crown area and automatically measured crown area (Figure 2.10). The best relationship between crown areas were obtained for isolated trees, such as for those in Sample 1 and 2, and the relationships were poor where the trees were difficult to detect, as in the case of Sample 3.

In general, the automatic delineation was underestimating the crown area. This underestimation may be due to several reasons. First, crown area of field-measured trees was computed as the area of a circle, which often is not representative of actual area of the trees, and crown area of automatically delineated trees as actual area. Secondly, increase in crown size during the two years between the lidar data collection and the field data collection may have contributed to the underestimation.

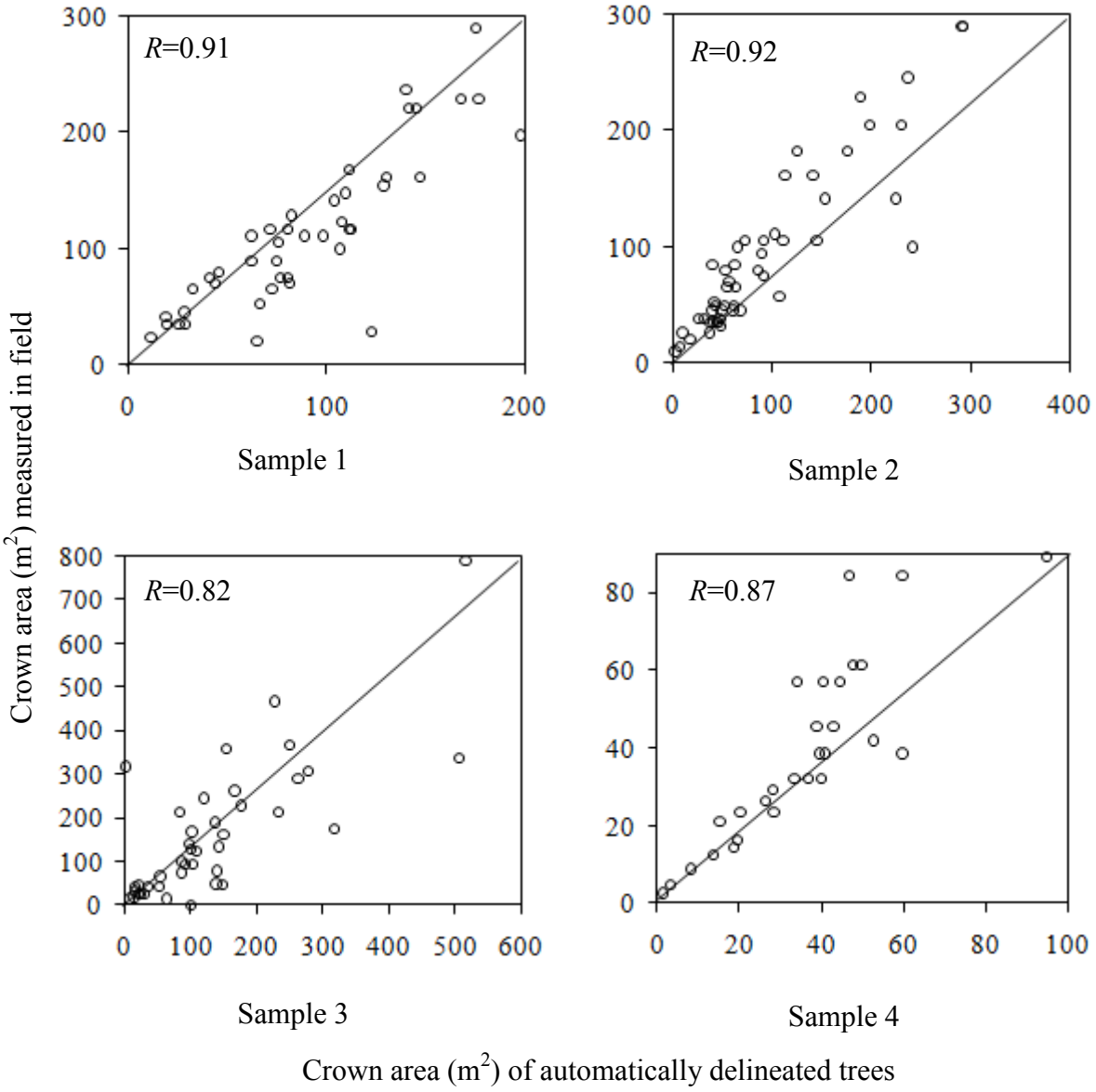

Figure 2.10. Relationship between crown area of automatically delineated trees and crown area of field measured trees in four sample areas. Field crown area were calculated using two radius measurements, perpendicular to each other, taken in the field.

2.7 Discussion

As far as the authors are aware, this study is one of the first studies to detect trees in an urban area at the individual tree level. There are few tree detection studies conducted in urban areas to compare the results from this study. One recent study by Chen and Zakhor (2009) used segmentation followed by classification using a random forests classifier to detect trees in urban areas in the USA and Europe, and obtained an accuracy over 95%. They were able to obtain higher accuracy in part because they were testing their results in areas both with and without trees, and not against individual trees. An earlier study by the same group (Secord and Zakhor, 2007) used a similar approach of segmentation followed by classification but also used hue, saturation and brightness values from a high-resolution orthoimage in addition to the lidar data to perform support vector machine based classification and achieved a high accuracy for tree cover. Chen and Zakhor (2009) indicated most of their errors were coming from noises along the building edges, along which they were finding too-much segmentation, which our marker-based segmentation approach was able to clearly filter out. Nevertheless, it should be noted that their test data sets were from areas where there were high variation in roof structures while the present study used mostly areas with far less heterogeneity.

The accuracy from our study was comparable or better than other studies of individual tree detection in forested areas. Chen et al. (2006) used variable window local maxima coupled with marker-based segmentation approach to isolate individual trees in open wood savanna in California, and obtained an absolute accuracy of 64.1%. As with the case of the present study, they also found separating trees difficult when the crowns are intertwined or when smaller trees are growing close to larger trees. Chen et al. (2006)'s approach also suffered from over-segmentation of larger trees resulting in a higher commission errors. In contrast, in our study, we noticed a higher omission error due to under-segmentation of larger trees. This must be due to the selection method for the markers for segmentation, which resulted in larger markers than Chen et al. (2006)'s method who used smaller marker using mainly local maxima and centre of the crown.

Kwak et al. (2007) used morphological segmentation with transformation distance to detect individual trees in coniferous and deciduous forests in Korea, and correctly detected 74.1% of the trees. They found conifers with a distinct cone shaped crown were better segmented

than deciduous trees with not much slope difference between the tree tops and the crown edges. Similar to their observation, we also found more difficulty in separating deciduous trees occurring in clumps (Sample Area 3).

Koch et al. (2006) used classical watershed segmentation. 61.7% of the trees in deciduous and mixed temperate forests were correctly delineated compared to photogrammetrically-delineated reference crowns. They also observed a better delineation of dominant conifers compared to the deciduous trees, where they found, similar to our observation, a high commission error due to merging of adjacent crown segments.

Two problem areas were distinctly noticeable where the morphological algorithm failed to detect individual trees – when smaller trees are occurring beneath the crown area of larger trees and when tree crowns are overlapping with no distinct tops. The first problem has to do with the issue of lidar data itself rather than the algorithm. At the given point density, lidar was not able to penetrate the denser crown and record the returns from smaller trees underneath, and when it was able to penetrate, because tree tops of smaller trees were overlapping with crowns of overstory trees, it was very difficult to separate those trees.

Detecting smaller trees underneath larger trees is one of the ubiquitous problems of tree detection using lidar for most of the currently available algorithms (Koch et al., 2006; Kaartinen et al., 2008). A very high density lidar dataset should be able to get more returns of the smaller trees underneath larger trees, but this may be only useful to a certain extent using presently available methods. Using a clustering approach (e.g., using mean-shift segmentation (Melzer, 2008)) in the lidar point data itself rather than using an interpolated raster nDSM is one area that can be explored in the future to improve detection of smaller trees that are underneath the larger trees. Wang et al. (2008) were able to detect sub-canopy trees in a spruce beech forest using statistical distribution and voxel analysis of lidar point clouds within a 3D single tree model. Their approach merits investigation for trees in urban landscapes. In areas, where trees are occurring in clumps, first identifying the tree clumps instead of individual trees using the morphological approach, and then applying other individual tree detection algorithms within the tree clump areas (e.g., using local maxima with variable moving window (Popescu and Wynne, 2004)) should improve the accuracy of tree detection. Zhang et al. (2009) have found grey-level concurrence matrix (GLCM) texture to perform better than grey-level texture for detection of

buildings. Because GLCM texture considers both height and position of pixel, the resulting features have more information about the surface. If the grey-level texture used in our study were replaced with GLCM texture, it has strong potential to yield similar results.

2.8 Conclusions

We have presented an automatic workflow that takes advantage of image morphological methods for detecting individual trees in the urban area using small-footprint airborne imaging lidar. This makes it possible to use lidar data for regular inventory of individual urban trees and for estimating urban tree cover. In the current stage, the algorithm, while performing well in removing the non-tree objects like buildings, electric wires, etc. and identifying isolated trees, still needs improvement in separating individual trees when trees occur in clumps. While the morphological method described in this paper was evaluated for detecting individual trees using a test area of a typical suburb with fairly homogeneous buildings, in future, it should also be tested with data from other urban areas with more heterogeneity, for example with more variation in roof structures.

Morphological based image processing methods can be sensitive to the size and shape of the structural elements. A detailed study of those parameters is necessary. There are other recent variants of the watershed segmentation approach (e.g., Rambabu and Chakrabarti, 2007) which might be superior to marker-based watershed segmentation for lidar-based tree detection. Future studies to compare performance of a combination of different morphological-based methods in similar vein to Forzieri et al. (2009) are recommended.

2.9 Literature Cited

Andersen, H., Reuterbuch, S.E. and Schreuder, G.F., 2001. Automated individual tree measurement through morphological analysis of a LiDAR-based canopy surface model, Proceedings of 1st International Precision Forestry Symposium. University of Washington, Seattle, WA, pp. 11-22.

Andersen, H.E., 2009. Using Airborne Light Detection and Ranging (LIDAR) to Characterize Forest Stand Condition on the Kenai Peninsula of Alaska. Western Journal of Applied Forestry, 24: 95-102.

Bortolot, Z.J. and Wynne, R.H., 2005. Estimating forest biomass using small footprint LiDAR data: An individual tree-based approach that incorporates training data. ISPRS Journal of Photogrammetry and Remote Sensing, 59(6): 342-360.

Brandtberg, T. and Walter, F., 1998. Automated delineation of individual tree crowns in high spatial resolution aerial images by multiple-scale analysis. Machine Vision and Applications, 11(2): 64-73.

Chen, G. and Zakhor, A., 2009. 2D tree detection in large urban landscapes using aerial lidar data, IEEE International Conference on Image Processing (ICIP), Cairo, Egypt.

Chen, L., Chiang, T. and Teo, T., 2005. Fusion of LIDAR data and high resolution images for forest canopy modelling, Proc. 26th Asian Conference on Remote Sensing, Hanoi, Vietnam.

Chen, L.C., Teo, T.A., Shao, Y.C., Lai, Y.C. and Rau, J.Y., 2004. Fusion of LIDAR data and optical imagery for building modeling. International Archives of Photogrammetry and Remote Sensing, 35(B4): 732-737.

Chen, Q., Baldocchi, D., Gong, P. and Kelly, M., 2006. Isolating individual trees in a Savanna woodland using small footprint lidar data. Photogrammetric Engineering & Remote Sensing, 72(8): 923-932.

Cho, W., Jwa, Y., Chang, H. and Lee, S., 2004. Pseudo-grid based building extraction using airborne LIDAR data. International Archives of Photogrammetry and Remote Sensing, 35(B3): 378-381.

Culvenor, D.S., 2002. TIDA: an algorithm for the delineation of tree crowns in high spatial resolution remotely sensed imagery. Computers & Geosciences, 28(1): 33-44.

Dralle, K. and Rudemo, M., 1997. Automatic estimation of individual tree positions from aerial photos. Canadian Journal of Forest Research, 27: 1728-1736.

Eckstein, W. and Munkelt, O., 1995. Extracting objects from digital terrain models, Remote Sensing and Reconstruction for Three-Dimensional Objects and Scenes, SPIE, pp. 43-51.

Eriksson, M., Perrin, G., Descombes, X. and Zerubia, J., 2006. A comparative study of three methods for identifying individual tree crowns in aerial images covering different types of forests, Proceedings International Society for Photogrammetry and Remote Sensing (ISPRS), Marne La Vallee, France.

Falkowski, M.J.S., Alistair M.S. , Hudak, A.T.H., Gessler, P.E., Vierling, L.A. and Crookston, N.L., 2007. Automated estimation of individual conifer tree height and crown diameter via two-dimensional spatial wavelet analysis of lidar data. Canadian Journal of Remote Sensing, 32(2): 153-161.

Filin, S., 2002. Surface clustering from airborne laser scanning data. International Archives of Photogrammetry Remote Sensing and Spatial Information Sciences, 34(3/A): 119-124.

Forzieri, G., Guarnieri, L., Vivoni, E.R., Castelli, F. and Preti, F., 2009. Multiple attribute decision making for individual tree detection using high-resolution laser scanning. Forest Ecology and Management, 258(11): 2501-2510.

Gonzalez, R. and Woods, R., 2002. Digital image processing. Prentice-Hall, Englewood Cliffs, NJ.

Gougeon, F.A., 1995. A crown-following approach to the automatic delineation of individual tree crowns in high spatial resolution aerial images. Canadian Journal of Remote Sensing, 21(3).

Gruen, A., Baltsavias, E.P. and Henricsson, O., 1998. Automatic extraction of man-made objects from aerial and space images (II). Birkhauser Boston.

Guan, H., Deng, F. and Zhang, J., 2007. Building detection from LIDAR and images in urban areas, MIPPR 2007: Pattern Recognition and Computer Vision. SPIE, Wuhan, China, pp. 67880V-6.

Haralick, R., Sternberg, S. and Zhuang, X., 1987. Image analysis using mathematical morphology. IEEE Transactions on Pattern Analysis and Machine Intelligence, 9(4): 532-550.

Hecht, R., Meinel, G. and Buchroithner, M.F., 2008. Estimation of urban green volume based on single-pulse LiDAR data. IEEE Transactions on Geoscience and Remote Sensing, 46(11): 3832-3840.

Hyyppa, J., Matikainen, L., Kaartinen, H., Xiaowei, Y., Hyyppa, H. and Ronnholm, P., 2007. Improving automation in map updating based on national laser scanning, classification trees, object-based change detection and 3D object reconstruction, Urban Remote Sensing Joint Event, 2007, pp. 1-10.

Hyyppä, J., Mielonen, T., Hyyppä, H., Maltamo, M., Yu, X., Honkavaara, E. and Kaartinen, H., 2005. Using individual tree crown approach for forest volume extraction with aerial images and laser point clouds, Proceedings of ISPRS Workshop Laser Scanning, pp. 144-149.

Imai, Y., M., S., Y., Y. and N, F., 2004. Tree-height measuring characteristics of urban forests, Proceedings of XXth ISPRS Congress 'Geo-Imagery Bridging Continents', Commission VII, 12-23 July 2004, Istanbul, Turkey.

Kaartinen, H. and Hyyppä, J., 2008. EuroSDR-Project Commission 2 ‘‘Tree Extraction’’, Final Report, EuroSDR-European Spatial Data Research, Official Publication.

Kaartinen, H., Hyyppä, J., Liang, X., Litkey, P., Kukko, A., Yu, X., Hyyppä, H. and Holopainen, M., 2008. Accuracy of automatic tree extraction using airborne laser scanner data, SilviLaser, Edinburgh, UK.

Kilian, J., Haala, N. and Englich, M., 1996. Capture and evaluation of airborne laser scanner data. International Archives of Photogrammetry and Remote Sensing, 31: 383-388.

Koch, B., Heyder, U. and Weinacker, H., 2006. Detection of individual tree crowns in airborne lidar data. Photogrammetric Engineering & Remote Sensing, 72(4): 357-363.

Kwak, D.-A., Lee, W.-K., Lee, J.-H., Biging, G. and Gong, P., 2007. Detection of individual trees and estimation of tree height using LiDAR data. Journal of Forest Research, 12(6): 425-434.

Leckie, D., Gougeon, F., Hill, D., Quinn, R., Armstrong, L. and Shreenan, R., 2003. Combined high-density lidar and multispectral imagery for individual tree crown analysis. Canadian Journal of Remote Sensing, 29(5): 633-649.

Liu, J., Li, D., Qin, X. and Yang, J., 2006. Automatic extraction of tree crowns from aerial imagery in urban environment, Geoinformatics 2006: Remotely Sensed Data and Information. SPIE, pp. 64190G-5.

Lohmann, P., Koch, A. and Schaeffer, M., 2000. Approaches to the filtering of laser scanner data. International Archives of Photogrammetry and Remote Sensing, 33(B3/1; PART 3): 540-547.

Mayer, H., 1999. Automatic Object Extraction from Aerial Imagery-A Survey Focusing on Buildings. Computer Vision and Image Understanding, 74: 138-149.

Meinel, G. and Hecht, R., 2004. Urban vegetation volume on the basis of laser-scan data at non-leaf aerial flight times. In: M. Thies, B. Koch, H. Spiecker and H. Weinacker (Editors), ISPRS Working Group VIII/2 Laser-Scanners Forest and Landscape Assessment, Vol. XXXVI, No. 8/W2, 03-06 October 2004, Freiburg, Germany, pp. 334-339.

Melzer, T., 2008. Non-parametric segmentation of ALS point clouds using mean shift. Journal of Applied Geodesy, 1(3): 159-170.

Omasa, K., Hosoi, F., Uenishi, T., Shimizu, Y. and Akiyama, Y., 2008. Three-dimensional modeling of an urban park and trees by combined airborne and portable on-ground scanning LIDAR remote sensing. Environmental Modeling and Assessment, 13(4): 473-481.

Palenichka, R.M. and Zaremba, M.B., 2007. Multiscale isotropic matched filtering for individual tree detection in LiDAR images. IEEE Transactions on Geoscience and Remote Sensing, 45(12): 3944-3956.

Persson, A., Holmgren, J. and Soderman, U., 2002. Detecting and measuring individual trees using an airborne laser scanner. Photogrammetric Engineering & Remote Sensing, 68(9): 925-932.

Popescu, S.C. and Wynne, R.H., 2004. Seeing the trees in the forest: using lidar and multispectral data fusion with local filtering and variable window size for estimating tree height. Photogrammetric Engineering & Remote Sensing, 70(5): 589-604.

Rambabu, C. and Chakrabarti, I., 2007. An efficient immersion-based watershed transform method and its prototype architecture. Journal of System Architecture, 53(4): 210-226.

Rivest, J., Soille, P. and Beucher, S., 1993. Morphological gradients. Journal of Electronic Imaging, 2(04): 326-336.

Rottensteiner, F. and Briese, C., 2002. A new method for building extraction in urban areas from high-resolution LIDAR data. International Archives of Photogrammetry Remote Sensing and Spatial Information Sciences, 34(3/A): 295-301.

Schenk, T. and Csatho, B., 2002. Fusion of LIDAR data and aerial imagery for a more complete surface description. International Archives of Photogrammetry and Remote Sensing, 34(3A): 310-317.

Secord, J. and Zakhor, A., 2007. Tree detection in urban regions using aerial lidar and image data. IEEE Geoscience and Remote Sensing Letters, 4(2): 196-200.

Soille, P., 2002. On morphological operators based on rank filters. Pattern Recognition, 35(2): 527-535.

Soille, P., 2003. Morphological image analysis: principles and applications. Springer-Verlag New York, Inc. Secaucus, NJ, USA.

Sugumaran, R. and Voss, M., 2007. Object-oriented classification of LIDAR-fused hyperspectral imagery for tree species identification in an urban environment. In: M. Voss (Editor), Proceedings of 2007 Urban Remote Sensing Joint Event, 11-13 April 2007, Paris, France.

Theo, P., 1982. Algorithms for graphics and image processing. USA: Computer Science Press, Inc.

Wang, Y., Weinacker, H. and Koch, B., 2008. A lidar point cloud based procedure for vertical canopy structure analysis and 3D single tree modelling in forest. Sensors, 8(6): 3938-3951.

Weidner, U., 1997. Digital surface models for building extraction. Automatic Extraction of Man-Made Objects from Aerial and Space Images (II): 193-202.

Wulder, M., Niemann, K.O. and Goodenough, D.G., 2000. Local maximum filtering for the extraction of tree locations and basal area from high spatial resolution imagery. Remote Sensing of Environment, 73(1): 103-114.

Yu, X., Hyyppä, J., Kaartinen, H. and Maltamo, M., 2004. Automatic detection of harvested trees and determination of forest growth using airborne laser scanning. Remote Sensing of Environment, 90(4): 451-462.

Zhang, H., Zhang, Y., Liu, J. and Ji, S., 2009. Automatic building detection using airborne LIDAR data, Information Technology and Applications, 2009. IFITA '09. International Forum on, pp. 668-671.

Zhang, K., 2008. Identification of gaps in mangrove forests with airborne LIDAR. Remote Sensing of Environment, 112(5): 2309-2325.

Zhang, K., Shu-Ching, C., Whitman, D., Mei-Ling, S., Jianhua, Y. and Chengcui, Z., 2003. A progressive morphological filter for removing nonground measurements from airborne LIDAR data. IEEE Transactions on Geoscience and Remote Sensing, 41(4): 872-882.

Zhang, K. and Whitman, D., 2005. Comparison of three algorithms for filtering airborne lidar data. Photogrammetric Engineering & Remote Sensing, 71(3): 313-324.

Zhang, Y., 2001. Texture-integrated classification of urban treed areas in high-resolution color-infrared imagery. Photogrammetric Engineering & Remote Sensing, 67(12): 1359-1365.

3: DISCRIMINATING THE TAXONOMIC GROUP OF INDIVIDUAL TREES IN AN URBAN LANDSCAPE USING SMALL FOOTPRINT DISCRETE-RETURN IMAGING LIDAR

3.1 Abstract

This study examines the potential of using small-footprint discrete-return airborne lidar data for taxonomic classification of urban trees. Using various distribution metrics of lidar returns, random forests classification was performed to test the separability of different taxonomic classes (broadleaves/conifers, genera, and species) of individual trees in central Oklahoma, USA. A classification accuracy of 80.5% was obtained when separating trees only into broadleaf and conifer classes, 50.0% for genera, and 51.3% for species. Using spectral metrics from high-resolution satellite imagery in addition to lidar-derived predictors improved the classification accuracies by 10.4% (to 90.9%) for broadleaf and conifer, 8.4% (to 58.4%) for genera and 8.8% (to 60.1%) for species compared to using lidar metrics alone.

3.2 Introduction

Urbanization is occurring at an unprecedented rate both globally and locally. By 2050, the world's population is expected to increase by 3 billion and this growth will be primarily concentrated in urban areas (U.N., 2007). While urbanization often degrades the environment due to concentrated human activity, trees in urban areas improve environmental quality through carbon sequestration, and provide several social and economic benefits (McPherson et al., 1997; Tyrväinen et al., 2005; Nowak and Dwyer, 2007). Identification of species is important for planning and management of existing urban trees, due to the variability between species in recreation potential, carbon/biomass sequestration, and insect and disease susceptibility. Information about urban trees species is now an integral part of the urban planning process (Miller, 1996).

Traditionally classification of urban vegetation cover has relied upon multispectral and hyperspectral remote sensing methods (Wang, 1988; Friedl and Brodley, 1997; Zhang, 2001). However, most of these methods rely on using the vegetation reflectance to classify trees, which may not be effective due to difficulty in separating trees from other urban objects (Zhang, 2001).

With the capability of lidar systems to collect dense point clouds, there is now potential to exploit the vertical structural information for tree identification and taxonomic discrimination.

There are number of studies that have used fusion of lidar and spectral data for taxonomic classification of individual trees, however few investigate the ability of lidar data alone to discriminate species or broader taxonomic groups at the individual tree level. Douglas et al. (2003) classified the forest into mature hardwood, and mature and immature conifers using the density and intensity of lidar returns. Holmgren and Persson (2004) reported an accuracy of 95% for classification of Scots pine and Norway spruce using lidar based variables derived from highly dense lidar data (footprint size 0.26 m). Using the difference between the first and last pulse, Liang et al. (2007) classified forest under leaf-off condition into conifer and deciduous. Brandtberg (2007) classified individual trees in both leaf-on and leaf-off conditions using the directed graph approach. Moffiet et al. (2005) suggested the use of lidar metrics such as the proportion of 'singular' returns and the number of returns per crown has potential for discriminating taxonomic classes of individual trees. Based on lidar point-height and canopy height model based distributional parameters, van Aardt et al. (2008) were able to classify per-object lidar points into broad taxonomic classes in a study area located in the Virginia Piedmont. Hecht et al. (2008) used a fuzzy classifier on the relative lidar point density and normalized height to separate conifers, broadleaves and shrubs in urban areas.

In recent years, lidar data have been successfully used to identify and measure urban trees (Imai et al., 2004; Meinel and Hecht, 2004; Secord and Zakhor, 2007). But there are only a few studies that investigate the ability of lidar data to classify tree species in urban areas (Table 1.1).

Alpha shape, a notion of computational geometry, is the generalization of a convex hull of a finite set of points (Edelsbrunner and Mücke, 1994). Vauhkonen et al. (2009) used alpha shape metrics along with height, density, intensity and textural metrics for classifying pine, spruce, and deciduous trees in Scandinavia using a very dense lidar data (40 returns/m^2), resulting in an overall accuracy of 95%. Vauhkonen et al. were able to achieve a higher level of classification accuracy because they only considered mature trees which generally have distinct crown shapes, and were not classifying within the deciduous group. Hecht et al. (2008) used normalized height and lidar point density as an input to fuzzy classification, and were able to separate shrubs, conifers and deciduous trees. They used lidar point density as representative of

the density of branches to separate deciduous from conifers, and normalized height to separate undergrowth shrubs from trees. This approach, while useful to separate broad vegetation categories, may not be useful for classification at finer scale when vegetation classes tend to have similar density of branches or height. Sugumaran and Voss (2007) used lidar data to improve accuracies of multispectral and hyperspectral imagery to classify species. They found using lidar in addition to optical data improved the accuracy by 12-24%, with the highest increase among the low vegetation and shrubs where spectral mixing complicates separating species. They did not evaluate the performance of using lidar data alone and the classification accuracy was not assessed at the individual tree level.

Table 3.1. Overview of approaches using lidar for taxonomic classification of individual urban trees

Classification level	**Approaches**	**Data used**	**Accuracy obtained**	**Study Area**
Pine, spruce, and deciduous	Alpha shape metrics	TopEye Mark II ALS, 200m alt, Leaf-on	95%	Finland (Vauhkonen et al., 2009)
Shrubs, conifers, deciduous	Fuzzy classifier	Optech ALTM 1225, 1.1 points/m^2	-	Germany (Hecht et al., 2008)
Species level	Object-oriented classification, Fusion with hyperspectral	Leica ALS50, 1m nDSM		Iowa (Sugumaran and Voss, 2007)

Generally lidar-based studies assume that each tree species has a distinctive crown shape and structure and the lidar data are capable of representing these parameters. However, the shape characteristics of tree crowns are dependent upon various factors. For example, within the same species, the shape of the crown changes with age, the condition in which it grows, and the extent of human influence. Trees growing in the open are wider and bushier, and trees growing in a limited space become taller with a narrow crown. These effects tend to be more pronounced in

urban trees which often grow on compacted soil, are subjected to intense pruning, have little space in which to grow, are improperly staked, etc. (Duryea and Malavasi, 1995). Given that 90% of the total trees in urban areas in the US are on private property (Miller, 1996), the management and cultural practices, and hence the crown shape, of urban trees vary immensely. All of these factors affect the ability of the tree crown shape to help distinguish among urban tree species.

Fine-scale taxonomic classifications of individual trees in urban landscapes need to be further developed. The objective of this study was to examine the potential of distribution metrics derived from normalized height of point clouds of small-footprint discrete-return imaging lidar data for classifying individual urban trees (defined as vegetation 1m or greater in height) at different taxonomic levels. We also evaluate if combination of the lidar and high-resolution optical imagery improves the classification accuracy.

3.3 Methodology

3.3.1 Study Area

The study area is on Tinker Air Force Base in central Oklahoma, USA (latitude: 35° 25' 35.43"N; longitude: 97° 24' 37.73"W) (Figure 3.1). The area represents a typical suburban residential area of the United States with detached and row houses with trees, both broadleaves and conifers, growing along the road and in the yards and parks. The base is approximately 20 km^2 (5000 acres) and has 472 buildings (TAFB, 2009). There are about 6600 trees, the most common species being Eastern red cedar (*Juniperus virgiana*), Austrian pine (*Pinus nigra*) and Siberian elm (*Ulmus pumila*) (Otey, 2007).

3.3.2 Lidar Data

Lidar data were acquired using an Optech ALTM 2050 lidar system in July 2004 in leaf-on condition. The system specifications of lidar data are shown as Table 3.2. Optech ALTM 2050 is a small-footprint multiple-return lidar system which uses a 1064 nanometer laser. The provided lidar data did not have any return numbers. There were approximately 8 returns per m^2.

Figure 3.1. Study Area at Tinker Air Force Base, Oklahoma. Trees measured are shown in darker shades.

Table 3.2. System Specification of Optech ALTM 2050

Flying Altitude	640m
Scan Overlap	40%
Scan Frequency	45Hz
Scan Angle	15 deg
Pulse Repetition Frequency	50KHz

3.3.3 High-resolution Satellite Image

High-resolution satellite data of the area was obtained from the Quickbird satellite (DigitalGlobe Inc., USA) in May 17, 2005. The image was radiometrically corrected, sensor corrected, and geometrically corrected. The image consisted of a panchromatic image of 0.6m resolution and 4-band multispectral image of 2m resolution (Table 3.3).

Table 3.3. Spectral resolution of the Quickbird image

Panchromatic	450-900nm
Blue	450-520nm
Green	520-600nm
Red	630-690nm
Near Infrared	780-900nm

A comparison of the spatial resolutions of the pan- and multispectral Quickbird imagery with that of a digital orthoimage (1:4500 scale, pixel resolution 0.076m) is shown in Figure 3.2. While the lower resolution of the Quickbird imagery may be sufficient to individually identify larger trees, it poses restrictions on the ability to identify and classify smaller trees when used alone.

(a) (b) (c)

Figure 3.2. Trees as they appear at the original resolution of (a) orthoimagery, and (b) pan- (c) multi-spectral Quickbird imagery of the area

3.3.4 Field Data

Baseline data from the urban trees used for this study were collected in 2006. The coordinates of each individual tree were recorded using a GPS unit. A high resolution digital orthoimage was used in the field to verify the location of each tree. Various tree attributes were recorded including species, diameter at breast height (dbh), tree height, condition of tree, crown radius, age class, etc. (Otey, 2007). For this study, a total of 3562 trees, which includes 60 broadleaved species and 12 conifer species, were considered (Table 3.4). Most of the conifers are in lower height classes compared to broadleaves. Among broadleaves, *Platanus occidentalis* and *Acer saccharinum* have more trees in higher height classes while other species have more trees in lower and medium height classes. *Ulmus pumila, Acer saccharinum,* and *Platanus occidentalis* are among those having larger diameter and crown widths. Conifers generally had smaller dbh and crown size than broadleaves.

3.3.5 Crown Shapes

Crown characteristics and the tree silhouettes in the study area were compiled using USFS Fact Sheets available at www.hort.ufl.edu/trees. Of the 12 major trees in the study area, it

seems some of the trees can be distinctly discriminated using the shape of the crown alone, while other trees had similar shapes (Figure 3.3). Based on crown shapes the trees can be categorized into the following groups:

- Group 1 – *Juniperus virgiana*
- Group 2 – *Platanus occidentalis*
- Group 3 – *Pinus nigra*, *Fraxinus pennsylvannica*, *Ulmus parvifolia*, *Quercus shumardii*, *Acer saccharinum*
- Group 4 – *Pyrus calleryana*, *Ulmus pumila*

Crown characteristics (horizontal spread of the crown, the height, crown shape, uniformity, and density) of major tree species in the study area are shown in Table 3.5. It should be noted that crown shapes hold only for mature trees, while the crown shape, spread and tree height of young trees of different species may overlap and thus are difficult to discriminate. Even at maturity the same tree species can attain different crown shape and size depending on growth spaces and other factors such as light and moisture. The standard crown shapes are based on isolated trees growing in open spaces while trees (a) growing in dense clumps with other trees or (b) overlapping with buildings may have entirely different shapes. Crown density characteristics, which quantify the amount, compactness, or depth of foliage in a tree crown, should relate well to lidar density metrics and can be exploited to discriminate species. Use of lidar metrics based on the geometry and form of the tree crown should improve classification of species. Our assumption is that as the height distributions of the lidar canopy returns have a distinct shape and dispersion for each species (Figure 3.4), the lidar metrics from the individual tree will enable discrimination among individual tree species.

Table 3.4. Number of trees measured in the field by height class and crown size

Species	Total trees	Height class[3] (m)					Crown radius (m)			
		<6	6-9	9-12	12-15	>15	Mean	St.dev	Min	Max
Juniperus virginiana[1]	475	156	208	102	8	1	11.9	4.0	2.5	24.5
Pinus nigra[1]	461	143	223	77	16	2	11.7	3.7	3.5	25.0
Ulmus pumila[2]	387	12	73	111	110	81	23.3	7.4	0.0	47.0
Pyrus calleryana[2]	280	116	132	30	2	0	9.7	4.4	3.5	25.0
Platanus occidentalis[2]	212	4	9	23	37	139	24.9	7.3	7.0	44.0
Fraxinus pennsylvannica[2]	184	17	43	49	46	29	18.5	7.1	2.0	35.0
Ulmus parvifolia[2]	172	44	76	39	11	2	13.9	5.8	4.5	34.0
Acer saccharinum[2]	163	1	8	16	50	88	25.5	6.6	8.0	41.0
Quercus shumardii[2]	118	33	49	22	10	4	11.9	4.0	2.5	24.5
Others conifers (10 species)	182	60	96	21	5	0	9.7	3.1	3.5	23.0
Other broadleaves (53 species)	928	313	272	151	122	70	14.8	7.7	0.0	44.5

[1]Conifer [2]Broadleaves

[3]Height of the tree was measured to the nearest foot (0.3048m) using an Opti-Logic100 LH Laser Rangefinder Hypsometer

Juniperus virgiana
(columnar; oval; pyramidal)

Pinus nigra
(oval; pyramidal)

Platanus occidentalis
(round; spreading; pyramidal)

Ulmus pumila
(vase shape)

Pyrus calleryana
(pyramidal)

Acer saccharinum
(dense and spreading)

Ulmus parvifolia
(round; vase shape)

Quercus shumardii
(pyramidal and spreading)

Fraxinus pennsylvannica
(oval; upright)

Figure 3.3. Shapes of the major trees of the study area

(Source: http://hort.ufl.edu/database/trees/trees_scientific.shtml, used with permission of University of Florida)

Table 3.5. Characteristics of major tree species of the study area[#]

Species	Crown spread (feet)	Height (feet)	Crown Shape	Crown Uniformity*	Crown Density
Juniperus virgiana	10 - 20	40 - 50	columnar; oval; pyramidal	1	moderate
Pinus nigra	25 - 35	40 - 60	oval; pyramidal	1	moderate
Ulmus pumila	35 - 50	50 - 70	vase shape	2	moderate
Pyrus calleryana	25 - 35	35 - 45	pyramidal	1	moderate
Fraxinus pennsylvannica	45 - 50	60 - 70	oval; upright	1	moderate
Platanus occidentalis	50 - 70	75 - 90	round; spreading; pyramidal	1	dense
Quercus shumardii	40 - 50	55 - 80	oval; round	2	open
Ulmus parvifolia	35 - 50	40 - 50	round; vase shape	2	moderate
Acer saccharinum	40 - 60	60 - 80	vase shape	2	moderate

[#]Source: USFS Fact Sheets: www.hort.ufl.edu/trees

*1 - symmetrical canopy with a regular (or smooth) outline, and individuals have more or less identical crown forms

2 - irregular outline or silhouette

3.3.6 Analysis of Lidar Data

To avoid complications arising from classifying lidar data using height-filtering algorithms in urban areas, the DEM delivered by the vendor (Tobin Aerial Surveys, Texas) was used. The DEM was evaluated by the vendor using ground control points and vertical accuracy within ± 15cm was reported. A normalized digital surface model (nDSM) of the point clouds was computed by subtracting elevation of DEM from the elevation of lidar returns (Figure 3.5). All returns with <1m surface height were removed, which resulted in retaining only the lidar returns from trees and other urban objects. Each tree crown was then manually delineated. We opted for a manual approach to minimize errors associated with finding and delineating individual tree crowns, especially in this area, where tree crowns overlapped with other trees or with buildings in many instances. Only a few automated individual tree crown delineating algorithms have been

tested in urban landscapes (e.g., Palenichka and Zaremba, 2007), where conditions are different than forested environments. With the help of the nDSM point cloud and a color orthophoto (acquired February 17, 2004 with a spatial resolution of 10.2cm), only the trees with distinctly separable crowns were selected. Lidar points below the height of 1m were removed. The boundary of each crown was delineated by computing the planimetric convex hull around the lidar points within each tree in ArcGIS. Descriptive statistics for the distribution of lidar returns within each individual tree were computed (Table 3.6).

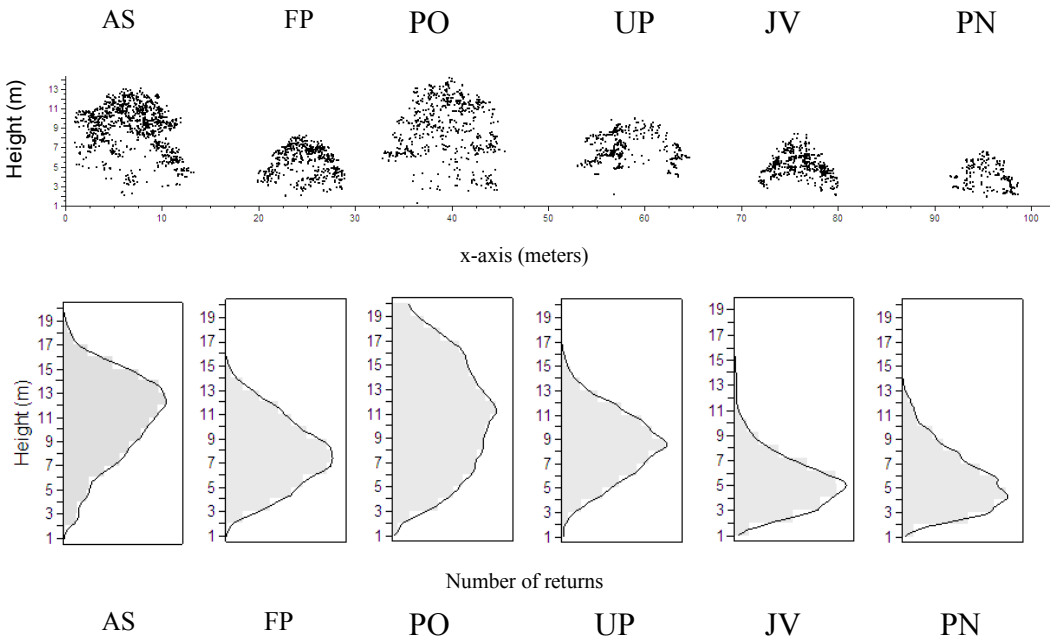

Figure 3.4. Distribution of lidar crown heights for six major species in the study area (AS=*Acer saccharinum*, FP=*Fraxinus pennsylvannica*, PO=*Platanus occidentalis*, UP= *Ulmus pumila*, JV=*Juniperus virginiana*, PN=*Pinus nigra*). The distributions of crown returns along the *x*-axis of an individual tree of the same species are shown in the histograms.

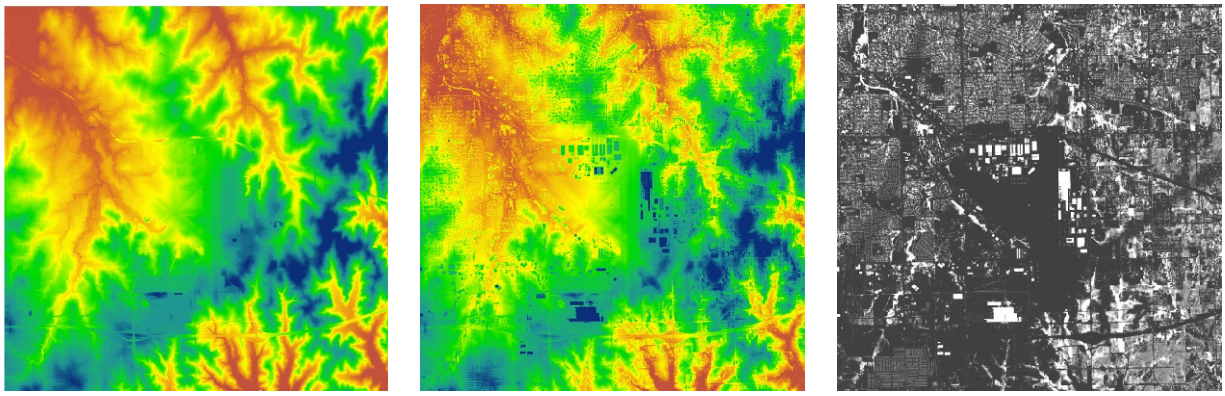

(a) (b) (c)

Figure 3.5. (a) Digital Elevation Model and (b) Digital Surface Model, (c) rasterized Normalized Digital Suface Model (nDSM) of the area

3.3.7 Random Forests

A random forests classification was performed for the lidar-based predictor variables (Table 3.6). In addition to the lidar-based predictors, different spectral variables from Quickbird imagery of the area were also computed for each individual tree, and used alone and in combination with lidar-based predictors for random forests classification. Individual tree boundaries were overlaid on the Quickbird imagery and derivative products (NDVI, SAVI and MSAVI) (Table 3.7), and basic statistics from each of the four bands and the derivative products were extracted for individual trees. NDVI enhances vegetation but is sensitive to optical properties of soil background, especially in areas with considerable soil-brightness variation. SAVI minimizes the effect of soil by introducing an adjustment factor to NDVI to account for first-order soil variation and differential red and near-infrared flux extinction through vegetation (Huete, 1988). Unlike NDVI, SAVI vegetation isolines do not converge to the origin and are independent of soil background (Baret and Guyot, 1991). The constant factor varies from 0 to infinity depending on the vegetation density. A factor of 0.5 was used for this study as it has been found optimal in a wide range of conditions. MSAVI replaces the constant factor of SAVI with an iterative self-adjusting factor.

Table 3.6. Candidate individual tree metrics used as a predictor variable

Height Distribution Statistics[1]	
H_{MEAN}	Mean height
H_{MODE}	Most frequent height of crown returns
H_{MIN}	Minimum height
H_{MAX}	Maximum height
H_R	Range of height ($H_{MAX} - H_{MIN}$)
H_{STD}	Standard deviation of height
H_{VAR}	Variance of height
H_{CV}	Coefficient of variation of height
H_{SE}	Standard error of mean of height
H_{KUR}	Kurtosis of height
H_{SKW}	Skewness of height
H_{QX}	x % Quantile of height (x = 5, 10, 25, 50, 75, 90, and 95)
Density Measures	
N_C	Number of crown returns
N_T	Number of total returns
N_P	Point density (N_C /N_T)
N_{CD}	N_C /C_A
N_{TD}	N_T /C_A
LPI	N_G(Number of total returns) / N_T
N_X	(Number of crown returns in x% of H_R)/ C_A (x = <20, 20-40, 40-60, 60-80, 80-90, >90)
Crown Dimension[2]	
C_A	Area of crown projected onto XY plane
C_p	Perimeter of crown projected onto XY plane

[1]Heights are lidar returns from tree crown. Only returns >1m in height were considered.

[2]Crown dimensions calculated by creating a convex hull around the planimetric projection of lidar returns from the tree crown

Table 3.7. Predictor variables computed from Quickbird imagery

$BandX_{MIN}$, $BandX_{MEAN}$, $BandX_{MAX}$, $BandX_{STD}$	Minimum, mean, maximum and standard deviation of spectral value of Band X, where X=1 to 4
$NDVI_{MIN}$, $NDVI_{MEAN}$, $NDVI_{MAX}$, $NDVI_{STD}$	Minimum, mean, maximum and standard deviation of normalized difference vegetation index (NDVI) computed as: $\frac{\text{Band 4} - \text{Band 3}}{\text{Band 4} + \text{Band 3}}$ (Rouse et al., 1974)
$SAVI_{MIN}$, $SAVI_{MEAN}$, $SAVI_{MAX}$, $SAVI_{STD}$	Minimum, mean, maximum and standard deviation of soil-adjusted vegetation index (SAVI) computed as: $\frac{(1+0.5)(\text{Band 4} - \text{Band 3})}{\text{Band 4} + \text{Band 3} + 0.5}$ (Huete, 1988)
$MSAVI_{MIN}$, $MSAVI_{MEAN}$, $MSAVI_{MAX}$, $MSAVI_{STD}$	Minimum, mean, maximum and standard deviation of modified soil-adjusted vegetation index (MSAVI) computed as: $\text{Band 4} + 0.5 - 0.5 * \left(\sqrt{(2 * \text{Band 4} + 1)^2 - 8 * (\text{Band 4} - \text{Band3})}\right)$ (Qi et al., 1994)

Variable importance was assessed using the Gini index (Breiman et al., 1984). When trees are grown using a minimum Gini impurity criterion, the impurity of two descendent nodes in a tree is less than the parents. Adding up the decrease in the Gini value for each variable over all the forest gives a variable importance that is often very consistent with the permutation importance measure. Random Forests™ version 1.0 software (Salford Systems, CA, USA) was used to perform the classification.

3.3.8 Classification Level

Individual trees were classified at three taxonomic levels – (1) conifers and broadleaves, (2) genera, and (3) species. Even though 3562 trees were measured, to ensure sufficient class representation, only those classes with more than 100 trees were considered. This resulted in 2452 trees for classification of species and 2874 trees for classification of genera, while all 3562 trees were considered for broadleaf/conifer classification. For broadleaf/conifer classification,

the broadleaf and conifer categories included 60 and 12 species, respectively (Table 3.4). There were 9 classes for species and 8 classes for genera (Table 3.8). The larger number of trees in the genera classification resulted from adding species which on their own could not qualify as a class for species classification due to the minimum 100 trees per class criterion.

Table 3.8. Total number of trees (*n*) considered for species and genera classification

Species classification		Genera classification	
Classes	*n*	Classes	*n*
Juniperus virginiana	475	*Pinus* (7 spp.)[1]	611
Pinus nigra	461	*Ulmus* (4 spp.)[2]	610
Ulmus pumila	387	*Juniperus* (1 spp.)[†]	475
Pyrus calleryana	280	*Quercus* (10 spp.)[3]	309
Platanus occidentalis	212	*Pyrus* (2 spp.)[4]	281
Fraxinus pennsylvannica	184	*Platanus* (1 spp.)[†]	212
Ulmus parvifolia	172	*Fraxinus* (2 spp.)[5]	189
Acer saccharinum	163	*Acer* (4 spp.)[6]	187
Quercus shumardii	118		

[1]*Pinus* included *P. echinata* (*n*=8), *P. elliottii* (*n*=33), *P. halepensis* (*n*=3), *P. nigra* (*n*=461), *P. sylvestris* (*n*=34), *P. taeda* (*n*=42), and *P. thunbergii* (*n*=30).

[2]*Ulmus* included *U. americana* (*n*=32), *U. crassifolia* (*n*=33), *U. parvifolia* (*n*=172), and *U. pumila* (*n*=387).

[3]*Quercus* included *Q. acutissima* (*n*=7), *Q. alba* (*n*=1), *Q. macrocarpa* (*n*=84), *Q. marilnadica* (*n*=27), *Q. muehlenbergii* (*n*=5), *Q. nigra* (*n*=2), *Q. palustris* (*n*=54), *Q. robur* (*n*=2), *Q. shumardii* (*n*=118), and *Q. virginiana* (*n*=9).

[4]*Pyrus* included *P. calleryana* (*n*=280), and *P. communis* (*n*=1).

[5]*Fraxinus* included *F. americana* (*n*=5), and *F. pennsylvannica* (*n*=184).

[6]*Acer* included *A. ginnala* (*n*=9), *A. negundo* (*n*=2), *A. rubrum* (*n*=7), *A. saccharinum* (*n*=163), and *A. saccharum* (*n*=6).

[†]*Juniperus* and *Platanus* included only one species *J. virginiana* and *P. occidentalis* respectively.

3.4 Results

The classification accuracy of broadleaf/conifer was 80.5%, genera 50.0% and species 51.3% (Table 3.9).

Table 3.9. Classification accuracies obtained using Random Forests at different taxonomy levels

Classification Level	Predictor Variables†	Accuracy
Broadleaf/Conifer		
Lidar only	H_{Q10}, H_{Q25}, C_P, H_{KUR}, H_{CV}, H_{Q50}	80.5%
Quickbird only	$Band4_{MEAN}$, $MSAVI_{MEAN}$, $MSAVI_{MIN}$, $Band4_{MAX}$, $NDVI_{MAX}$, $SAVI_{MAX}$	86.4%
Lidar + Quickbird	$MSAVI_{MEAN}$, $Band4_{MEAN}$, $MSAVI_{MIN}$, $Band4_{MAX}$, $NDVI_{MAX}$, H_{Q25}	90.9%
Genera		
Lidar only	H_{MEAN}, H_{Q50}, H_{Q75}, H_{VAR}, H_{Q25}, H_{Q50}, C_P	50.0%
Quickbird only	$MSAVI_{MEAN}$, $Band4_{MEAN}$, $NDVI_{MAX}$, $MSAVI_{MIN}$, $Band4_{MAX}$, $SAVI_{MAX}$	42.9%
Lidar + Quickbird	$MSAVI_{MEAN}$, $Band4_{MEAN}$, H_{Q50}, H_{MEAN}, $MSAVI_{MIN}$, N_C	58.4%
Species		
Lidar only	H_{Q25}, H_{Q50}, H_{MEAN}, H_{Q95}, H_{CV}, C_P	51.3%
Quickbird only	$MSAVI_{MEAN}$, $Band4_{MEAN}$, $Band4_{MAX}$, $MSAVI_{MIN}$, $NDVI_{MAX}$, $SAVI_{MAX}$	42.2%
Lidar + Quickbird	H_{Q25}, $MSAVI_{MEAN}$, $Band4_{MEAN}$, N_C, H_{Q90}, H_{MEAN}	60.1%

†Calculated using Gini index, important variables are to the left and less important variables to the right-side of the table

Using predictor variables based on Quickbird imagery only improved accuracies for the broadleaf/conifer classification. For genera and species classifications, the Quickbird-only variables performed worse than the lidar-only variables (Table 3.9). While spectral information from Quickbird imagery was useful in separating broadleaves and conifers, it was not very useful in discriminating genera and species of individual trees because of the documented need for improved spectral resolution for that task (e.g., van Aardt and Wynne, 2007; Banskota et al., in

press). However, using combined variables based on both lidar and Quickbird data increased the classification accuracy by as much as 10.4% for the broadleaf/conifer classification, 8.4% for the genera classification, and 8.8% for species classification (Table 3.9). It appears that shape and structure information from lidar and near-infrared information from Quickbird are complementary, and when combined enhances taxonomic discrimination potential of both sensors, resulting in higher accuracies. Producer's accuracies of broadleaves are noticeably higher than that of conifers while user's accuracies of conifers are higher than broadleaves (Table 3.10).

Among the predictor variables from Quickbird, $MSAVI_{MEAN}$ and $Band4_{MEAN}$ are consistently more important for classification at all three levels. MSAVI is the best performer among vegetation indices and, as expected, the near infrared band (Band 4) performed better at discriminating taxonomic classes. Different lidar-derived predictors were given different importance at different levels of classification.

Table 3.10. Classification results from Random Forests of broadleaves and conifers (actual vs predicted)

	Broadleaves	Conifers	Producer's accuracy
Lidar only			
Broadleaves	1911	533	**78.2%**
Conifers	162	956	**85.5%**
User's accuracy	**92.2%**	**64.3%**	Overall: 80.5%
Quickbird only			
Broadleaves	2092	352	**85.6%**
Conifers	131	987	**88.3%**
User's accuracy	**94.1%**	**73.7%**	Overall: 86.4%
Lidar + Quickbird			
Broadleaves	2214	230	**90.6%**
Conifers	94	1024	**91.6%**
User's accuracy	**95.9%**	**81.7%**	Overall: 90.90%

For classification of genera using variables based on lidar data only, *Fraxinus* and *Quercus* had the lowest accuracies (Table 3.11). This is probably because the crown shape of

Fraxinus does not stand out from that of *Acer* or *Ulmus* (Figure 3.3). The same is true with *Quercus,* whose shape is one of the most difficult to distinguish. *Quercus* has ten species within the genera (Table 3.8) with substantial variation in crown shape and structure; hence the low accuracy. *Pyrus, Platanus* and *Junipers* have very distinct crown shape, and as such lidar-derived variables were able to identify them with higher accuracies. It appears from the results of classification based on Quickbird-derived variables (Table 3.11) that *Quercus* and *Fraxinus* also have high spectral variance and hence low classification accuracy. Combining lidar and Quickbird-based variables improved the accuracy for most of the genera because having both the spectral and structural information improved separability. For example, while the pyramidal-shaped crown of *Quercus* may have been somewhat structurally similar to *Pinus,* these two genera, one being broadleaved and other being conifer, had different spectral characteristics (particularly in the near infrared).

As with the genera, *Fraxinus pennsylvannica* appears to be most difficult to discriminate both spectrally and structurally using variables from Quickbird, lidar and both combined (Table 3.12). *Pinus nigra* does not have a unique crown shape, as its crown shape tends to get confused with that of *Quercus shumardii* and *Juniper virginiana,* hence the low accuracy for the lidar only classification. However, *P. nigra* has distinct spectral characteristics that separate it clearly from other broadleaves; only *J. virginiana* has similar spectral properties. This explains the improved accuracy for *P. nigra* with Quickbird-based variables. For *Q. shumardii,* the lidar-only classification results in confusion with *P. nigra* and *Pyrus calleryana*, which contributes to the lower accuracy (45.8%). The classification based on Quickbird tends to get confused with *P. calleryana* and *Ulmus parviflora* but not with *P. nigra,* thereby further lowering the accuracy (29.7%). When lidar- and Quickbird-based variables are combined, the accuracy improves significantly to 62.7%. Combining lidar and Quickbird variables do not always increase the accuracy for all species, though. For example, *U. pumila*, which has a somewhat distinct vase-shaped crown, is best discriminated from other species using lidar data (55.0% accuracy), whereas Quickbird-based variables results in 30% accuracy due to similar spectral properties to *Acer saccharinum* and *U. parviflora*. Combing lidar with Quickbird resulted in amplification of the effect of similar crown shape and spectral characteristics with *F. pennsylvannica*, thus slightly diminishing resulting accuracy (42.2%).

Table 3.11. Genera classification results from Random Forests (actual vs predicted)

Genera[1]		*Ac*	*Fr*	*Ju*	*Pi*	*Pl*	*Py*	*Qu*	*Ul*	Producer's accuracy
Lidar only										
	Ac	103	26	5	6	14	10	5	18	**55.1**
	Fr	31	63	8	10	17	25	10	25	**33.3**
	Ju	5	18	297	73	16	32	24	10	**62.5**
	Pi	4	48	129	255	25	77	52	21	**41.7**
	Pl	13	25	5	7	145	5	8	4	**68.4**
	Py	6	17	15	13	3	211	15	1	**75.1**
	Qu	26	37	26	39	27	51	79	24	**25.6**
	Ul	80	96	23	23	25	57	23	283	**46.4**
User's accuracy		**38.4**	**19.1**	**58.5**	**59.9**	**53.3**	**45.1**	**36.6**	**73.3**	**Overall: 50.0%**
Quickbird only										
	Ac	81	26	5	3	35	7	16	14	**43.3**
	Fr	42	44	18	4	27	18	11	25	**23.3**
	Ju	10	26	244	132	9	37	7	10	**51.4**
	Pi	10	17	194	303	14	47	13	13	**49.6**
	Pl	28	7	2	5	140	10	4	16	**66.0**
	Py	16	19	14	14	12	168	23	15	**59.8**
	Qu	44	31	17	17	46	62	74	18	**23.9**
	Ul	141	93	14	18	43	98	24	179	**29.3**
User's accuracy		**21.8**	**16.7**	**48.0**	**61.1**	**42.9**	**37.6**	**43.0**	**61.7**	**Overall: 42.9%**
Lidar + Quickbird										
	Ac	114	26	1	0	13	13	11	9	**61.0**
	Fr	28	80	3	6	8	24	21	19	**42.3**
	Ju	2	8	347	82	6	19	8	3	**73.1**
	Pi	2	29	156	337	10	48	24	5	**55.2**
	Pl	17	18	0	7	159	3	5	3	**75.0**
	Py	1	15	7	8	1	231	18	0	**82.2**
	Qu	22	46	11	7	27	48	131	17	**42.4**
	Ul	78	103	7	7	21	89	25	280	**45.9**
User's accuracy		**43.2**	**24.6**	**65.2**	**74.2**	**64.9**	**48.6**	**53.9**	**83.3**	**Overall: 58.4%**

[1] *Ac=Acer, Fr= Fraxinus, Ju= Juniperus, Pi=Pinus, Pl=Platanus, Py=Pyrus, Qu= Quercus,* and *Ul= Ulmus*

Table 3.12. Species classification results from Random Forest (actual vs predicted)

Species[1]	*AS*	*FP*	*JV*	*PN*	*PO*	*PC*	*QS*	*UPa*	*UPu*	Prod. Ac.
Lidar only										
AS	106	18	1	0	15	1	5	3	14	**65.0**
FP	30	42	6	9	17	16	14	12	38	**22.8**
JV	2	15	241	70	12	31	70	31	3	**50.7**
PN	3	33	67	177	17	28	85	47	4	**38.4**
PO	17	23	1	4	143	3	12	4	5	**67.5**
PC	1	13	12	15	2	175	34	28	0	**62.5**
QS	7	7	9	16	4	17	54	3	1	**45.8**
UPa	3	10	4	3	5	20	6	106	15	**61.6**
UPu	49	50	1	7	18	14	7	28	213	**55.0**
User ac.	**48.6**	**19.9**	**70.5**	**58.8**	**61.4**	**57.4**	**18.8**	**40.5**	**72.7**	**Overall: 51.3%**
Quickbird only										
AS	80	17	3	2	29	0	7	10	15	**49.1**
FP	36	36	11	8	15	11	23	21	23	**19.6**
JV	8	16	197	156	7	22	29	20	20	**41.5**
PN	1	14	117	260	7	21	18	11	12	**56.4**
PO	26	7	2	5	131	5	11	12	13	**61.8**
PC	10	11	10	10	8	105	56	63	7	**37.5**
QS	8	8	3	1	11	26	35	23	3	**29.7**
UPa	2	12	2	5	7	21	29	75	19	**43.6**
UPu	104	40	6	11	20	11	12	67	116	**30.0**
User ac.	**29.1**	**22.4**	**56.1**	**56.8**	**55.7**	**47.3**	**15.9**	**24.8**	**50.9**	**Overall: 42.2%**
Lidar + Quickbird										
AS	108	19	0	0	12	2	8	1	13	**66.3**
FP	29	68	2	4	9	13	22	13	24	**37.0**
JV	2	4	297	109	6	13	28	13	3	**62.5**
PN	1	20	79	299	4	14	26	16	2	**64.9**
PO	16	15	1	3	153	2	12	4	6	**72.2**
PC	2	11	6	6	1	178	53	23	0	**63.6**
QS	2	10	6	2	3	16	74	5	0	**62.7**
UPa	4	9	0	3	2	19	13	108	14	**62.8**
UPu	57	63	1	3	14	13	10	37	189	**48.8**
User ac.	**48.9**	**31.1**	**75.8**	**69.7**	**75.0**	**65.9**	**30.1**	**49.1**	**75.3**	**Overall: 60.1%**

[1]*AS=Acer saccharinum, FP= Fraxinus pennsylvannica, JV= Juniperus virginiana, PN=Pinus nigra, PO=Platanus occidentalis, PC = Pyrus calleryana, QS= Quercus shumardii, UPa= Ulmus parvifolia, UPu= Ulmus pumila*

3.5 Discussion and Conclusions

The potential of lidar for taxonomic classification of individual trees in urban landscapes has been largely untested heretofore. Using a large set of field data of individual trees, this study evaluated the potential of height metrics derived from small-footprint discrete-return lidar data for taxonomic classification of individual trees. The results indicate that lidar data show promise in discriminating and classifying broad taxonomy, if not species, of individual trees in urban landscapes.

Our approach of classifying the tree is essentially a 'segmentation followed by classification' rather than classifying using the entire point cloud. Individual trees were manually delineated first, and classification formed using the points within the tree boundary. This means that the performance of the classification depends as much on the correct segmentation of individual crown boundaries as the classification itself. However, once the segmentation of individual crowns is achieved, with automatic or semi-automatic methods (e.g., Chapter 2 of the thesis), the classification will outperform a classification using all lidar points without knowing the individual tree crown boundaries. Secord and Zakhor (2007), while classifying an urban area into tree and non-tree segments using support vector machines (SVM) classifier, also found that classification of the segments gives better performance than a point-wise classification approach.

We also evaluated several other known pattern recognition methods, such as linear discriminant analysis, support vector machines (SVM), classification and regression trees (CART), and k-nearest neighbor (kNN), to test if these approaches yield better results. However, we found that the use of these classifiers resulted in no improvement in accuracy. Random Forests yielded moderate to high accuracies; it also provides an estimate of the relative importance of lidar metrics. Random Forests has been found to perform well in other similar studies, for example, in characterizing forest succession (Falkowski et al., 2009), estimating forest structure attributes (Hudak et al., 2008), and classifying urban land cover (Chehata et al., 2009).

Aerial photographs need to be of at least certain minimum scale for discriminating individual tree species, otherwise species can only be discriminated as stand level cover types or broad vegetation types (Avery and Berlin, 1992). Based on the present study, a similar conclusion can be made for lidar data with respect to the density of point clouds. Acquisition of

lidar data at a higher point density than the present study (8 returns/m^2) should improve classification at the individual tree level, at least for mature trees, as it will increase the ability to characterize crown shape and structure. However, higher density datasets may not necessarily help in taxonomic classification of smaller trees because the crown shapes of smaller trees are not distinctive enough between species.

Using spectral metrics from high-resolution multispectral data such as Quickbird in addition to lidar-derived variables improves the classification accuracy over using either of these data alone. This result is similar to that obtained by Sugumaran and Voss (2007) for urban tree cover and Holmgren et al. (2008) for a spruce-pine-deciduous forest.

In addition to traditional spectral information, lidar intensity data may help improve finer-scale classifications at the individual tree level. Lidar intensity has been used for landcover classification (Song et al., 2002; Antonarakis et al., 2008; Cheng and Glenn, 2009; Singh et al., 2010) and should improve the ability of lidar for taxonomic classification of trees, as demonstrated by Kim et al. (2009) and van Aardt et al. (2008) for broad classification (conifer/deciduous) of individual trees and structurally homogenous segments respectively.

3.6 Literature Cited

Antonarakis, A.S., Richards, K.S. and Brasington, J., 2008. Object-based land cover classification using airborne LiDAR. Remote Sensing of Environment, 112(6): 2988-2998.

Avery, T. and Berlin, G., 1992. Fundamentals of Remote Sensing and Airphoto Interpretation. Macmillan Publishing Company, New York, 472 pp.

Banskota, A., Wynne, R.H., Johnson, P. and Emessiene, B., in press. Synergistic use of very-high-frequency radar and discrete-return lidar for estimating biomass in temperate hardwood and mixed forests. Annals of Forest Science.

Baret, F. and Guyot, G., 1991. Potentials and limits of vegetation indices for LAI and APAR assessment. Remote Sensing of Environment, 35(2-3):161-173.

Brandtberg, T., 2007. Classifying individual tree species under leaf-off and leaf-on conditions using airborne lidar. ISPRS Journal of Photogrammetry and Remote Sensing, 61(5): 325-340.

Breiman, L., Friedman, J.H., Olshen, R.A. and Stone, C.J., 1984. Classification and Regression Trees. Wadsworth, Inc., Pacific Grave, California, 358 pp.

Chehata, N., Guo, L. and Mallet, C., 2009. Airborne lidar feature selection for urban classification using random forests. In: F. Bretar, M. Pierrot-Deseilligny and G. Vosselman (Editors), Laser scanning 2009, ISPRS, Vol. XXXVIII, Part 3/W8, 1-2 September, 2009, Paris, France, pp. 207-212.

Cheng, W. and Glenn, N.F., 2009. Integrating LiDAR intensity and elevation data for terrain characterization in a forested area. IEEE Geoscience and Remote Sensing Letters, 6(3): 463-466.

Douglas, T., Evans, D., Belli, K. and Roberts, S., 2003. Classification of pine and hardwood by the distribution and intensity of lidar returns, Proceedings of ISPRS Joint Workshop of ISPRS WG I/3 and II/2, Three-dimensional Mapping from InSAR and Lidar, 17-19 June 2003, Portland Oregon, USA.

Duryea, M.L. and Malavasi, M.M., 1995. Tree growth in the urban forest. Forestry Report R8-FR, USDA Forest Service, Southern Region, Atlanta, Georgia.

Edelsbrunner, H. and Mücke, E., 1994. Three-dimensional alpha shapes. ACM Transactions in Graphics, 13(1): 43-72.

Falkowski, M.J., Evans, J.S., Martinuzzi, S., Gessler, P.E. and Hudak, A.T., 2009. Characterizing forest succession with lidar data: An evaluation for the Inland Northwest, USA. Remote Sensing of Environment, 113(5): 946-956.

Friedl, M.A. and Brodley, C.E., 1997. Decision tree classification of land cover from remotely sensed data. Remote Sensing of Environment, 61(3): 399-409.

Hecht, R., Meinel, G. and Buchroithner, M.F., 2008. Estimation of urban green volume based on single-pulse LiDAR data. IEEE Transactions on Geoscience and Remote Sensing, 46(11): 3832-3840.

Holmgren, J. and Persson, Å., 2004. Identifying species of individual trees using airborne laser scanner. Remote Sensing of Environment, 90(4): 415-423.

Holmgren, J., Persson, A. and Soderman, U., 2008. Species identification of individual trees by combining high resolution lidar data with multi-spectral images. International Journal of Remote Sensing, 29(5): 1537-1552.

Hudak, A.T., Crookston, N.L., Evans, J.S., Hall, D.E. and Falkowski, M.J., 2008. Nearest neighbor imputation of species-level, plot-scale forest structure attributes from LiDAR data. Remote Sensing of Environment, 112(5): 2232-2245.

Huete, A.R., 1988. A soil-adjusted vegetation index (SAVI). Remote Sensing of Environment, 25(3): 295-309.

Imai, Y., M., S., Y., Y. and N, F., 2004. Tree-height measuring characteristics of urban forests, Proceedings of XXth ISPRS Congress 'Geo-Imagery Bridging Continents', Commission VII, 12-23 July 2004, Istanbul, Turkey.

Kim, S., McGaughey, R.J., Andersen, H.E. and Schreuder, G., 2009. Tree species differentiation using intensity data derived from leaf-on and leaf-off airborne laser scanner data. Remote Sensing of Environment, 113(8): 1575-1586.

Liang, X., Hyyppa, J. and Matikainen, L., 2007. Deciduous–coniferous tree classification using difference between first and last pulse laser signatures. In: P. Rönnholm, H. Hyyppä and J. Hyyppä (Editors), Proceedings of the ISPRS Workshop ‘Laser Scanning 2007 and SilviLaser 2007’, Vol. XXXVI, Part 3/W52, September 12-14, 2007, Espoo, Finland, pp. 12–14.

McPherson, E.G., Nowak, D., Heisler, G., Grimmond, S., Souch, C., Grant, R. and Rowntree, R., 1997. Quantifying urban forest structure, function, and value: the Chicago Urban Forest Climate Project. Urban Ecosystems, 1(1): 49-61.

Meinel, G. and Hecht, R., 2004. Urban vegetation volume on the basis of laser-scan data at non-leaf aerial flight times. In: M. Thies, B. Koch, H. Spiecker and H. Weinacker (Editors), ISPRS Working Group VIII/2 Laser-Scanners Forest and Landscape Assessment, Vol. XXXVI, No. 8/W2, 03-06 October 2004, Freiburg, Germany, pp. 334-339.

Miller, R.W., 1996. Urban Forestry: Planning and Managing Urban Greenspaces. Prentice Hall, New Jersey, USA, 480 pp.

Moffiet, T., Mengersen, K., Witte, C., King, R. and Denham, R., 2005. Airborne laser scanning: Exploratory data analysis indicates potential variables for classification of individual trees or forest stands according to species. ISPRS Journal of Photogrammetry and Remote Sensing, 59(5): 289-309.

Nowak, D. and Dwyer, J., 2007. Understanding the benefits and costs of urban forest ecosystems. In: J.E. Kuser (Editor), Urban and Community Forestry in the Northeast. Springer, pp. 25-46.

Otey, J.K., 2007. GIS Applications in Urban Tree Inventory. Master of Forestry Thesis, Virginia Polytechnic Institute and State University, Blacksburg, Virginia, USA.

Palenichka, R.M. and Zaremba, M.B., 2007. Multiscale isotropic matched filtering for individual tree detection in LiDAR images. IEEE Transactions on Geoscience and Remote Sensing, 45(12): 3944-3956.

Qi, J., Chehbouni, A., Huete, A.R., Kerr, Y.H. and Sorooshian, S., 1994. A modified soil adjusted vegetation index. Remote Sensing of Environment, 48(2): 119-126.

Rouse, J., Haas, R., Schell, J., Deering, D. and Harlan, J., 1974. Monitoring the vernal advancement of retrogradation of natural vegetation. Final report. National Aeronautics & Space Administration/Goddard Space Flight Centre, Greenbelt, Maryland, USA.

Secord, J. and Zakhor, A., 2007. Tree detection in urban regions using aerial lidar and image data. IEEE Geoscience and Remote Sensing Letters, 4(2): 196-200.

Singh, K.K., Vogler, J.B. and Meentemeyer, R.K., 2010. Estimation of land-use in an urbanized landscape using lidar intensity data: A regional scale approach, Proceedings of Geospatial Data and Geovisualization: Environment, Security and Society, Special joint symposium of ISPRS Technical Commission IV and Auto Carto 2010, November 15-19, 2010, Orlando, Florida, USA.

Song, J.H., Han, S.H., Yu, K.Y. and Kim, Y.I., 2002. Assessing the possibility of land-cover classification using lidar intensity data. International Archives of Photogrammetry Remote Sensing and Spatial Information Sciences, 34(3/B): 259-262.

Sugumaran, R. and Voss, M., 2007. Object-oriented classification of LIDAR-fused hyperspectral imagery for tree species identification in an urban environment. In: M. Voss (Editor), Proceedings of 2007 Urban Remote Sensing Joint Event, 11-13 April 2007, Paris, France.

TAFB, 2009. Tinker Air Force Base Fact Sheet. Tinker Air Force Base.

Tyrväinen, L., Pauleit, S., Seeland, K. and Vries, S., 2005. Benefits and uses of urban forests and trees. In: C.C. Konijnendijk, K. Nilsson, T.B. Randrup and J. Schipperijn (Editors), Urban Forests and Trees. Springer, pp. 81-114.

U.N., 2007. World Urbanization Prospects: The 2007 Revision Population Database. U.N. Department of Economic and Social Affairs, New York, U.S.A.

van Aardt, J.A. and Wynne, R.H., 2007. Examining pine spectral separability using hyperspectral data from an airborne sensor: An extension of field-based results. International Journal of Remote Sensing, 28(2): 431-436.

van Aardt, J.A., Wynne, R.H. and Scrivani, J.A., 2008. Lidar-based mapping of forest volume and biomass by taxonomic group using structurally homogenous segments. Photogrammetric Engineering & Remote Sensing, 74(8): 1033-1044.

Vauhkonen, J., Tokola, T., Packalen, P. and Maltamo, M., 2009. Identification of Scandinavian commercial species of individual trees from airborne laser scanning data using alpha shape metrics. Forest Science, 55(1): 37-47.

Wang, S.C., 1988. An analysis of urban tree communities using Landsat Thematic Mapper data. Landscape and Urban Planning, 15(1-2): 11-22.

Zhang, Y., 2001. Texture-integrated classification of urban treed areas in high-resolution color-infrared imagery. Photogrammetric Engineering & Remote Sensing, 67(12): 1359-1365.

4: ESTIMATING BIOPHYSICAL PARAMETERS OF INDIVIDUAL TREES IN AN URBAN ENVIRONMENT USING SMALL FOOTPRINT DISCRETE-RETURN IMAGING LIDAR

4.1 Abstract

The quantification of biophysical parameters of urban trees is important for urban planning, and for assessing carbon sequestration and ecosystem services. However, uncertainties exist in such quantification due to a lack of direct measurements of urban tree allometry. Airborne lidar has been used extensively in recent years to estimate biophysical parameters of trees in forested ecosystems. However, similar studies are largely lacking for individual trees in urban landscapes. Prediction models to estimate several biophysical parameters such as height, crown area, diameter at breast height, and biomass was developed for individual trees in central Oklahoma, USA using point cloud distributional metrics from an Optech ALTM 2050 lidar system. A high level of accuracy was attained for estimating tree height (R^2=0.89), dbh (R^2=0.82), crown diameter (R^2=0.90) and biomass (R^2=0.67). Species-specific relationships had a much higher R^2 (0.68 to 0.84) than for general broadleaves and conifer relationships (0.45 to 0.67). The metric crown area performed particularly well for most of the species biomass equations, which suggests that tree crowns should be delineated accurately, whether manually or using automatic individual tree detection algorithms, to obtain a good estimation of biomass using lidar-based metrics.

4.2 Introduction

Urban trees perform ecosystem functions such as sequestering carbon, improving air quality and providing general amenities (McPherson et al., 1997; Bolund and Hunhammar, 1999). Urban trees in the USA store 700 million tonnes of carbon (tC) with a gross carbon sequestration rate of 22.8 million tC/yr (Nowak and Crane, 2002). The quantification of urban tree carbon storage can lead to a better understanding of the role of urban trees in global carbon accounting for greenhouse gas emissions (Myeong et al., 2006). However, uncertainties exist in such quantification due to a lack of direct measurements of urban tree allometry and biomass (Pataki et al., 2006).

Only 10% of the total trees in urban areas in the USA are publicly-owned and the remaining 90% are on private property (Miller, 1996). Thus the management of urban trees varies immensely. At the same time, urban trees are subjected to different stresses – they often grow on compacted soil, are subjected to intense pruning, have very little space in which to grow, are improperly staked, etc. (Duryea and Malavasi, 1995). These factors affect the rate of growth as well as the shape and form of the trees, which makes the ability to predict biophysical parameters such as tree height, biomass, and crown dimensions more difficult than with forests, where trees are more homogenous in their growth and form for a particular locality and species. Unlike traditional forests, where trees experience a change in growth and allocation after certain events like thinning, low density of trees in urban environments reduces potential competition for light and other resources (McHale et al., 2009).

Urban tree inventories can provide estimates of trees biophysical parameters. But urban tree inventories are labor intensive, and thus expensive, because they often place emphasis on measuring individual trees (Wood, 1999). Cost-effective approaches such as using optical remote sensing and airborne lidar data may provide alternatives for urban tree inventories. In forests, lidar based inventories have been found to save as much as 10 weeks of time and $15,000 (e.g., Means et al., 2000). Additional cost-savings may occur in urban tree inventories because they are more complex and take into account a wider range of parameters at the individual tree level.

High-resolution to moderate or coarser resolution satellite images and airborne hyperspectral data have been widely used to estimate forest biophysical parameters (Boyd and Danson, 2005; Lu, 2006). Some examples include estimating forest biomass using moderate resolution Landsat Thematic Mapper (Nelson et al., 2000), estimating leaf area index using hyperspectral HyMap data (Schlerf et al., 2005), and estimating several forest inventory parameters using high resolution IKONOS imagery (Chubey et al., 2006). Wulder (1998) and Lutz et al. (2009) have reviewed issues on using remote sensing for estimation of forest biophysical parameters.

Because of their ability to record vertical structure, airborne lidar data are more useful than two-dimensional optical images in estimating forest biophysical parameters like tree height, aboveground biomass, leaf area index, crown, etc. (Nelson et al., 1988; Hyyppä and Inkinen, 1999; Hyyppa and Hyyppa, 2001; Brandtberg et al., 2003; Todd et al., 2003; Popescu and

Wynne, 2004; Bortolot and Wynne, 2005; Boudreau et al., 2008; Dean et al., 2008). Lidar based estimation of forest biophysical parameters has been implemented at the grid level (Means et al., 2000; Naesset, 2002), stand level (Magnussen and Boudewyn, 1998; Naesset and Bjerknes, 2001; Naesset and Okland, 2002), sub-stand segment level (van Aardt et al., 2006), plot level (Popescu and Wynne, 2002; Popescu et al., 2004; Tesfamichael et al., 2010), tree cluster level (Bortolot, 2006), and individual tree level (Persson et al., 2002; Roberts et al., 2005; Chen et al., 2007). Only a few parameters, such as height and crown diameter, can be measured directly from the lidar data (e.g. Hyyppä et al., 2001; Popescu et al., 2003). For most biophysical parameters, lidar-based estimation generally involves establishing the relationship between the metrics describing the distribution of lidar-derived heights in a given area and metrics measured (or derived from) in situ measurements (e.g., Means et al., 2000; Næsset and Gobakken, 2008).

The synergistic integration of vertical structure information from lidar data with spectral information from optical remote sensing data improves forest canopy characterisation (Hudak et al., 2002). Such integration has been used to increase accuracy for species classification (Dalponte et al., 2008; Holmgren et al., 2008), height estimation (St-Onge et al., 2008), and biomass/volume estimation (Popescu et al., 2004).

The estimation of biophysical parameters, such as biomass, using lidar relies on a strong relationship between the amount of foliage and the various tree components since foliage normally is the main element blocking laser pulses (Næsset and Gobakken, 2008). However, most of the studies using distributional approaches are based on metrics derived from a raster canopy height model rather than from point clouds. These interpolated canopy models only represent the outer canopy return data and miss the returns from the inner foliage. Our assumption is that metrics computed directly from the lidar point cloud, rather than from an interpolated raster surface, will improve the estimation of the biophysical parameters.

Despite a growing body of studies in using small-footprint discrete return lidar for forest parameter estimation, studies using distributional approaches, which exploit the relationships between distributional height metrics (e.g., mean, range, skewness, percentiles, etc.) and forest biophysical parameters are rare (Means et al., 2000; Naesset and Gobakken, 2005; Bortolot, 2006; van Aardt et al., 2008), and especially at the individual tree level (Chen et al., 2007;

Popescu, 2007). Furthermore, there are few to no related studies for individual trees in urban landscapes.

This study evaluates the potential of distribution metrics derived from normalized height of lidar-point clouds in estimating total height, diameter, crown radius, and biomass for urban trees (defined as vegetation 1m or greater in height) at the individual tree level. The study also evaluates the potential gains to be realized in biomass estimation of urban trees by coupling high-resolution spectral remote sensing with airborne lidar data.

4.3 Biomass Estimation Using Airborne Lidar

Forest biomass estimation using lidar data is dependent on how well the height of the tree is related to diameter. Naesset (2004) found bias of the difference between predicted and actual diameter at the stand level to be 0.15 - 0.74cm, which was better than using methods based on field inventory and photo interpretation. Biomass is estimated based on height metrics obtained from lidar data (Means et al., 2000; Nelson et al., 2003; Nelson et al., 2004) or based on lidar-measured crown variables, e.g., crown width (Popescu et al., 2003) or canopy cover density (Naesset, 2004). Table 4.1 shows the results of recent biomass/volume studies in primarily coniferous forests (with some deciduous forests) conducted using lidar data. Because these studies were conducted using different sensors in different forest types, the R^2 values may not be directly comparable, but in general less of the overall variance is explained in deciduous stands.

Popescu et al. (2003) found the explanatory power of the lidar-derived metrics for predicting biomass for deciduous plots lower than that for pines. One factor attributing to this may be the deliquescent tree forms of hardwoods which result in greater amounts of woody biomass into lateral branches, thereby making the height-volume or height-biomass relationship noisier (Nelson et al., 2007; Boudreau et al., 2008). But, additional differences between coniferous and deciduous species related to the crown material (leaves versus needles) and branch size and structure, which may affect the lidar penetration depth, and hence the precision of stand characteristics derived from laser data, should be considered (Naesset, 2004). Naesset (2004) observed a penetration rate of less than 2- 3% below 2 m above ground in a young deciduous forest plot, and 20-25% in a mature conifer stand. The difference in penetration rates may affect the residuals for stand variables that are related to canopy density. Difference in

crown shape between hardwoods and softwoods have an effect on the height estimation from lidar data, and hence on the prediction of biomass or volume. Nelson (1997) found that, as the crown shape changes from conical (most softwood) to spherical (most hardwoods), the estimates of lidar-based forest height tend to be 16-25% higher with elliptical and spherical canopies than with a conical canopy.

Table 4.1. Studies using small foot-print lidar to estimate above-ground biomass/volume of the forests

Study	Variable	*RMSE**			Remarks
		Deci.	Coni.	Mixed	
Naesset (2004)	Volume	-	0.22[§]	-	Pine /Spruce
van Aardt et al. (2008)	Volume	55.98	8.24	28.02	3-class volume
Næsset and Gobakken (2008)	Biomass	-	0.21[§]	-	coniferous boreal
Popescu (2007)	Biomass	-	16.70	-	individual loblolly pines
Nelson et al. (2007)	Biomass	-	33.90	-	Loblolly pine
Hyde et al. (2007)	Biomass	-	24.85	-	Pondorosa pine
Hall et al. (2005)	Biomass	-	35.79	-	Ponderosa pine
	Foliage	-	2.06	-	
Bortolot and Wynne (2005)	Biomass	-	13.70	-	Loblolly pine
Popescu et al. (2004)	Biomass	44.0	29.00	-	

*Volume m^3 ha^{-1}, Biomass t ha^{-1}; [§] ln-ln model RMSE

Later studies (Naesset, 2004; Næsset and Gobakken, 2008) reported a higher biomass and volume for spruce compared to deciduous trees of similar size. The narrow and conical-shaped crown of spruce trees allows for a relatively large portion of the laser pulses to hit low in the tree crowns, whereas more rounded crown shapes of deciduous trees normally will result in laser point clouds located higher up in the canopy.

A mixture of coniferous and deciduous trees within stands degrades the precision of lidar-based biomass estimation and presents a major challenge in practical applications (Naesset, 2004). There is a relative scarcity of component biomass equations, along with substantial variation in the observed estimates from existing equations (Jenkins et al., 2003). Jenkins et al. (2003) compiled component biomass equations for several hardwood and softwood species and developed equations to estimate component biomass as a proportion of total above ground

biomass (Figure 4.1), which shows that hardwoods distribute more biomass in the branches than the stem as compared to softwoods, especially for trees with smaller diameters. Contrary to assumption, the hardwood trees distribute less biomass in foliage than the softwood trees.

Naesset (1997) estimated stand volume of Norway spruce and Scots pine using various tree lidar-based metrics of canopy height and canopy cover density. Two test sites were used one with 97% pine and the other with 69% spruce and 28% pine. The pine site had a coefficient of determination of 0.4 and the spruce site had 0.8. Norway spruce is usually taller (24-30m) as compared to crown spread (8-12m). Scots pine is usually shorter (9-12m) with a larger crown spread of 8-9m. Even though both are conifers, the Norway spruce has a greater height to spread ratio. According to the "apical-deliquescent" hypothesis, a spruce distributes its biomass more on to stem than to branches. This might explain the difference in the coefficient of determination, though Naesset (1997) points out several other factors – such as a larger footprint size and lack of stratification – that may also have contributed to the low R^2 in pine.

Biomass is dependent on site properties, management regime, and stand age. Thinning changes the distribution of biomass within the crown. Gary (1978) found a strongly skewed distribution of needles and branchwood in the top half of the canopy of unthinned 80-year old lodgepole pine stand compared to a normal distribution in thinned stands. Within species, the distribution of aboveground biomass among the various components changes with stand age. Peichl and Arain (2007) found the relative proportion of stem biomass to total tree biomass increased from 25% for a 2 year old stand to 69% for a 65 year old stand of white pine, while the relative contribution of foliage and branches decreased with stand age.

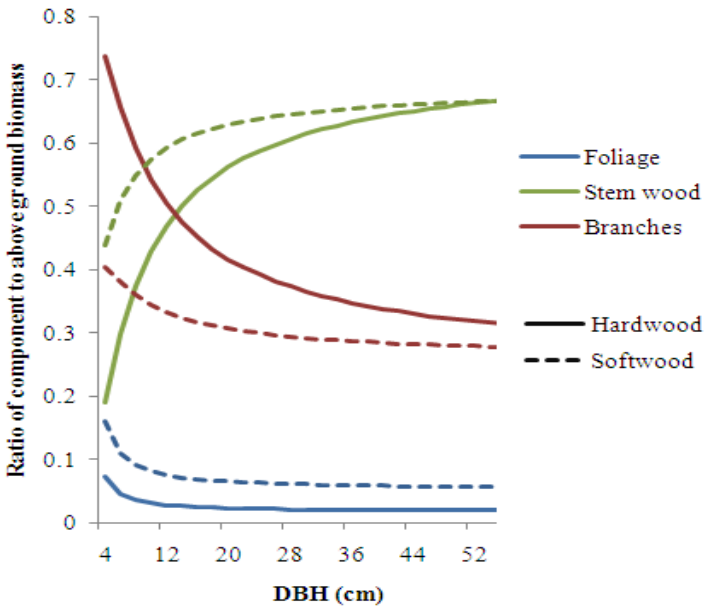

Figure 4.1 Proportion of components (foliage, stem and branches) to the total above ground biomass of hardwood and softwood species. Component ratios for hardwood and softwood species of United States as given in Jenkins et al. (2003) were used.

4.4 Methodology

4.4.1 Study Area

The study area is on Tinker Air Force Base in central Oklahoma, USA (latitude: 35° 25' 35.43"N; longitude: 97° 24' 37.73"W) (Figure 4.2). The area represents a typical suburban residential area with detached and row houses with trees, both broadleaves and conifers, growing along the road and in the yards and parks. The base is around 20 km^2 (5000 acres) in area and has 472 buildings (TAFB, 2009). There are about 6600 trees, the most common species being Eastern red cedar (*Juniperus virgiana*), Austrian pine (*Pinus nigra)* and Siberian elm (*Ulmus pumila*) (Otey, 2007).

Figure 4.2. Study Area at Tinker Air Force Base, Oklahoma. Trees measured are shown in darker shades

4.4.2 Lidar Data

Lidar data were acquired using an Optech ALTM 2050 lidar system in July 2004 in leaf-on condition. The acquisition parameters for the lidar data are shown in Table 4.2. The Optech ALTM 2050 is a small-footprint multiple-return lidar system which uses a 1064 nanometer laser. The provided lidar data did not have any return numbers. There were about 8 returns per m^2.

Table 4.2. System Specification of Optech ALTM 2050

Flying Altitude	640m
Scan Overlap	40%
Scan Frequency	45Hz
Scan Angle	15 deg
Pulse Repetition Frequency	50KHz

To do away with any complications arising from classifying lidar data using height-filtering algorithms in urban areas, a 2m-resolution bare-earth digital elevation model (DEM) delivered by the vendor (Tobin Aerial Surveys, Texas) was used. The DEM was evaluated by the vendor using ground control points and vertical accuracy within ± 15cm was reported. A normalized digital surface model (nDSM) was computed by subtracting the digital elevation model (DEM) of the area from the elevation of lidar returns. In the nDSM point cloud, all points

with less than 1m height were filtered out, and the trees, which were measured during the field survey of 2006/2007, were delineated manually in ArcGIS. We opted for a manual approach to avoid the discrepancies from an automated crown-delineation algorithm, especially in cases where tree crowns are overlapping with other trees or with buildings. Only a few individual tree crown delineating algorithms have been tested in urban landscapes (e.g., Palenichka and Zaremba, 2007), where conditions are different than forested environments. With the help of the nDSM point cloud and a color orthophoto (acquired February 17, 2004 with a spatial resolution of 10.2cm), only the trees with distinctly separable crowns (3564 in total) were selected. Lidar points below the height of 1m were removed. The boundary of each crown was delineated by computing the planimetric convex hull around the lidar points within each tree in ArcGIS. Various lidar metrics were computed for lidar returns within each individual tree (Table 4.3).

Table 4.3. Candidate individual tree metrics used as a predictor variable

Height Distribution Statistics[1]		**Density Measures**	
H_{MEAN}	Mean height	N_C	Number of crown returns
H_{VAR}	Variance of height	N_T	Number of total returns
H_{MIN}	Minimum height	N_P	Point density (N_C /N_T)
H_{MAX}	Maximum height	N_{CD}	N_C /C_A
H_R	Range of height ($H_{MAX} - H_{MIN}$)	N_{TD}	N_T /C_A
H_{STD}	Standard deviation of height	N_X	(Number of crown returns in x% of H_R)/ C_A (x = <20, 40, 80, 90, 95, >95)
H_{MODE}	Most frequent height of crown returns		
H_{CV}	Coefficient of variation of height		
H_{SE}	Standard error of mean of height	**Crown Dimension**[2]	
H_{KUR}	Kurtosis of height	C_A	Area of crown projected onto XY plane
H_{SKW}	Skewness of height	C_p	Perimeter of crown projected onto XY plane
H_{QX}	x % Quantile of height (x = 5, 10, 25, 50, 75, 90, and 95)		

[1]Heights are lidar returns from tree crown. Only returns >1m in height were considered.

[2]Crown dimensions calculated by creating a convex hull around the planimetric projection of lidar returns from the tree crown

4.4.3 High-resolution Satellite Image

High-resolution satellite data of the area was obtained from a Quickbird satellite image (DigitalGlobe Inc., USA) acquired May 17, 2005. The image was radiometrically corrected, sensor corrected, and geometrically corrected. The image consisted of a panchromatic image of 0.6m resolution and 4-band multispectral image of 2m resolution (Figure 4.3). The spectral resolution of the Quickbird image is shown in Table 3.3.

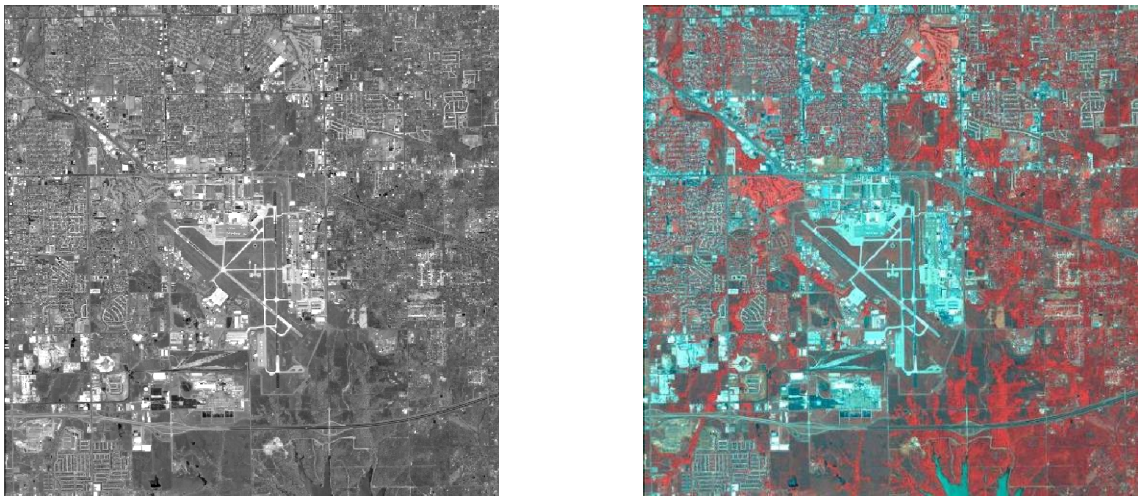

(a) (b)

Figure 4.3. (a) Panchromatic and (b) multispectral Quickbird imagery of the area

Table 4.4. Spectral resolution of the Quickbird image

Panchromatic	450-900nm
Blue	450-520nm
Green	520-600nm
Red	630-690nm
Infra-red	780-900nm

Subsequent to preprocessing, three vegetation indices were computed as follows: normalized difference vegetation index (NDVI; Rouse et al., 1974), soil-adjusted vegetation index (SAVI; Huete, 1988), and modified soil-adjusted vegetation index (MSAVI; Qi et al., 1994). For each of these three indices, and for spectral bands on through four, tree-specific descriptive statistics (minimum, maximum, mean, and standard deviation) were calculated (Table 3.7). NDVI enhances vegetation but is sensitive to optical properties of soil background,

especially in areas with considerable soil-brightness variation. SAVI minimizes the effect of soil by introducing an adjustment factor to NDVI to account for first-order soil variation and differential red and near-infrared flux extinction through vegetation (Huete, 1988). Unlike NDVI, SAVI vegetation isolines do not converge to the origin and are independent of soil background (Baret and Guyot, 1991). The constant factor varies from 0 to infinity depending on the vegetation density. A factor of 0.5 was used for this study as it has been found optimal in a wide range of conditions. MSAVI replaces the constant factor of SAVI with an iterative self-adjusting factor.

Table 4.5. Predictor variables computed from Quickbird imagery

$BandX_{MIN}$, $BandX_{MEAN}$, $BandX_{MAX}$, $BandX_{STD}$	Minimum, mean, maximum and standard deviation of spectral value of Band X, where X=1 to 4
$NDVI_{MIN}$, $NDVI_{MEAN}$, $NDVI_{MAX}$, $NDVI_{STD}$	Minimum, mean, maximum and standard deviation of normalized difference vegetation index (NDVI) computed as: $\frac{\text{Band 4} - \text{Band 3}}{\text{Band 4} + \text{Band 3}}$ (Rouse et al., 1974)
$SAVI_{MIN}$, $SAVI_{MEAN}$, $SAVI_{MAX}$, $SAVI_{STD}$	Minimum, mean, maximum and standard deviation of soil-adjusted vegetation index (SAVI) computed as: $\frac{(1+0.5)(\text{Band 4} - \text{Band 3})}{\text{Band 4} + \text{Band 3} + 0.5}$ (Huete, 1988)
$MSAVI_{MIN}$, $MSAVI_{MEAN}$, $MSAVI_{MAX}$, $MSAVI_{STD}$	Minimum, mean, maximum and standard deviation of modified soil-adjusted vegetation index (MSAVI) computed as: $\text{Band 4} + 0.5 - 0.5 * \left(\sqrt{(2 * \text{Band 4} + 1)^2 - 8 * (\text{Band 4} - \text{Band3})}\right)$ (Qi et al., 1994)

4.4.4 Field Measurement

Base line data of the urban trees used for this study were collected in 2006. The coordinates of each individual tree were recorded using a GPS unit. A high resolution digital orthoimage was used in the field to verify the location of each tree. Various tree attributes were recorded including species, diameter at breast height, tree height, condition of tree, crown radius,

age class, etc. (Otey, 2007). Diameter at breast height (dbh) was measured to the nearest inch using a logger's tape. If the tree was co-dominant, the largest leader at breast height (1.37m) was measured and recorded. Tree height was measured to the nearest foot (0.3048m) using an Opti-Logic100 LH Laser Rangefinder Hypsometer. On windy days several measurements were taken and averaged. Crown radius was measured at two directions perpendicular to each other with a logger's tape to the nearest foot from the center of the trunk to the dripline of the canopy by using a nail to secure the tape to the trunk. For this study, a total of 3562 trees, 60 broadleaf species and 12 conifer species, were used (Table 4.6). Most of the conifers are shorter than the broadleaf trees. Among broadleaf species, *Platanus occidentalis* and *Acer saccharinum* are, in general, taller than the other species. The descriptive statistics for diameter at breast height and crown size are shown in Table 4.7. *Ulmus pumila, Acer saccharinum,* and *Platanus occidentalis* are among those having larger diameter and crown widths. Conifers generally have smaller dbh and crown size than broadleaf trees.

Table 4.6. Number of trees measured in the field by height class

Species	Total trees	Height class (m)					
		<6	6-9	9-12	12-15	15-18	>18
Conifers							
Juniperus virginiana	475	156	208	102	8	1	0
Pinus nigra	461	143	223	77	16	2	0
Others conifer (10 species)	182	60	96	21	5	0	0
Broadleaf Species							
Ulmus pumila	387	12	73	111	110	53	28
Pyrus calleryana	280	116	132	30	2	0	0
Platanus occidentalis	212	4	9	23	37	43	96
Fraxinus pennsylvannica	184	17	43	49	46	26	3
Ulmus parvifolia	172	44	76	39	11	2	0
Acer saccharinum	163	1	8	16	50	55	33
Quercus shumardii	118	33	49	22	10	3	1
Other broadleaf species (53)	928	313	272	151	122	52	18

Table 4.7. Statistics for diameter at breast height and crown radius of the trees measured in the field

Species	Diameter at breast height (cm)				Crown radius (m)			
	Mean	St.dev	Min	Max	Mean	St.dev	Min	Max
Conifers								
Juniperus virginiana	30.9	14.4	5.1	68.6	11.9	4.0	2.5	24.5
Pinus nigra	31.9	11.8	7.6	66.0	11.7	3.7	3.5	25.0
Others conifers (10 species)	25.9	11.5	7.6	66.0	9.7	3.1	3.5	23.0
Broadleaf species								
Ulmus pumila	60.7	19.7	0.0	139.7	23.3	7.4	0.0	47.0
Pyrus calleryana	20.9	10.0	7.6	48.3	9.7	4.4	3.5	25.0
Platanus occidentalis	54.0	19.4	10.2	124.5	24.9	7.3	7.0	44.0
Fraxinus pennsylvannica	43.4	20.4	2.5	96.5	18.5	7.1	2.0	35.0
Ulmus parvifolia	26.0	18.4	7.6	111.8	13.9	5.8	4.5	34.0
Acer saccharinum	64.3	21.2	17.8	119.4	25.5	6.6	8.0	41.0
Quercus shumardii	25.0	16.0	5.1	86.4	11.9	4.0	2.5	24.5
Other broadleaf species (53)	31.3	22.9	0.0	200.7	14.8	7.7	0.0	44.5

4.4.5 Variables Predicted

The biophysical parameters of the trees, including tree height, diameter at breast height, mean crown radius, and biomass were estimated.

4.4.5.1 Tree height

Tree height is defined as the vertical distance from ground level to the highest green point (or 'tip') of the tree (West, 2004). Measurement of tree-height is important because tree height is included in calculation of volume and biomass of the trees and, especially in forests, tree height is an important measure to assess site quality (West, 2004).

4.4.5.2 Diameter at breast height

Diameter at breast height (dbh) of the tree is highly correlated with the volume/biomass and height of the trees. Dbh has been found to be the most reliable variable for biomass estimation (Crow, 1971; Schroeder et al., 1997).

4.4.5.3 Crown radius

As the size of a tree crown is an indicator of the growth and vigor of the tree, the measurement of crown size can help to quantify and understand growth of the tree. In urban forests, crown size can give useful cues to urban planners as to its aesthetic and hazard potential. One of the commonly measured parameter of crown size is crown width, which is defined as the horizontal width of the crown as projected to the ground and measured along one axis from edge to edge through the crown centre. Usually two axes perpendicular to each other are measured and an average taken.

4.4.5.4 Biomass

Even though volume has been traditionally used to quantify timber, biomass is increasingly used in recent years to quantify forest products such as firewood, pulpwood, and wood for bioenergy. Tree biomass is usually estimated either through direct measurement such as destructive sampling, or through use of biomass equations and tables (Avery and Burkhart, 2002). Direct measurement involves cutting the whole tree and, if underground biomass is of interest, excavating the root systems, and oven drying

for several days to get dry biomass. Because the direct method of biomass measurement is often impractical, allometric equations developed for specific tree species and localities are often used to estimate biomass. In ground-based mensuration, biomass is generally estimated using an allometric relationship between plant dimensions and biomass, and usually expressed as a function of height and diameter at breast height (dbh) (Reed et al., 1996) or as a function of dbh only (Jenkins et al., 2004). Allometric equations to estimate biomass are of two basic functional forms (West, 2004):

$$B = aD^b \tag{1.1}$$

$$B = aD^bH^c \tag{1.2}$$

where D is diameter at breast height, H is total tree height, and a, b, c...are regression parameters.

Equation 1.1 is more commonly used than Equation 1.2 because it provides a good balance of accurate prediction and low data requirements, and addition of an extra variable (in Equation 1.2) does not increase R^2 or decrease the sum of squares error substantially (Ter-Mikaelian and Korzukhin, 1997).

As there are few allometric equations developed specifically for urban trees (e.g. Pillsbury et al., 1995), most studies rely on the equations based on forest trees. Allometric equations developed for different tree species in different part of the world differ little in the values of the parameters (Ter-Mikaelian and Korzukhin, 1997; Snowdon et al., 2001), which suggest that biomass equations developed for certain tree species in one part of the world can satisfactorily predict the biomass of different species in another part of the world, albeit with some bias in the predictions (West, 2004). The USDA Forest Service has developed and evaluated models to quantify the benefit of urban trees – namely STRATUM[1] and UFORE[2]. These models also use allometric equations from urban trees of the specific region where available.

For the present study, due to lack of availability of urban tree allometry, forest-derived aboveground biomass equations were used in most cases. The species-specific allometric equations were chosen such that they represent the climatic conditions of the

[1] http://www.itreetools.org/stratum.shtm

[2] http://www.fs.fed.us/ne/syracuse/Tools/UFORE.htm

study area, where available, and they were based on trees with sufficient range of DBH. Equations used to estimate above ground biomass for major species are listed in Table 4.8. McHale et al. (2009) compared biomass equations derived from terrestrial lidar scanning of urban trees to equations developed from traditional forests and found that depending on scale and species or population and community characteristics, variability ranged from 60–300%, but when a variety of equations are used for the entire urban forest community, variability was reduced to 10%. In the present study, we used multiple species-specific biomass equations, rather than one or two general biomass equations for all the trees in the area, as this should reduce the potential errors associated with using forest-based allometry.

Table 4.8. Biomass equations used to estimate individual tree aboveground biomass

Species[§]	Biomass equation[#]	R^2	DBH range	N	Locality	Source
JUVI	Ln (*Y*, kg)= - 0.912+2.322 Ln (*DBH*, cm)	0.98	13.3 - 37.3cm	12	Kansas, Oklahoma	Norris et al. (2001)
ULPU	(*Y*, lb) = 2.17565 (*DBH*, in) $^{2.4962}$	0.98	6.5 - 69.7cm	15	Piedmont (SE USA)	Clark III et al. (1986)
FRPE	Ln(*Y*, lb) = -1.104+0.88814 ln((*DBH*, in)^2(*H*, ft))	0.91	0.9 - 30.6in	70	W.C. Mississipi	Schlaegel (1984)
ULPA	(*Y*, lb) = 2.17565 (*DBH*, in) $^{2.4962}$	0.98	6.5 - 69.7cm	15	Piedmont (SE USA)	Clark III et al. (1986)
ACSA	$\log_{10}$(*Y*, lb) = $\log_{10}$(2.4439)+ 2.5735 $\log_{10}$(*DBH*, in)	0.98	5-50cm	119	W. Virginia	Brenneman et al. (1978)
QUSH	Ln(*Y*, kg)= -2.0127 + 2.4342 Ln(*DBH*, cm)	0.99	Up to 73cm	485	-	Jenkins et al. (2004)
PYCA	(*Y*, kg) =0.0029 ((*DBH*, cm)^2(*H*, m))$^{1.4607}$	0.89	4.0 - 11.0cm	6	Pennsylvania, Ohio	Johnson and Gerhold (2001)
PINI	Ln (*Y*, kg) = –2.5356+ 2.4349 Ln (*DBH*, cm)	0.99	Up to 180cm	331	-	Jenkins et al. (2004)
PLOC	(*Y*, lb) = 1.57573 (*DBH*, in) $^{2.5801}$	0.98	12.3 - 60.7	14	Piedmont (SE USA)	Clark III et al. (1986)

[§]JUVI=*Juniperus virginiana*, PINI = *Pinus nigra*, ULPU=*Ulmus pumila,* PYCA= *Pyrus calleryana,* PLOC= *Platanus occidentalis,* FRPE = *Fraxinus pennsylvanica,* ULPA= *Ulmus parviflora,* ACSA= *Acer saccharinum,* QUSH=*Quercus shumardii*

[§]*Y*=Above-ground biomass*, DBH*=diameter at breast height, *H*=total height

1 lb = 0.4536 kg

The regression models were evaluated using the following three criteria to select the best model (Montgomery and Peck, 2006):

1. $\boldsymbol{R^2_{adj}}$: Adjusted coefficient of multiple regression R^2_{adj} is the most commonly used criterion, which is given as:

$$R^2_{adj} = 1 - \frac{MSE}{MST}$$

where MSE is the mean sum of square of error and MST is mean sum of square of regression with p terms. In contrast to the R^2, adding more variables to the model does not automatically increase R^2_{adj}, because the decrease in error sum of square (SSE) used to calculate R^2 may be offset by the corresponding decrease in the error degrees of freedom. The model with a maximum R^2_{adj} value is preferred assuming model parsimony and physical plausibility.

2. $\boldsymbol{C_p}$**:** Mallows C_p is a measure of the fit for the regression model given as:

$$C_p = \frac{SSE}{\hat{\sigma}^2} - n + 2p$$

where SSE is the error sums of square with p terms, $\hat{\sigma}^2 = MSE$ is the mean square error from the full $k+1$ term and n is the sample size. The regression models that have negligible bias will have values of near $C_p = p$. The best regression model is either a model with minimum C_p or a model with a slightly larger C_p that contains less bias than the minimum.

3. ***MSE:*** MSE is the mean square error for the p-variable equation:

$$MSE = \frac{SSE}{n - p}$$

Generally *MSE* decreases as p increases. But, if adding variables in the p term does not improve *SSE* by the amount equal to *MSE* in the $p-1$ term model, then *MSE* will increase. *MSE* is plotted versus p and the model is chosen based on the choice of p on the following:

- Minimum *MSE*
- Value of p such that *MSE* is approximately equal to *MSE* for the full model
- Value of p near the point where the smallest *MSE* turns upward.

If the objective of the model is to obtain a good description of data, a model with small residual sums of squares is chosen. If the model is to be used for prediction and estimation, a model with minimum mean square error of prediction (such as the PRESS statistic) is chosen. If the objective is parameter estimation, then the bias resulting from deleting variables and the variances of estimated coefficients are considered. If the model is to be used for control, the standard errors of the regression coefficient should be small. In this study, only the models that have $Cp \leq (p + 1)$, where p is the number of variables in the model, were included for choosing the best model.

The model was subjected to residual and influential analysis. While selecting the final model, the parsimony principle was employed whereby fewer variables were preferred over slightly better values of R^2_{adj} or Cp. The predictive capability of the selected model was assessed using cross-validation multiple-correlation (Rozeboom, 1978) and prediction sum of squares (PRESS) (Allen, 1974). Cross-validation, R_r^2, was estimated as:

$$R_r^2 = 1 - \left(\frac{N + p}{N - p}\right)(1 - R^2)$$

where N is sample size, p is number of predictors, and R^2 is squared multiple correlation coefficient. The *PRESS* residual was computed as:

$$PRESS = \sum_{i=1}^{n} \left(Y - \hat{Y}_{(i)}\right)$$

where $\hat{Y}_{(i)}$ is the predicted mean of the i^{th} observation if that observation is excluded in the estimation of regression coefficient.

Outliers in the model were identified using jackknife residuals (Kleinbaum et al., 2007), where the multivariate distance for each observation is calculated using means, variances, and covariances that do not include the observation itself. For the *i*th observation, the jackknife residual is calculated as:

$$r_{(-i)} = \frac{E_i}{S_{(-i)}\sqrt{1 - h_i}}$$

where E_i is the regression residual of the *i*th observation, $S_{(-i)}$ is the square root of mean square error (MSE) calculated excluding *i*th observation, and h_i is the leverage of the *i*th observation or a measure of the extremeness of the observation with respect to the

independent variables. Jackknife residuals have a *t* distribution, and if the absolute residual value is greater than 95th percentile of the distribution, they are considered as an outlier. Each outlier, as defined by Jacknife residuals, was investigated carefully to determine the cause of the outlier. Only when the outlier was due to unnatural causes, such as lidar returns from power wires or dead trees, or anomalous measurements, it was discarded from the data analysis. Outlier removal is particularly important for this study because there is a lapse of two years between the lidar flight and the field data collection. In the two years between lidar data collection in 2004 and field data collection in 2006, some trees had growth in the height and crown, while others were pruned, and some were completely removed.

4.5 Results and Discussions

4.5.1 Tree Height

4.5.1.1 Relationship between Tree Height and H_{MAX}

The lidar return with maximum height (H_{MAX}) from an individual tree is representative of the return coming from the topmost branch of the tree, and is most often related to the field-measured height of the tree. The mean field-measured height was higher compared to H_{MAX} in both conifers (field measured 7.2m; H_{MAX} 7.1m) and broadleaf trees (field measured 10.1m; H_{MAX} 9.6m). The height underestimation may have become compounded because of the two year lapse between the lidar flight (2004) and field data collection (2006), in which period the height of tree may have grown.

Previous studies (e.g. Hopkinson et al., 2005) using the individual tree height with lidar have found similar underestimation in forested environments. Hyyppä et al. (2000) and Persson et al. (2002) found an underestimation of 0.14m and 1.73m respectively in Norway spruce and Scots pine forests. Difference in bias between the two studies was attributed to lidar point density. Hyyppä et al. (2000) used a point density of 24 pts/m^2, which was considerably denser than the present study. Using fairly dense lidar data (10 pts/m^2) in mixed Bavarian forest in Germany, Heurich et al. (2004) obtained similar underestimation of 0.42 m for deciduous trees, but much larger underestimation of 0.65 m for coniferous trees. The smaller underestimation of conifers in the present study can be attributed to lower growth during the two year lapse period compared to broadleaf trees.

The distribution of the field-measured total height and H_{MAX} for broadleaf trees shows a larger number of trees in taller height classes having lower H_{MAX} than field-measured height, while for shorter trees fewer numbers of trees had lower H_{MAX} (Figure 4.4). This positive shift in height distribution of field-measured broadleaf trees is likely due to growth during the two year lapse. In conifers, however, the total number of trees was lower for most of the trees in the middle height range (Figure 4.4). For very tall and very short trees, H_{MAX} overestimated the total height. This result does not conform to the findings by other studies which have shown lidar underestimates the tree height consistently. In mixed temperate forests of Northern Idaho, Falkowski et al. (2008) found that lidar underestimated high tree height and overestimated low tree height, which is similar to the results obtained for broadleaf trees by the present study. Brandtberg et al. (2003) also found similar results in oak-dominated forest of West Virginia using leaf-off lidar data. Since the overall height growth for the conifers over two years' period was minimal, the height underestimation in upper height class may also be due to lidar pulses missing the conifer top or to random errors in field measurement where it is sometimes harder to locate the tree-tops, leading to over- or under-estimation of tree heights (Hyyppä and Inkinen, 1999; Clark et al., 2004).

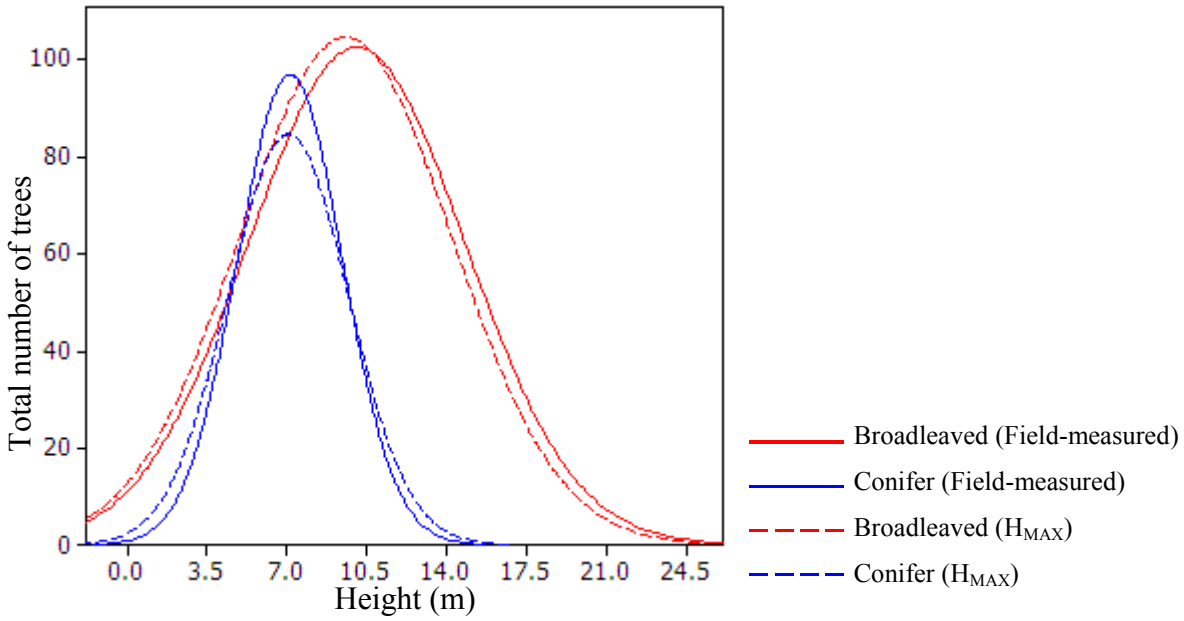

Figure 4.4. Distribution of trees in each class showing field measured total height (solid line) and lidar measured maximum height H_{MAX} (dotted line) of conifers and broad leaves

The field-measured tree height and H_{MAX} of 3562 total trees had an R^2 of 0.887 and *RMSE* of 1.34m (Figure 4.5). Conifers (R^2=0.789), had a poorer relationship with

H_{MAX} than the broadleaf trees (R^2=0.889) (Figure 4.6). The increased probability that lidar pulses missed the conical and pointed tip of the conifers may have contributed to the lower R^2 than in broadleaf trees, whose tips are not as pronounced as that of conifers.

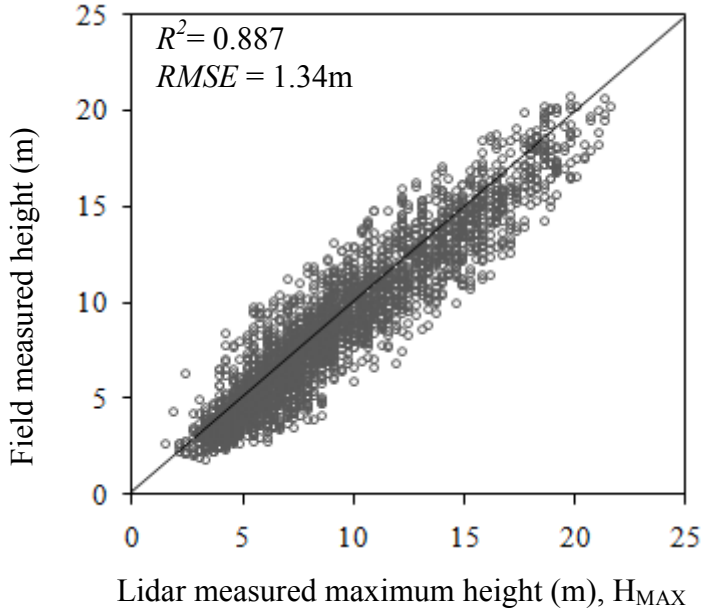

Figure 4.5. Relationship between field-measured height and lidar-measured maximum height.

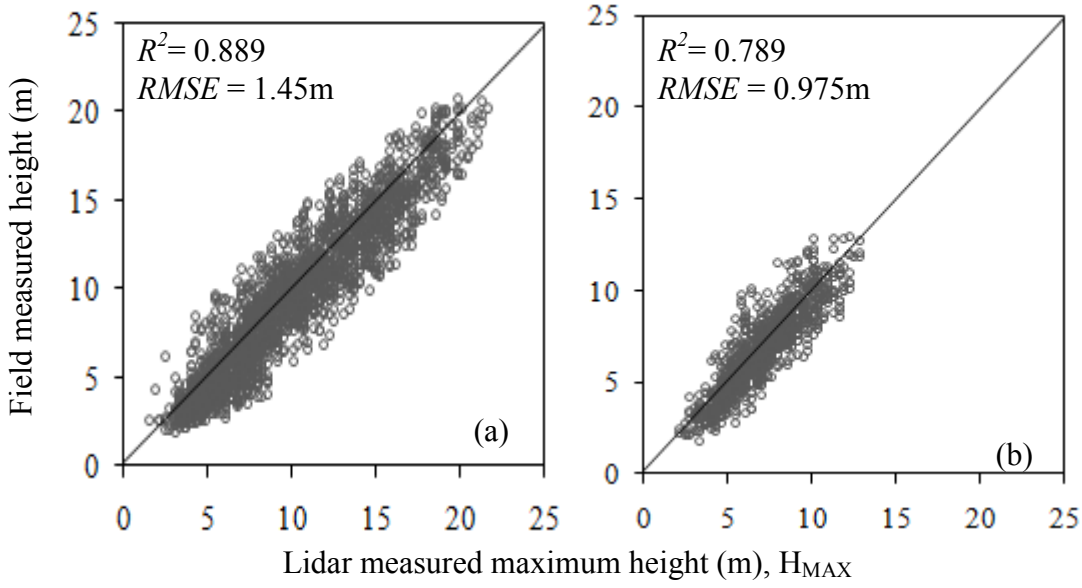

Figure 4.6. Relationship between field-measured height and lidar-measured maximum height in (a) broadleaf trees (total 2292 trees) and (b) conifers (total 1058 trees)

The less-pronounced tips of broadleaf trees also contribute to error in field-measured height. The well-defined tips of conifers, on the other hand, make it easier to spot the tip in the field. Two factors are important for achieving good height estimation of

individual trees using lidar: (1) correct height filtering and hence accurate estimation of bare-earth surface, and (2) correct delineation of crown, which reduces error due to false tree tops. Poorer crown boundary delineation can attribute to false tree tops and reduce the R^2 considerably (Kwak et al., 2007).

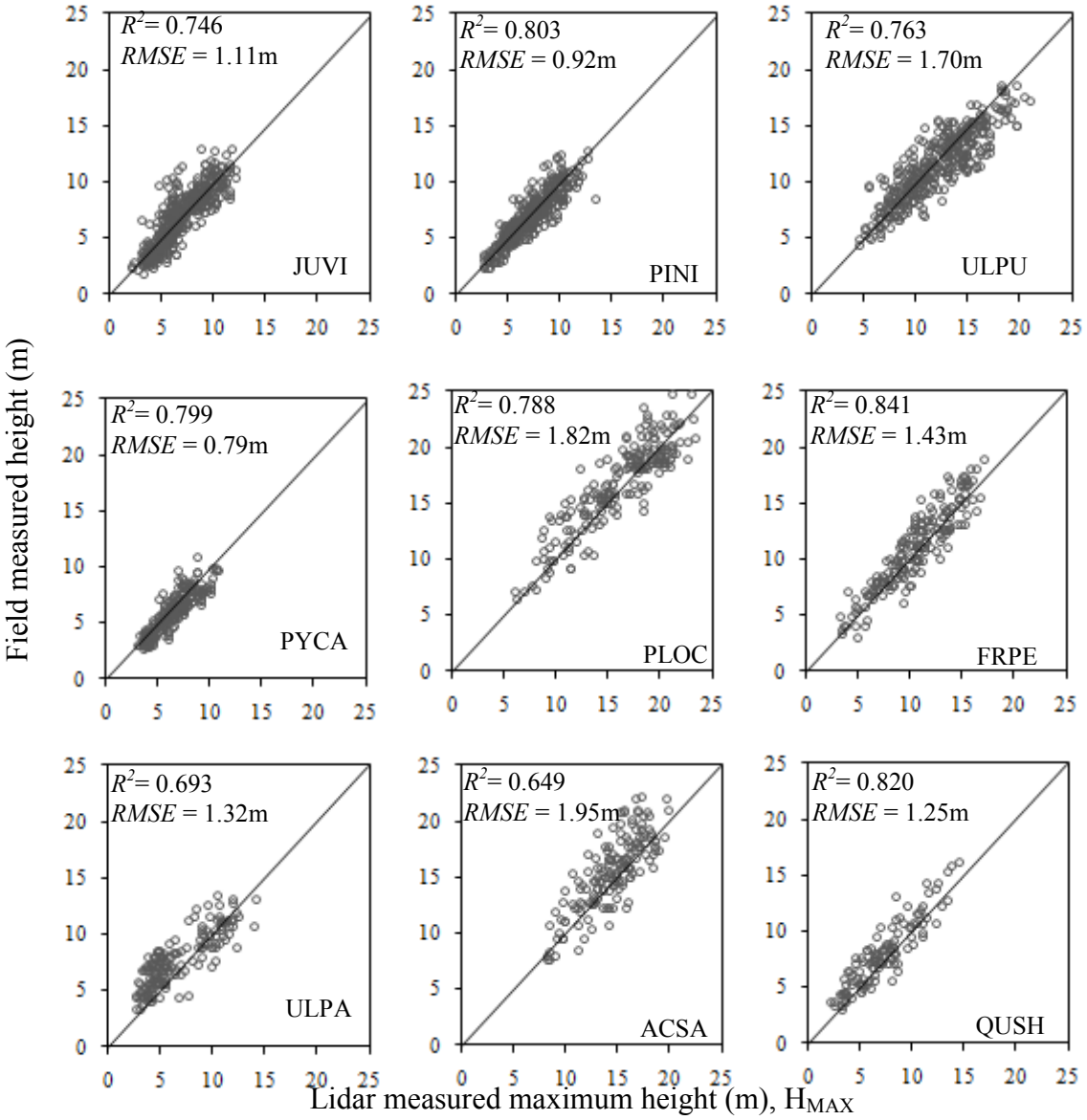

Figure 4.7. Relationship between field-measured height and lidar-measured maximum height in major species of the study area. Tree species abbreviations: JUVI=*Juniperus virginiana*, PINI = *Pinus nigra*, ULPU=*Ulmus pumila,* PYCA= *Pyrus calleryana,* PLOC= *Platanus occidentalis,* FRPE = *Fraxinus pennsylvanica,* ULPA= *Ulmus parviflora,* ACSA= *Acer saccharinum,* QUSH=*Quercus shumardii*

Some species had a better relationship and others had a poorer relationship with H_{MAX} (Figure 4.7). *Ulmus parviflora* and *Acer saccharinum* had R^2 below 0.7. These

species have a rounded crown with no distinct tree top, thus making it difficult to identify the tree top for the lidar as well as for the field measurer.

4.5.2 Diameter at Breast Height

Diameter at breast height (dbh) was estimated with crown-based metrics and height-based metrics separately (Table 4.9). For both sets, one variable with the best relationship was chosen. Among crown-metrics, crown perimeter, C_p, performed best in all cases, and among height-based metrics different variables performed best in different cases. H_{MEAN} had a good fit with all trees, broadleaf trees, and both conifer species, while for broadleaf species the best variables were H_{MAX} or one of the upper quantiles.

Crown metrics had a better R^2 value than height-based metrics. The result is similar to that reported by Chen et al. (2007) who also found that crown metrics performed better than height metrics to predict basal area and stem volume for individual trees in a deciduous oak woodland in California.

Broadleaf dbh is better estimated using either crown or height metrics than conifer dbh. If measuring crown size with relatively high accuracy is achievable, crown metrics are better predictors of dbh than height-based metrics. Height-based metrics can also give a robust estimate of dbh for individual trees for broadleaf trees, but are not as good for conifers. Estimation of diameter at breast height can be greatly improved through complementary use of terrestrial lidar, as has been demonstrated for urban trees by Omasa et al. (2008).

Table 4.9. Relationship of diameter at breast height (cm) with crown-size and height metrics

Species[a]	*N*	Crown-size metrics						Height metrics					
		Metrics[b]	R^2	R^2_{adj}	R^2_{pred}[c]	*PRESS*	*RMSE*	Metrics[b]	R^2	R^2_{adj}	R^2_{pred}[c]	*PRESS*	*RMSE*
All trees	3505	C_P	0.818	0.818	0.817	289605	9.1	H_{MEAN}	0.723	0.723	0.722	440754	11.2
Broadleaf species	2414	C_P	0.843	0.843	0.843	220242	9.5	H_{MEAN}	0.761	0.761	0.760	336470	11.8
ULPU	378	C_P	0.738	0.737	0.735	36110	9.7	H_{MAX}	0.603	0.602	0.599	54683	12.0
PYCA	273	C_P	0.706	0.705	0.701	7079	5.1	H_{Q75}	0.620	0.619	0.614	9164	5.8
PLOC	207	C_P	0.830	0.829	0.827	12292	7.7	H_{Q95}	0.820	0.819	0.817	12983	8.7
FRPA	175	C_P	0.794	0.793	0.789	13645	8.8	H_{MAX}	0.701	0.700	0.694	19796	10.6
ULPA	167	C_P	0.888	0.887	0.885	5619	5.8	H_{Q75}	0.855	0.854	0.850	7340	6.6
ACSA	160	C_P	0.715	0.713	0.708	20233	11.2	H_{Q75}	0.643	0.640	0.635	25359	12.5
QUSH	114	C_P	0.911	0.910	0.908	2310	4.5	H_{MAX}	0.851	0.849	0.844	3902	5.8
Conifers	1093	C_P	0.739	0.738	0.738	48057	6.6	H_{MEAN}	0.541	0.540	0.538	84655	8.8
JUVI	475	C_P	0.673	0.672	0.669	32366	8.2	H_{MEAN}	0.510	0.509	0.501	48788	10.1
PINI	461	C_P	0.691	0.690	0.687	20069	6.6	H_{MEAN}	0.572	0.572	0.567	27737	7.7

[a] *ACSA=Acer saccharinum, FRPA= Fraxinus pennsylvannica, JUVI= Juniperus virginiana, PINI=Pinus nigra, PLOC=Platanus occidentalis, PYCA = Pyrus calleryana, QUSH= Quercus shumardii, ULPA= Ulmus parvifolia, ULPU= Ulmus pumila*

[b] C_P=crown perimeter, H_{MEAN}=mean lidar height, H_{MAX}=maximum lidar height, H_{Qx}=*x*% quantile of height

[c] R^2_{pred} calculated using leave one out cross-validation assessment. Only one variable with best relationship was chosen.

4.5.3 Crown Radius

A strong correlation (R^2=0.90) was obtained from the relationship between field measured crown radius and the radius measured on the trees identified with lidar (Figure 4.8a). Field-measured crown radius was the average of the two perpendicular measurements taken in the field. Lidar-based radius was computed by assuming the tree crown as a circle: $radius = \sqrt{crown\ area/\pi}$.

Because crown radius is often a function of tree height – taller trees have larger crowns and smaller trees have smaller crowns – field-measured crown radius is related to lidar-measured maximum height but has lower R^2 of 0.75 (Figure 4.8b).

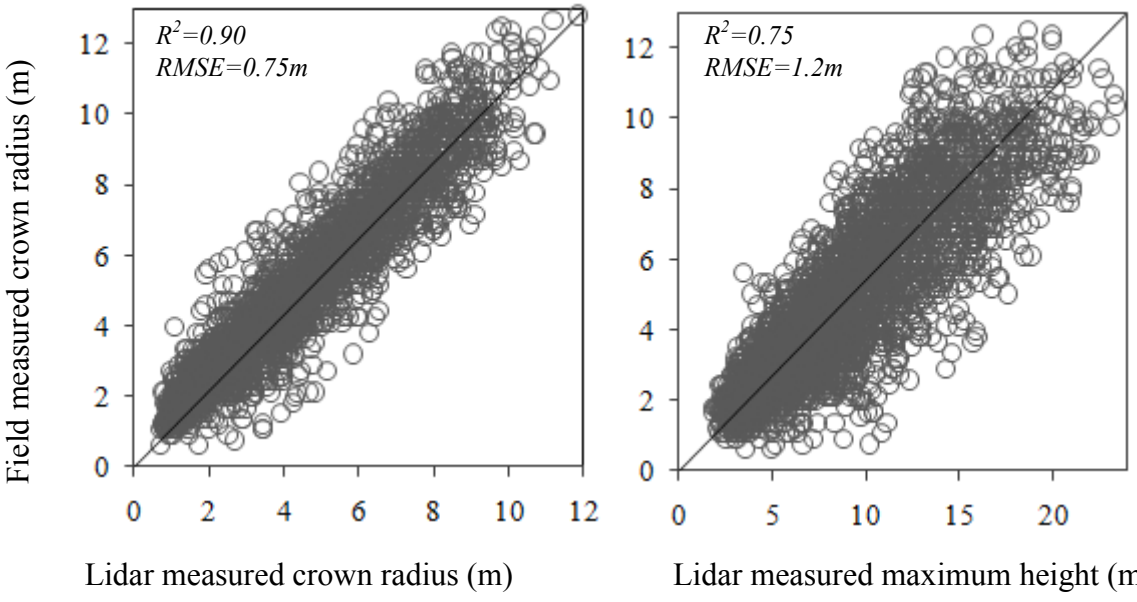

Figure 4.8. Relationship of field-measured crown radius (m) with (a) lidar-measured crown-radius (m) and (b) lidar-measured maximum height (m) for all trees.

An attempt was made to estimate the crown radius using only height-based lidar distribution metrics (Table 4.10). Lidar height metrics from conifers have a poorer relationship with crown radius compared to those from broadleaf trees. Among broadleaf species only *Acer saccharinum* has the lowest R^2. Among the metrics, H_{MEAN}, H_{MAX}, and the upper quantiles resulted in the best fit with crown-diameter.

Table 4.10. Results of regression analysis of crown radius with height-metrics

Species[a]	*N*	Model[b]	R^2	R^2_{adj}	R^2_{pred}[c]	*PRESS*	*RMSE*
All trees	3517	$Y = 0.30898 + 0.74960*H_{MEAN}$	0.771	0.770	0.770	4558	1.1
All broadleaf species	2414	$Y = 0.21928 + 0.76909*H_{MEAN}$	0.779	0.778	0.778	3616	1.2
ULPU	378	$Y = 0.71799 + 0.59987*H_{Q95}$	0.643	0.642	0.639	616	1.3
PYCA	272	$Y = -0.36681 + 0.76381*H_{MED}$	0.733	0.732	0.729	116	0.7
PLOC	205	$Y = 0.84456 + 0.42798*H_{MAX}$	0.770	0.768	0.766	210	1.0
FRPA	178	$Y = -0.24987 + 0.67583*H_{Q75}$	0.730	0.729	0.724	228	1.1
ULPA	167	$Y = 0.70168 + 0.58483* H_{Q90}$	0.818	0.817	0.813	88	0.7
ACSA	160	$Y = 0.39968 + 0.56739*H_{Q90}$	0.589	0.587	0.580	279	1.3
QUSH	114	$Y = -0.05268 + 0.50024*H_{MAX}$	0.810	0.809	0.804	55	0.7
All conifers	1092	$Y = 1.19172 + 0.38139*H_{Q90}$	0.460	0.459	0.458	767	0.8
JUVI	449	$Y = 1.28095 + 0.33242*H_{MAX}$	0.530	0.529	0.525	274	0.8
PINI	440	$Y = 1.05681 + 0.39898* H_{Q90}$	0.531	0.530	0.527	228	0.7

[a] *ACSA=Acer saccharinum, FRPA= Fraxinus pennsylvannica, JUVI= Juniperus virginiana, PINI=Pinus nigra, PLOC=Platanus occidentalis, PYCA = Pyrus calleryana, QUSH= Quercus shumardii, ULPA= Ulmus parvifolia, ULPU= Ulmus pumila*

[b] H_{MEAN}=mean lidar height, H_{MAX}=maximum lidar height, H_{MED}=median lidar height, H_{Qx}=x% quantile of height

[c] R^2_{pred} calculated using leave one out cross-validation assessment

4.5.4 Aboveground Biomass

Aboveground biomass of conifers had the lowest R^2 value among broadleaf trees and all trees combined (Table 4.11). The lower performance of the biomass models for all trees, broadleaf trees, and conifers compared to individual species (Table 4.12) might have resulted from aggregating the species-wise models to estimate biomass for broader categories. This might have compounded the variation of biomass between species within the category.

Predictors based on Quickbird performed poorly for all trees, broadleaves and conifers (Table 4.11). While studies have found good stand-level biomass prediction capacity using hyperspectral or multispectral data in forested areas (e.g., Smith et al., 2002; Zheng et al., 2004; Hall et al., 2006; Heiskanen, 2006; Blackard et al., 2008), studies exploring the relationship between spectral metrics from high-resolution imagery and forest biomass are largely lacking. Instead of using spectral metrics, most studies have used crown-size information from high-resolution imagery to predict forest biomass. Leboeuf et al. (2007) used Quickbird-derived tree shadow fraction, which is calculated as the ratio of the area of tree shadows to the ground reference, to predict biomass in black spruce stands in Canada. Gonzalez et al. (2010) used Quickbird-derived crown diameter to predict biomass of old-growth forests in California, but found higher uncertainty and lower accuracy than with lidar-derived height. This is due to the poorer relationship between crown diameter and biomass than between lidar-derived height and biomass.

Species-specific relationships had a much higher R^2 (from 0.68 to 0.84), Table 4.12 and Figure 4.9. Naesset (2004) also suggested the use of careful stratification to improve accuracy. The metric crown area (C_A) performed well in all the species biomass models, except for *Q. schumardii*. In *Q. schumardii* the number of crown returns explained more variance than crown area. Popescu et al. (2003) similarly found that lidar-derived crown diameter alone explained 78% of the variance associated with pine biomass.

Table 4.11. Results of regression analysis of aboveground biomass (kg) of individual trees

	R^2	R^2_{adj}	*MSE*	R^2_{pred} [a]	*PRESS*	Best Model [b, c]
All trees (*n=2425)*						
Lidar only	0.665	0.665	1093.1	0.663	2907146469	$Y = -828.1762 + 18.135676\ C_A + 242.3016\ H_{Q5}$
Quickbird only	0.405	0.404	14569	0.403	5156216255	$Y = 1261.291 + 0.00617\ MSAVI_{MAX} - 0005016\ MSAVI_{MEAN} - 17.67353 * Band4_{STDEV}$
Broadleaf trees (*n=1489)*						
Lidar only	0.634	0.633	1303.3	0.632	2538508726	$Y = -808.7527 + 18.106044\ C_A + 264.14317\ H_{Q5}$
Quickbird only	0.432	0.430	1625.5	0.428	3945573886	$Y = 9421.6382 - 0.002867\ MSAVI_{MIN} - 5.64675\ Band2_{MEAN} - 12.89806\ Band4_{MIN} - 31.22805\ Band4_{STD}$
Conifers (*n=897)*						
Lidar only	0.453	0.451	680.2	0.447	417899538	$Y = -84.97512 + 25.5688\ C_A - 306.7143\ N_{>90} + 144.889\ N_{40\text{-}60}$
Quickbird only	0.336	0.333	750.1	0.328	507518718	$Y = -1045.448 + 0.003535\ MSAVI_{MAX} + 1925.2053\ SAVI_{MAX} + 4.552205\ Band4_{MAX} - 13.70097\ Band4_{STDEV}$

[a] R^2_{pred} calculated using leave one out cross-validation assessment

[b] *MSAVI* = Modified soil-adjusted vegetation index, *SAVI*=Soil-adjusted vegetation index, and *BandX* = X^{th} band of Quickbird imagery

[c] C_A=crown area, H_{Q5}=5% quantile of height,

Table 4.12. Results of regression analysis of aboveground biomass (kg) of individual trees

Species[a]	*N*	R^2	R^2_{adj}	*MSE*	R^2_{pred}[b]	*PRESS*	Model[c]
Broadleaf species							
ULPU	377	0.702	0.699	1098.9	0.694	461324986	$Y = - 932.5395 + 16.3418\ C_A + 161.10597\ H_{VAR} + 263.449\ H_{Q5}$
PYCA	274	0.697	0.695	450.1	0.688	56429872	$Y = -345.3206 + 34.9041\ C_A + 1808.5412\ H_{SE}$
PLOC	210	0.803	0.800	780.7	0.792	132648518	$Y = 1517.2267 + 9.46736\ C_A + 158.7919\ H_{VAR} – 79.73756\ H_{CV}$
FRPA	175	0.783	0.779	259.2	0.767	12325526	$Y = -351.1855 + 4.197\ C_A + 67.9569\ H_{VAR} + 89.8835\ H_{Q5}$
ULPA	171	0.841	0.839	354.3	0.833	22231502	$Y = -171.942 + 19.2475\ C_A – 0.5355\ N_T$
ACSA	158	0.706	0.701	1964.1	0.687	631371424	$Y = - 3674.714 + 24.5642\ C_A + 286.0985\ H_{VAR} + 593.973\ H_{Q5}$
QUSH	115	0.838	0.833	330.1	0.771	17107190	$Y = -569.97 + 1.9247\ N_C + 141.973\ H_{VAR} + 198.2907\ H_{Q5}$
Conifers							
JUVI	459	0.684	0.683	737.1	0.678	250770557	$Y = - 660.1173 + 44.694116\ C_A + 327.94367\ H_{MIN}$
PINI	449	0.715	0.713	197.6	0.708	17814771	$Y = - 284.7497 + 12.792\ C_A + 1043.889\ H_{SE} + 77.7504\ H_{Q5}$

[a] R^2_{pred} calculated using leave one out cross-validation assessment

[b] *ACSA=Acer saccharinum, FRPA= Fraxinus pennsylvannica, JUVI= Juniperus virginiana, PINI=Pinus nigra, PLOC=Platanus occidentalis, PYCA = Pyrus calleryana, QUSH= Quercus shumardii, ULPA= Ulmus parvifolia, ULPU= Ulmus pumila*

[c] C_A=crown area, H_{Q5}=5% quantile of height, H_{VAR}=variance of height, H_{SE} = standard error of height, H_{MIN} = minimum of height, H_{CV} = coefficient of variation of height, N_T = number of total returns, and N_C= number of crown returns

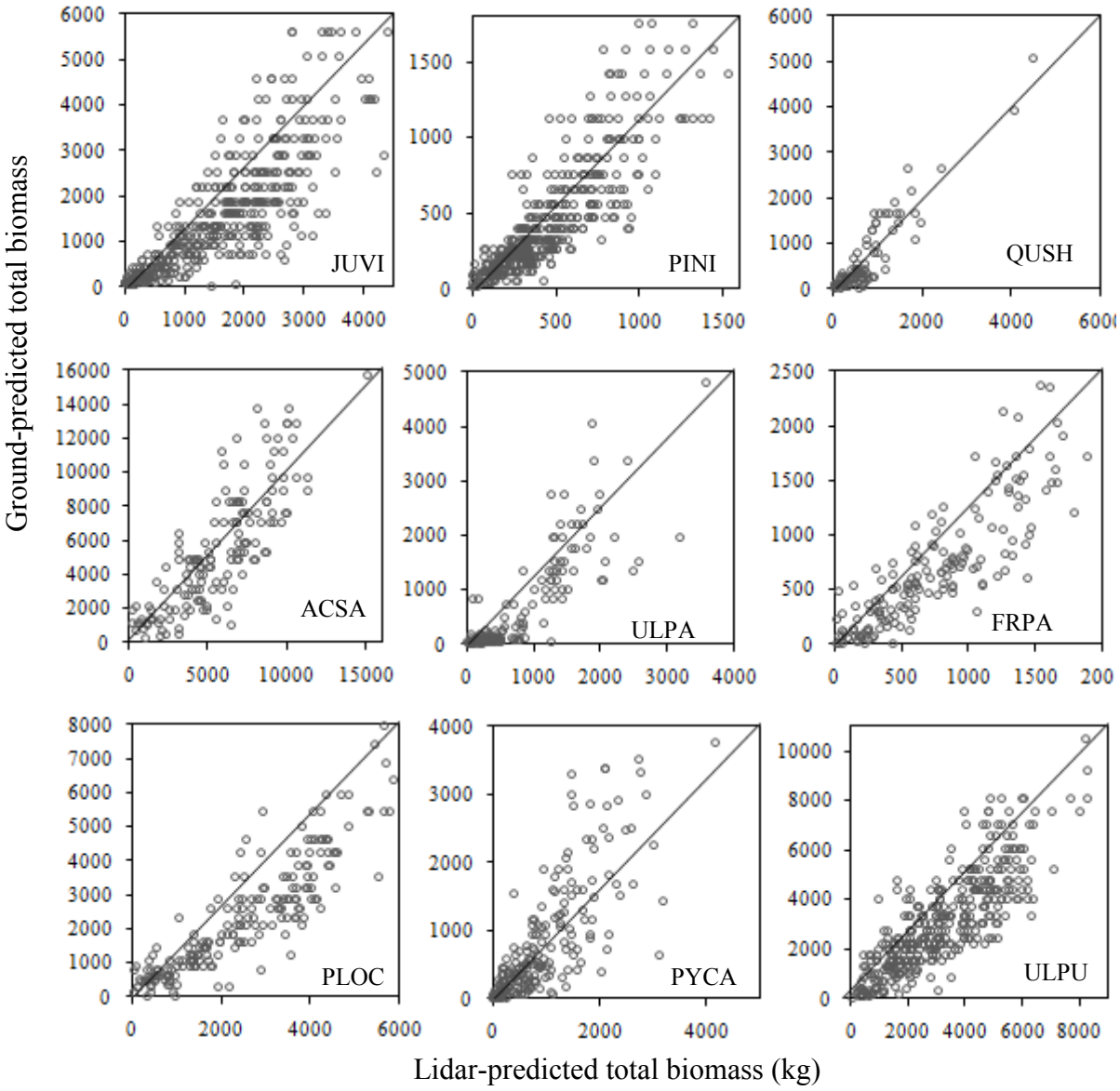

Figure 4.9. Relationship between total ground-predicted tree biomass and lidar-predicted biomass of major species of the study area. Tree species abbreviations: JUVI=*Juniperus virginiana*, PINI = *Pinus nigra*, ULPU=*Ulmus pumila,* PYCA= *Pyrus calleryana,* PLOC= *Platanus occidentalis,* FRPE = *Fraxinus pennsylvanica,* ULPA= *Ulmus parviflora,* ACSA= *Acer saccharinum,* QUSH=*Quercus shumardii*

4.6 Conclusions

This study is one of the early attempts at developing biophysical estimation models for individual trees in an urban area based on point-based lidar distributional metrics. A high level of accuracy was attained for estimating tree height (R^2=0.89), dbh (R^2=0.82), crown diameter (R^2=0.90) and biomass (R^2=0.67). Tree height of most species

had a good relationship with lidar-measured maximum height, except for species with a round crown and no distinct tree top, which makes it difficult to detect the tree-top for the lidar as well as for the field measurer. The good relationship between field-measured and lidar-measured crown radius indicates that individual tree crown delineation from lidar data was fairly accurate. Species-specific relationships had much higher R^2 (0.68 to 0.84) than for general broadleaves and conifer relationships (0.45 to 0.67). Using a general, instead of species-specific, allometric relationship should improve the biomass models for broadleaves and conifers. When estimating the biomass of individual trees during an urban forest inventory, it is recommended to first stratify the trees by species and use lidar-based biomass equations developed for the particular species than using the biomass equations developed for broader classes. We found that the metric crown area (C_A) performed particularly well for most of the species biomass equations. It is imperative that tree crown be delineated accurately, whether manually or using automatic individual tree detection algorithms, to obtain a good estimation of biomass using lidar-based metrics. Though spectral metrics from high-resolution satellite imagery did not perform particularly well in predicting individual tree biomass, future studies can explore other vegetation indices and grey-level texture (such as Kayitakire et al., 2006; Ouma and Tateishi, 2006) to improve prediction capacity of high-resolution imagery.

Prediction models from this study, even though developed from trees from a specific urban area, can be applied to other urban areas with similar landscape and species composition, and when the lidar data were acquired with mission parameters similar to this study, e.g., point density of 8 pulses/m^2 and similar footprint size. These kinds of lidar-based prediction models will help in accurate quantification of urban carbon storage at the individual tree level. Future studies should develop models that can predict other biophysical parameters such as leaf area index, stem volume, etc., and management attributes useful for urban planner such as pruning level required, potential hazard rate, and age-class of the individual trees. Applicability of the models can be improved by incorporating data from other urban areas, and, if available, using allometric equations based on trees from urban areas rather than based on trees from forests.

4.7 Literature Cited

Allen, D., 1974. The relationship between variable selection and data agumentation and a method for prediction. Technometrics, 16(1): 125-127.

Avery, T.E. and Burkhart, H.E., 2002. Forest Measurements. McGraw-Hill, Boston, 456 pp.

Baret, F. and Guyot, G., 1991. Potentials and limits of vegetation indices for LAI and APAR assessment. Remote Sensing of Environment, 35(2-3):161-173.

Blackard, J.A., Finco, M.V., Helmer, E.H., Holden, G.R., Hoppus, M.L., Jacobs, D.M., Lister, A.J., Moisen, G.G., Nelson, M.D., Riemann, R., Ruefenacht, B., Salajanu, D., Weyermann, D.L., Winterberger, K.C., Brandeis, T.J., Czaplewski, R.L., McRoberts, R.E., Patterson, P.L. and Tymcio, R.P., 2008. Mapping U.S. forest biomass using nationwide forest inventory data and moderate resolution information. Remote Sensing of Environment, 112(4): 1658-1677.

Bolund, P. and Hunhammar, S., 1999. Ecosystem services in urban areas. Ecological Economics, 29(2): 293-301.

Bortolot, Z.J., 2006. Using tree clusters to derive forest properties from small footprint lidar data. Photogrammetric Engineering & Remote Sensing, 72(12): 1379-1388.

Bortolot, Z.J. and Wynne, R.H., 2005. Estimating forest biomass using small footprint LiDAR data: An individual tree-based approach that incorporates training data. ISPRS Journal of Photogrammetry and Remote Sensing, 59(6): 342-360.

Boudreau, J., Nelson, R.F., Margolis, H.A., Beaudoin, A., Guindon, L. and Kimes, D.S., 2008. Regional aboveground forest biomass using airborne and spaceborne LiDAR in Québec. Remote Sensing of Environment, 112(10): 3876-3890.

Boyd, D.S. and Danson, F.M., 2005. Satellite remote sensing of forest resources: three decades of research development. Progress in Physical Geography, 29(1): 1-26.

Brandtberg, T., Warner, T.A., Landenberger, R.E. and McGraw, J.B., 2003. Detection and analysis of individual leaf-off tree crowns in small footprint, high sampling density lidar data from the eastern deciduous forest in North America. Remote Sensing of Environment, 85(3): 290-303.

Brenneman, B.B., Frederick, D.J., Gardner, W.E., Schoenhofen, L.H. and Marsh, P.L., 1978. Biomass of species and stands of West Virginia hardwoods. In: P.E. Pope (Editor), Proceedings of Central Hardwood Forest Conference II. Purdue University, West LaFayette, Indiana, USA, pp. 159-178.

Chen, Q., Gong, P., Baldocchi, D. and Tian, Y.Q., 2007. Estimating basal area and stem volume for individual trees from lidar data. Photogrammetric Engineering & Remote Sensing, 73(12): 1355-1365.

Chubey, M., Franklin, S. and Wulder, M., 2006. Object-based analysis of Ikonos-2 imagery for extraction of forest inventory parameters. Photogrammetric Engineering & Remote Sensing, 72(4): 383–394.

Clark III, A., Phillips, D.R. and Frederick, D.J., 1986. Weight, volume, and physical properties of major hardwood species in the Piedmont, Southeastern Forest Experiment Station. North Carolina State University, Raleigh, pp. 88.

Clark, M.L., Clark, D.B. and Roberts, D.A., 2004. Small-footprint lidar estimation of sub-canopy elevation and tree height in a tropical rain forest landscape. Remote Sensing of Environment, 91(1): 68-89.

Crow, T.R., 1971. Estimation of biomass in an even-aged stand--regression and “mean tree" techniques. In: H.E. Young (Editor), Forest Biomass Studies, 17th IUFRO Congress, 15-20 March, 1971. IUFRO Yield and Growth Working Group on forest biomass studies, Gainsville, Florida, pp. 35-47.

Dalponte, M., Bruzzone, L. and Gianelle, D., 2008. Fusion of hyperspectral and lidar remote sensing data for classification of complex forest areas. IEEE Transactions on Geoscience and Remote Sensing, 46(5): 1416-1427.

Dean, T.J., Cao, Q.V., Roberts, S.D. and Evans, D.L., 2008. Measuring heights to crown base and crown median with LiDAR in a mature, even-aged loblolly pine stand. Forest Ecology and Management, 257(1): 126-133.

Duryea, M.L. and Malavasi, M.M., 1995. Tree growth in the urban forest. Forestry Report R8-FR, USDA Forest Service, Southern Region, Atlanta, Georgia.

Falkowski, M., Smith, A., Gessler, P., Hudak, A., Vierling, L. and Evans, J., 2008. The influence of conifer forest canopy cover on the accuracy of two individual tree measurement algorithms using lidar data. Canadian Journal of Remote Sensing, 34(Suppl 2): S338-S350.

Gary, H., 1978. The vertical distribution of needles and branchwood in thinned and unthinned 80-year-old lodgepole pine. Northwest Science, 52(4): 303-309.

Gonzalez, P., Asner, G.P., Battles, J.J., Lefsky, M.A., Waring, K.M. and Palace, M., 2010. Forest carbon densities and uncertainties from Lidar, QuickBird, and field measurements in California. Remote Sensing of Environment, 114(7): 1561-1575.

Hall, R.J., Skakun, R.S., Arsenault, E.J. and Case, B.S., 2006. Modeling forest stand structure attributes using Landsat ETM+ data: Application to mapping of aboveground biomass and stand volume. Forest Ecology and Management, 225(1-3): 378-390.

Hall, S.A., Burke, I.C., Box, D.O., Kaufmann, M.R. and Stoker, J.M., 2005. Estimating stand structure using discrete-return lidar: an example from low density, fire prone ponderosa pine forests. Forest Ecology and Management, 208(1/3): 189-209.

Heiskanen, J., 2006. Estimating aboveground tree biomass and leaf area index in a mountain birch forest using ASTER satellite data. International Journal of Remote Sensing, 27(6): 1135 - 1158.

Heurich, M., Persson, A., Holmgren, J. and Kennel, E., 2004. Detecting and measuring individual trees with laser scanning in mixed mountain forest of Central Europe using an algorithm developed for Swedish boreal forest conditions. In: M. Thies, B. Koch, H. Spiecker and H. Weinacker (Editors), Proceedings of the ISPRS Working Group VIII/2 'Laser-Scanners for Forest and Landscape Assessment', 03-06 October 2004, Freiburg, Germany, pp. 307-312.

Hocking, R., 2003. Methods and applications of linear models: Regression and the analysis of variance. Wiley-Interscience, 776 pp.

Holmgren, J., Persson, A. and Soderman, U., 2008. Species identification of individual trees by combining high resolution LiDAR data with multi-spectral images. International Journal of Remote Sensing, 29(5): 1537-1552.

Hopkinson, C., Chasmer, L., Sass, G., Creed, I., Sitar, M., Kalbfleisch, W. and Treitz, P., 2005. Vegetation class dependent errors in lidar ground elevation and canopy height estimates in a boreal wetland environment. Canadian Journal of Remote Sensing, 31(2): 191–206.

Hudak, A.T., Lefsky, M.A., Cohen, W.B. and Berterretche, M., 2002. Integration of lidar and Landsat ETM+ data for estimating and mapping forest canopy height. Remote Sensing of Environment, 82(2/3): 397-416.

Huete, A.R., 1988. A soil-adjusted vegetation index (SAVI). Remote Sensing of Environment, 25(3): 295-309.

Hyde, P., Nelson, R., Kimes, D. and Levine, E., 2007. Exploring LiDAR-RaDAR synergy--predicting aboveground biomass in a southwestern ponderosa pine forest using LiDAR, SAR and InSAR. Remote Sensing of Environment, 106(1): 28-38.

Hyyppä, H.J. and Hyyppä, J.M., 2001. Effects of stand size on the accuracy of remote sensing-based forest inventory. Geoscience and Remote Sensing, 39(12): 2613-2621.

Hyyppä, J. and Inkinen, M., 1999. Detecting and estimating attributes for single trees using laser scanner. Photogrammetric Journal of Finland, 16(2): 27-42.

Hyyppä, J., Kelle, O., Lehikoinen, M. and Inkinen, M., 2001. A segmentation-based method to retrieve stem volume estimates from 3-D tree height models produced by laser scanners. IEEE Transactions on Geoscience and Remote Sensing, 39(5): 969-975.

Hyyppä, J., Pyysalo, U., Hyyppä, H. and Samberg, A., 2000. Elevation accuracy of laser scanning-derived digital terrain and target models in forest environment, Proceedings of EARSeL-SIG-Workshop LIDAR, Dresden/FRG, June 16 – 17, 2000, pp. 14-17.

Jenkins, J., Chojnacky, D., Heath, L. and Birdsey, R., 2003. National-scale biomass estimators for United States tree species. Forest Science, 49(1): 12-35.

Jenkins, J., Chojnacky, D., Heath, L. and Birdsey, R., 2004. Comprehensive database of diameter-based biomass regressions for North American tree species. NE-319, United States Forest Service, Northeastern Research Station, New Town Square, Pennsylvania.

Johnson, A. and Gerhold, H., 2001. Carbon storage by utility-compatible trees. Journal of Arboriculture, 27(2): 57-68.

Kayitakire, F., Hamel, C. and Defourny, P., 2006. Retrieving forest structure variables based on image texture analysis and IKONOS-2 imagery. Remote Sensing of Environment, 102(3-4): 390-401.

Kleinbaum, D., Kupper, L., Nizam, A. and Muller, K., 2007. Applied regression analysis and other multivariable methods. Thompson Higher Education, Belmont, CA, 928 pp.

Kwak, D.A., Lee, W.K., Lee, J.H., Biging, G. and Gong, P., 2007. Detection of individual trees and estimation of tree height using LiDAR data. Journal of Forest Research, 12(6): 425-434.

Leboeuf, A., Beaudoin, A., Fournier, R.A., Guindon, L., Luther, J.E. and Lambert, M.C., 2007. A shadow fraction method for mapping biomass of northern boreal black spruce forests using QuickBird imagery. Remote Sensing of Environment, 110(4): 488-500.

Lim, K.S., Treitz, P., Morrison, I. and Baldwin, K., 2003. Estimating above-ground biomasss using lidar remote sensing. In: M. Owe, G. D'Urso and L. Toulios (Editors), Proceedings of SPIE Remote Sensing for Agriculture, Ecosystems, and Hydrology IV, Agia Pelagia, Crete, Greece, pp. 289-296.

Lu, D., 2006. The potential and challenge of remote sensing-based biomass estimation. International Journal of Remote Sensing, 27(7): 1297-1328.

Lutz, D., Washington-Allen, R. and Shugart, H., 2009. Remote sensing of boreal forest biophysical and inventory parameters: a review. Canadian Journal of Remote Sensing, 34(Suppl. 2): S286-S313.

Magnussen, S. and Boudewyn, P., 1998. Derivations of stand heights from airborne laser scanner data with canopy-based quantile estimators. Canadian Journal of Forest Research, 28(7): 1016-1031.

McHale, M., Burke, I., Lefsky, M., Peper, P. and McPherson, E., 2009. Urban forest biomass estimates: is it important to use allometric relationships developed specifically for urban trees? Urban Ecosystems, 12(1): 95-113.

McPherson, E.G., Nowak, D., Heisler, G., Grimmond, S., Souch, C., Grant, R. and Rowntree, R., 1997. Quantifying urban forest structure, function, and value: the Chicago Urban Forest Climate Project. Urban Ecosystems, 1(1): 49-61.

Means, J.E., Acker, S.A., Fitt, B.J., Renslow, M., Emerson, L. and Hendrix, C.J., 2000. Predicting forest stand characteristics with airborne scanning lidar. Photogrammetric Engineering & Remote Sensing, 66(11): 1367-1371.

Miller, R.W., 1996. Urban Forestry: Planning and Managing Urban Greenspaces. Prentice Hall, Englewood Cliffs, New Jersey, USA, 480 pp.

Montgomery, D. and Peck, E., 2006. Introduction to Linear Regression Analysis. Wiley, New York, USA, 640 pp.

Myeong, S., Nowak, D. and Duggin, M., 2006. A temporal analysis of urban forest carbon storage using remote sensing. Remote Sensing of Environment, 101(2): 277-282.

Naesset, E., 1997. Estimating timber volume of forest stands using airborne laser scanner data. Remote Sensing of Environment, 61(2): 246-253.

Naesset, E., 2002. Predicting forest stand characteristics with airborne scanning laser using a practical two-stage procedure and field data. Remote Sensing of Environment, 80(1): 88-99.

Naesset, E., 2004. Practical large-scale forest stand inventory using a small-footprint airborne scanning laser. Scandinavian Journal of Forest Research, 19(2): 164 - 179.

Naesset, E. and Bjerknes, K.O., 2001. Estimating tree heights and number of stems in young forest stands using airborne laser scanner. Remote Sensing of Environment, 78(3): 328-340.

Næsset, E. and Gobakken, T., 2008. Estimation of above- and below-ground biomass across regions of the boreal forest zone using airborne laser. Remote Sensing of Environment, 112(6): 3079-3090.

Naesset, E. and Gobakken, T., 2005. Estimating forest growth using canopy metrics derived from airborne laser scanner data. Remote Sensing of Environment, 96(3-4): 453-465.

Naesset, E. and Okland, T., 2002. Estimating tree height and tree crown properties using airborne scanning laser in a boreal nature reserve. Remote Sensing of Environment, 79(1): 105-115.

Nelson, R., 1997. Modeling forest canopy heights: The effects of canopy shape. Remote Sensing of Environment, 60(3): 327-334.

Nelson, R., Krabill, W. and Tonelli, J., 1988. Estimating forest biomass and volume using airborne laser data. Remote Sensing of Environment, 24(2): 247-267.

Nelson, R., Parker, G. and Horn, M., 2003. A portable airborne laser system for forest inventory. Photogrammetric Engineering and Remote Sensing, 69(3): 267-273.

Nelson, R., Short, A. and Valenti, M., 2004. Measuring biomass and carbon in Delaware using an airborne profiling LIDAR. Scandinavian Journal of Forest Research, 19(6): 500-511.

Nelson, R.F., Hyde, P., Johnson, P., Emessiene, B., Imhoff, M.L., Campbell, R. and Edwards, W., 2007. Investigating RaDAR-LiDAR synergy in a North Carolina pine forest. Remote Sensing of Environment, 110(1): 98-108.

Nelson, R.F., Kimes, D.S., Salas, W.A. and Routhier, M., 2000. Secondary forest age and tropical forest biomass estimation using thematic mapper imagery. BioScience, 50(5): 419-431.

Norris, M.D., Blair, J.M., Johnson, L.C. and McKane, R.B., 2001. Assessing changes in biomass, productivity, and C and N stores following *Juniperus virginiana* forest expansion into tallgrass prairie. Canadian Journal of Forest Research, 31(11): 1940-1946.

Nowak, D.J. and Crane, D.E., 2002. Carbon storage and sequestration by urban trees in the USA. Environmental Pollution, 116(3): 381–389.

Omasa, K., Hosoi, F., Uenishi, T., Shimizu, Y. and Akiyama, Y., 2008. Three-dimensional modeling of an urban park and trees by combined airborne and portable on-ground scanning LIDAR remote sensing. Environmental Modeling and Assessment, 13(4): 473-481.

Otey, J.K., 2007. GIS Applications in Urban Tree Inventory. Master of Forestry Thesis, Virginia Polytechnic Institute and State University, Blacksburg, Virginia, USA.

Ouma, Y. and Tateishi, R., 2006. Optimization of second-order grey-level texture in high-resolution imagery for statistical estimation of above-ground biomass. Journal of Environmental Informatics, 8(2): 70-85.

Palenichka, R.M. and Zaremba, M.B., 2007. Multiscale isotropic matched filtering for individual tree detection in LiDAR images. IEEE Transactions on Geoscience and Remote Sensing, 45(12): 3944-3956.

Pataki, D.E., Alig, R.J., Fung, A.S., Golubiewski, N.E., Kennedy, C.A., Mcpherson, E.G., Nowak, D.J., Pouyat, R.V. and Lankao, P.R., 2006. Urban ecosystems and the North American carbon cycle. Global Change Biology, 12(11): 2092-2102.

Peichl, M. and Arain, M.A., 2007. Allometry and partitioning of above- and belowground tree biomass in an age-sequence of white pine forests. Forest Ecology and Management, 253(1-3): 68-80.

Persson, A., Holmgren, J. and Soderman, U., 2002. Detecting and measuring individual trees using an airborne laser scanner. Photogrammetric Engineering & Remote Sensing, 68(9): 925-932.

Pillsbury, N., Reimer, J. and Thompson, R., 1995. Tree volume equations for fifteen urban species in California, California Polytechnic State University, Urban Forest Ecosystems Institute, San Louis Obispo, California, USA.

Popescu, S.C., 2007. Estimating biomass of individual pine trees using airborne lidar. Biomass and Bioenergy, 31(9): 646-655.

Popescu, S.C. and Wynne, R.H., 2002. Esimating plot-level forest biophysical parameters using small-footprint airborne lidar measurements. Computers and Electronics in Agriculture, 37: 71-95.

Popescu, S.C. and Wynne, R.H., 2004. Seeing the trees in the forest: using lidar and multispectral data fusion with local filtering and variable window size for estimating tree height. Photogrammetric Engineering & Remote Sensing, 70(5): 589-604.

Popescu, S.C., Wynne, R.H. and Nelson, R.F., 2003. Measuring individual tree crown diameter with lidar and assessing its influence on estimating forest volume and biomass. Canadian Journal of Remote Sensing, 29(5): 564-577.

Popescu, S.C., Wynne, R.H. and Scrivani, J.A., 2004. Fusion of small-footprint lidar and multispectral data to estimate plot-level volume and biomass in deciduous and pine forests in Virginia, USA. Forest Science, 50(4): 551-565.

Qi, J., Chehbouni, A., Huete, A.R., Kerr, Y.H. and Sorooshian, S., 1994. A modified soil adjusted vegetation index. Remote Sensing of Environment, 48(2): 119-126.

Reed, D., Liechty, H., Jones, E. and Zhang, Y., 1996. Above- and below-ground dry matter accumulation pattern derived from dimensional biomass relationships. Forest Science, 42(2): 236-241.

Roberts, S.D., Dean, T.J., Evans, D.L., McCombs, J.W., Harrington, R.L. and Glass, P.A., 2005. Estimating individual tree leaf area in loblolly pine plantations using LiDAR-derived measurements of height and crown dimensions. Forest Ecology and Management, 213(1-3): 54-70.

Rouse, J., Haas, R., Schell, J., Deering, D. and Harlan, J., 1974. Monitoring the vernal advancement of retrogradation of natural vegetation. Final report. National Aeronautics & Space Administration/Goddard Space Flight Centre, Greenbelt, Maryland, USA.

Rozeboom, W., 1978. Estimation of cross-validated multiple correlation: a clarification. Psychological Bulletin, 85(6): 1348-1351.

Schlaegel, B., 1984. Green ash volume and weight tables, Res. Pap. SO-206., US Department of Agriculture, Forest Service, Southern Forest Experiment Station, New Orleans, LA.

Schlerf, M., Atzberger, C. and Hill, J., 2005. Remote sensing of forest biophysical variables using HyMap imaging spectrometer data. Remote Sensing of Environment, 95(2): 177-194.

Schroeder, P., Brown, S., Mo, J., Birdsey, R. and Cieszewski, C., 1997. Biomass estimation for temperate broadleaf forests of the United States using inventory data. Forest Science, 43(3): 424-434.

Smith, M.-L., Ollinger, S.V., Martin, M.E., Aber, J.D., Hallett, R.A. and Goodale, C.L., 2002. Direct estimation of aboveground forest productivity through hyperspectral remote sensing of canopy nitrogen. Ecological Applications, 12(5): 1286-1302.

Snowdon, P., Eamus, D., Gibbons, P., Khanna, P., Keith, H., Raison, R. and Kirschbaum, M., 2001. Synthesis of allometrics, review of root biomass, and design of future woody biomass sampling strategies, The Australian Greenhouse Office, Canberra, Australia.

St-Onge, B., Hu, Y. and Vega, C., 2008. Mapping the height and above-ground biomass of a mixed forest using lidar and stereo Ikonos images. International Journal of Remote Sensing, 29(5): 1277-1294.

Ter-Mikaelian, M.T. and Korzukhin, M.D., 1997. Biomass equations for sixty-five North American tree species. Forest Ecology and Management, 97(1): 1-24.

Tesfamichael, S.G., van Aardt, J.A.N. and Ahmed, F., 2010. Estimating plot-level tree height and volume of *Eucalyptus grandis* plantations using small-footprint, discrete return lidar data. Progress in Physical Geography, 34(4): 515-540.

Todd, K.W., Csillag, F. and Atkinson, P.M., 2003. Three-dimensional mapping of light transmittance and foilage distribution using lidar. Canadian Journal of Remote Sensing, 29(5): 544-555.

van Aardt, J.A.N, Wynne, R.H. and Scrivani, J.A., 2008. Lidar-based mapping of forest volume and biomass by taxonomic group using structurally homogenous segments-an evaluation of an object-oriented approach to deciduous and coniferous forest. Photogrammetric Engineering & Remote Sensing, 74(8): 1033-1044.

van Aardt, J.A.N., Wynne, R.H. and Oderwald, R.G., 2006. Forest volume and biomass estimation using small-footprint lidar-distributional parameters on a per-segment basis. Forest Science, 52(6): 636-649.

West, P.W., 2004. Tree and Forest Measurement. Springer, 167 pp.

Wood, J.P., 1999. Tree inventories and GIS in urban forestry. M.S. Thesis, Virginia Polytechnic Institute and State University, Blacksburg, Virginia, USA. http://scholar.lib.vt.edu/theses/available/etd-012499-141520.

Wulder, M., 1998. Optical remote-sensing techniques for the assessment of forest inventory and biophysical parameters. Progress in Physical Geography, 22(4): 449-476.

Zheng, D., Rademacher, J., Chen, J., Crow, T., Bresee, M., Le Moine, J. and Ryu, S.-R., 2004. Estimating aboveground biomass using Landsat 7 ETM+ data across a managed landscape in northern Wisconsin, USA. Remote Sensing of Environment, 93(3): 402-411.

5: CONCLUSIONS

It has been more than a decade since small-footprint airborne lidar has been widely and successfully adopted in the forestry community to assist in assessment and inventory of forest lands. However, the utility of lidar data for urban tree inventory, which poses a different set of challenges and conditions compared to forest inventory, has not been extensively explored and tested so far. Based on remote sensing and field data from a suburban residential area of central United States, this dissertation has presented a methodology for utilizing airborne small-footprint lidar data in inventory of urban trees. The study proposes approaches that have potential to automate three main activities of urban tree inventory – identifying the locations of trees, classifying the trees into taxonomic categories, and estimating biophysical parameters of individual trees – using airborne lidar data.

An image morphology-based approach was evaluated to delineate the crown of individual trees and separate urban trees from other urban non-tree structures. This approach can be used within an acceptable level of accuracy for separating individual trees especially along the pathways or in backyards, where the trees are fairly isolated. As with most of other individual tree detection algorithms using lidar data, our approach also had some trouble separating the trees when the crowns are overlapping and detecting smaller trees underneath larger crowns. This is more an issue associated with nature of airborne lidar data than with the methodology in detecting the trees. Until a very high density lidar collection becomes affordable, we can either resort to sampling using terrestrial laser scanning or other forms of field data collection, or do away with measuring individual trees and measure an estimate of tree clumps when these conditions predominated.

Random forests imputation was used to assess the ability of the lidar data to classify the trees into taxonomic groups. This approach is based on the notion that tree shapes of each taxonomic group are unique and representative, and the lidar data has ability to characterize the shape and size of the tree crowns. While the latter has been proven and tested by this investigation and other studies, crown shapes alone cannot be used for taxonomic classification at finer scales. Our results also indicate that while lidar data are useful to classify the individual trees at broad taxonomy level, such as deciduous and conifers, they do not perform particularly well when classifying at species or genera

level. Given that requirements of urban tree inventory often entail the information on species of each individual tree, use of additional spectral data with a finer resolution of infrared spectrum (such as hyperspectral data) may be necessary to achieve an acceptable species-level classification of individual trees.

Prediction models to estimate several biophysical parameters such as height, crown area, diameter at breast height, and biomass were developed using lidar point cloud distributional metrics from individual trees. As was found by other earlier studies focussing on trees in forested environments, lidar has potential to estimate biophysical parameters of individual urban trees to the accuracy levels required. Since a high-resolution lidar data set can capture information on branching and crown characteristics, there is potential in the future for studies to develop models that can estimate other management attributes useful for urban planners such as the pruning level required, potential hazard rate, and age-class of the individual trees. Applicability of the models can also be improved by incorporating data from other urban areas, and, if available, using allometric equations based on trees from urban areas rather than based on trees from forests.

Our results indicate that, while using lidar data alone can achieve the automation of major urban forest inventory tasks to an acceptable level of accuracy, a synergistic use of lidar data with other spectral data such as hyperspectral data or orthoimages, the latter of which are usually available at least in the United States for most urban areas, can considerably improve the performance of the lidar-based method. Automation of tree inventory can be a good incentive for urban planners and policy-makers to adopt lidar and other remote-sensing based approaches in their current workflow, not only to improve cost-effectiveness, but also to improve both the quality and quantity of information available for ever-expanding urban forest ecosystems.

APPENDIX A: IDL PROGRAM TO IMPLEMENT URBAN TREE DETECTION ALGORITHM

```
pro set_filename

common set_filename, filedem, filedtm, fileortho
filedem = ''
filedtm =''
fileortho=''

common set_filename, progversion
progversion=''

end

PRO overlayortho_event, event


common set_filename, filedem, filedtm, fileortho

if ((file_test('tempimg.tif', /read)) AND KEYWORD_SET(fileortho)) then begin

        imgdisp = Read_TIFF('tempimg.tif')
        tvscl, imgdisp, /order
        wait, 1


        dataortho = Read_TIFF(fileortho)

        widget_control, event.top, get_uvalue=infoptr
        info = *infoptr
        widget_control, event.id, get_uvalue=widget
        widget_control, info.draw_id, GET_VALUE = dindex
        wset, dindex

        *infoptr = info

        if (size(dataortho, /N_DIMENSIONS) gt 2) then begin
                tvscl, dataortho, /order, true=1
                wait, 1
        endif
        if (size(dataortho, /N_DIMENSIONS) eq 2) then begin
                tvscl, dataortho, /order
                wait, 1
        endif
endif

end
```

```
PRO opendem_event, event

widget_control, event.top, get_uvalue=infoptr
info = *infoptr

widget_control, event.id, get_uvalue=widget

common set_filename, filedem, filedtm, fileortho

filedem= dialog_pickfile(/read, title='Select the DEM file', filter='*.tif')

if KEYWORD_SET(filedem) then begin

        data = Read_TIFF(filedem, GEOTIFF = geo)


        imgsize = size(data)

        draw_x = imgsize[1]
        draw_y = imgsize[2]

        widget_control, info.draw_id , draw_xsize=draw_x, draw_ysize=draw_y

        widget_control, info.draw_id, GET_VALUE = dindex

        wset, dindex

        *infoptr = info

        write_tiff, 'tempimg.tif', data, /float, GEOTIFF = geo
        tvscl, data, /order

endif

PRO drawimage_event, event

widget_control, event.top, get_uvalue=infoptr
info = *infoptr

widget_control, event.id, get_uvalue=widget

if (file_test('tempimg.tif', /read)) then begin

        if (event.press gt 0) then begin

                tempimg = Read_TIFF('tempimg.tif', GEOTIFF = geo)

                tempsize = size(tempimg)

                xscale  = geo.ModelPixelScaleTag[0]
                yscale  = geo.ModelPixelScaleTag[1]
```

```
            origpt  = geo.ModelTiePointTag[3:4]

            label_text = string('X:', (origpt[0] + (event.x*xscale)), $
                          '     Y:', (origpt[1]+ (event.y*xscale)), '    Z:', $
                          tempimg[(event.x), ((tempsize[2]-1)-event.y)])

            widget_control, info.pixellabel , set_value=label_text

        endif

endif

*infoptr = info

End

PRO findtrees_event, event

widget_control, /hourglass

common set_filename, filedem, filedtm, fileortho

if keyword_set(filedem) AND keyword_set(filedtm) then begin

        datadem = read_tiff(filedem, GEOTIFF = geo)
        datadtm = read_tiff(filedtm, GEOTIFF = geo)

        datachm = datadtm-datadem

        blankchm = datachm * 0

        trees = where(datachm GT 1.0, count)
        blankchm[trees] = datachm[trees]

        radius = 5
        strucElem = shift_tree(dist(2*radius+1), radius, radius) LE radius

        tophatchm = morph_tophat_tree(blankchm , strucElem)

        topchm = temporary(tophatchm ) GT 3.0

        thinchm = THIN(topchm, /prune)

        closechm = morph_close_tree(thinchm, strucElem)

        radius2 = 1
        strucElem2 = shift(dist(2*radius2+1), radius2, radius2) LE radius2

        erodechm = erode_tree(closechm, strucElem2)

        gradchm = morph_gradient_tree(blankchm, strucElem2)
```

```
        tgradchm= temporary(gradchm) GE 1.0

        imgsize = size(tgradchm)

        image = tgradchm*0

        for i = 0, 5 do begin
        for r = 1, (imgsize[1]-2) do begin
                for c = 1, (imgsize[2]-2) do begin
                        if tgradchm[r,c] ge 1 then begin
                                tindex=where(erodechm[r-1:r+1,c-1:c+1] ge 1, count)
                                if count NE 0 then image[r,c]=1
                        endif
                endfor
        endfor
        erodechm = image
        endfor

        labelchm=label_region(image)

        openw, lun, 'treelocation.txt' , /get_lun
        header1 = 'TreeID, X, Y, CrownArea, Height, Crown Height'
        printf,lun, header1

        xscale  = geo.ModelPixelScaleTag[0]
        yscale  = geo.ModelPixelScaleTag[1]
        origpt  = geo.ModelTiePointTag[3:4]

        FOR i=1, max(labelchm)-1 DO BEGIN

                p1 = where(labelchm eq i, count)

                a = count * xscale * yscale

                hmax = max(blankchm[p1], maxd, min=hmin)

                hloc = array_indices(blankchm, maxd)

                printf,lun, i, ',', hloc[0] - origpt[0],',', origpt[1]- hloc[1],',', a,',',
hmax,',', hmin


        ENDFOR

        image = labelchm

        widget_control, event.top, get_uvalue=infoptr
        info = *infoptr
        widget_control, event.id, get_uvalue=widget
        widget_control, info.draw_id, GET_VALUE = dindex
```

```
        wset, dindex

        widget_control, info.butopenlidar, SENSITIVE=1

        write_tiff, 'tempimg.tif', image, /float, GEOTIFF = geo

        DEVICE, DECOMPOSED = 0
        LOADCT, 29
        tvscl, image, /order

        close, /all

endif
end

PRO locatetree

common set_filename, progversion

progversion='LocateTrees v 1.0'

device, get_screen_size=screen_size

xoffset = screen_size[0]/5

yoffset = screen_size[1]/5

base = widget_base(title=progversion, bitmap='icon/tree_small.bmp', $
               xsize=830, ysize=660, mbar = mbar, xoffset=xoffset, yoffset=yoffset)

viewmenu = widget_button(mbar, value='File')

vmenu1 = widget_button(viewmenu, value='View tree info...',  $
               uvalue='tree', event_pro='menu_viewtreeinfo')

vmenu2 = widget_button(viewmenu, value='View lidar metrics...',  $
               uvalue='lidar', event_pro='menu_viewlidarmetrics')

vmenu3 = widget_button(viewmenu, value='View image in iTool...',  $
               uvalue='itool', event_pro='menu_viewimage', /SEPARATOR)

vmenu4 = widget_button(viewmenu, value='Exit', uvalue='exit', $
               event_pro='menu_exit', /SEPARATOR)

helpmenu = widget_button(mbar, value=' Help')

hmenu1 = widget_button(helpmenu, value='Contents...', uvalue='helpcontent', $
               event_pro='menu_helpcontent')

hmenu2 = widget_button(helpmenu, value='About...', uvalue='helpabout', $
                event_pro='menu_about')
```

```
butbase = widget_base(base,column=1, frame=1, yoffset=20)

butdem = widget_button(butbase, value='1. Open DEM', $
               uvalue='OpenDEM', event_pro='opendem_event', xsize=105)

butdtm = widget_button(butbase, value='2. Open DTM', $
               uvalue='OpenDTM', event_pro='opendtm_event', xsize=105)
butfindtrees = widget_button(butbase, value='3. Find Trees', $
               uvalue='FindTrees', event_pro='findtrees_event', xsize=105)

draw_x=695
draw_y=625

draw_id = widget_draw(base, uvalue='DrawImage', event_pro='drawimage_event', $
               /button_events, /scroll, x_scroll_size=695, y_scroll_size=625, $
               xsize=draw_x, ysize=draw_y, xoffset=115)

butopenlidar = widget_button(base, value='Open lidar', uvalue='Openlidar', $
               event_pro='openlidar_event', xoffset=5, yoffset=300, xsize=100,
SENSITIVE=0)

butopenortho = widget_button(base, value='Open ortho', uvalue='OpenOrtho', $
               event_pro='openortho_event', xoffset=5, yoffset=575, xsize=100)

butoverlay = widget_button(base, value='Overlay Trees', uvalue='OverlayOrtho', $
               event_pro='overlayortho_event', xoffset=5, yoffset=605, xsize=100, $
               SENSITIVE=0)

pixellabel = widget_label(base, value ='X:    Y:    Z:', $
               xoffset=115, yoffset=642, /dynamic_resize)

widget_control, base, /realize,  /hourglass

widget_control, draw_id, GET_VALUE = dindex

wset, dindex

info = {dindex:dindex, draw_x: draw_x, draw_y:draw_y, draw_id:draw_id,  $
               butfindtrees:butfindtrees, pixellabel:pixellabel,butoverlay:butoverlay,  $
               butopenlidar:butopenlidar, x:-1L, y:-1L}

infoptr = ptr_new(info)

widget_control, base, set_uvalue=infoptr

xmanager, 'locatetree', base, cleanup='locatetree_cleanup', /no_block


END
PRO locatetree_cleanup, ID
```

```
widget_control, id, get_uvalue=infoptr

info = *infoptr

;FILE_DELETE,'tempimg.tif',  /ALLOW_NONEXISTENT

ptr_free, infoptr

END

pro menu_helpcontent, event

        ONLINE_HELP, BOOK='help\help.pdf', /FULL_PATH

end

pro about_idlvm, event

BOOK='http://www.ittvis.com/ProductServices/IDL/VirtualMachine.aspx', /FULL_PATH

end

pro menu_about, event

device, get_screen_size=screen_size
xoffset = screen_size[0]/3
yoffset = screen_size[1]/3
base_about = widget_base(title='About LocateTrees', bitmap='icon/tree_small.bmp', col=2, $
                      xsize=330, ysize=170, xoffset=xoffset, yoffset=yoffset)


textbase = widget_base(base_about, row=9, /base_align_center, /ALIGN_CENTER)

common set_filename, progversion

buttonlogo =widget_button(textbase, VALUE='icon/idl_logo.bmp', /BITMAP,
event_pro='about_idlvm')

widget_control, base_about, /realize

xmanager, 'menu_about', base_about, /no_block

end

pro menu_viewtreeinfo, event

file = 'treelocation.txt'
if (file_test(file,/read)) then begin
        xdisplayfile, file, DONE_BUTTON='Close', GROUP=base, /GROW_TO_SCREEN
endif else begin
```

```
        result = DIALOG_MESSAGE('No output file exists!', /CENTER, DIALOG_PARENT=base)

endelse

end

pro menu_viewlidarmetrics, event

file = 'treelocation.txt'

if (file_test(file,/read)) then begin

        xdisplayfile, file, DONE_BUTTON='Close', GROUP=base, /GROW_TO_SCREEN

endif else begin

        result = DIALOG_MESSAGE('No output file exists!', /CENTER, DIALOG_PARENT=base)

endelse

end

pro menu_viewimage, event

if (file_test('tempimg.tif', /read)) then begin
        data = Read_TIFF('tempimg.tif', GEOTIFF = geo)

        iimage, data, TITLE = 'Trees', /FIT_TO_VIEW, /order

endif  else begin

        result = DIALOG_MESSAGE('No output image exists!', /CENTER, DIALOG_PARENT=base)

endelse

end

pro menu_exit, event

widget_control, event.top, get_uvalue=infoptr

WIDGET_CONTROL, event.top, /DESTROY

end
```